POLITECNICO DI TORINO

Master of Science in Mechanical Engineering

Master's Degree Thesis

Design Selection of Multimode Power Split Hybrid Electric Vehicle Powertrains

Supervisors

Prof. Giovanni Belingardi

Prof. Ali Emadi

Co-Supervisor

Ing. Pier Giuseppe Anselma

Candidate

Giuseppe Buccoliero

December 2018

To my parents, grandparents, family and friends:
without your love and support, none of this would have been possible.

Index

List of Figures

List of Tables

Nomenclature

BEV	Battery Electric Vehicle
CS	Charge Sustaining
DOF	Degree of Freedom
DP	Dynamic Programming
ECMS	Equivalent Consumption Minimization Strategy
EPA	Environmental Protection Agency
EVT	Electrical Variable Transmission
HEV	Hybrid Electric Vehicle
HWFET	Highway Fuel Economy Test
ICE	Internal Combustion Engine
MGU	Motor/Generator Unit
MY	Model Year
PEARS	Power-weighted Efficiency Analysis for Rapid Sizing
PMP	Pontryagin's Minimum Principle
PGs	Planetary Gear set
PHEV	Plug-in Hybrid Electric Vehicle
SERCA	Slope-weighted Energy-based Rapid Control Analysis
SOC	State of Charge
SOH	State of Health
UDDS	Urban Dynamometer Driving Schedule

Abstract

The new challenges of reducing the fuel consumption and the pollutant emissions are leading the transport sector towards a paradigm shift. Among the sustainable alternatives to the carbon fossil dependency the electrification is one of the most appealing solutions. In fact, the technological progress, especially in the power electronic field, is making electrified vehicles increasingly attractive for the mobility scenario. Nevertheless, some know-how limitations, as the ones related with the battery energy density, represent the current obstacle for a massive penetration of the fully Electric Vehicle (EV). Consequently, in the near future the market will likely be dominated by the Hybrid Electric Vehicles (HEVs). In this case, both the internal combustion engine and the electric motors can contribute to the propulsion with a significative efficiency improvement. Among the HEV state of art possible design architectures, the power split HEV are the most interesting for the market. Indeed, they can the exploit the advantages of both parallel and series configurations. These types of transmissions typically use the Planetary Gear sets (PGs) as power split devices to divide the engine power in an electrical and a mechanical path. Current market applications are the transmissions of Toyota Prius 2010, Chevrolet Volt II Generation, Ford Fusion and Chrysler Pacifica. Moreover, the addition of clutches allows to greatly improve the powertrain flexibility enabling multimode operations. Being for this type of HEV the design stage a crucial activity, the aim of the whole project is to create a tool capable to select design and size providing the best compromise solution among fuel economy, emissions and vehicle performances. This thesis deals with the first step of the tool development, which is related to the selection of the best design candidate based on the fuel consumption value fixing as input parameters the component dimensions. For this purpose, the selection of the proper Energy Management Strategy (EMS) is crucial. A design tool, called "Analytical Transmission Design Tool" (ATDT), has already been built in MATLAB, using as EMS the "Power-weighted Efficiency Analysis for Rapid Sizing" (PEARS) algorithm. Since the results produced have been found to be in some cases far from the optimal benchmark, the scope of this dissertation is to find a new and more suitable optimization algorithm for the design analysis. First, the "Slope-weighted Energy-based Rapid Control Analysis" (SERCA) is implemented in the ATDT. Subsequently, after

some consistency analysis, another strategy called SERCA$^+$ is introduced. This algorithm, which represents the main intellectual contribution of this research, is obtained combining the strengths of PEARS and SERCA. Finally, some case studies are presented to confirm the value of the proposed methodology.

Chapter 1: Introduction to HEV

This chapter explains the drive behind this research justifying the creation of the proposed transmission design tool (ATDT). In the first paragraph, the reasons pushing the electrification process of the transportation sector are presented. Subsequently, it is discussed the current HEV state-of-art debating advantages and disadvantages of the possible arrangements. In particular, the benefits of the multimode power split design are underlined. Nowadays, most of the HEVs sold in the market belong to this category due to the usage flexibility which can be further enhanced with the addition of clutches, obtaining a multimode transmission. This category of powertrains is the focus of the overall analysis. Finally, in the last part of the chapter, some examples from existing vehicle applications are presented.

1.1 Automotive Industry: A New Paradigm Shift

The transportation sector, one on the biggest industry in the world, is not sustainable. In fact, the dependence by fossil fuel creates serious limitations both in terms of resources availability and air quality [1]. In United States the interest in reducing the dependency from oil started between 1973 and 1974, with the oil embargo imposed by the OPEC (Organization of Petroleum Countries). As consequence, in 1975, the Congress created the CAFE (Corporate Average Fuel Economy) with the aim of issue standards to regulate the fuel consumption [2]. Over the years, the interest towards the reduction of pollutant emissions and greenhouse gases (GHG), to which the transportation sector greatly contributes, has been increased all over the world. The first European regulations for passenger trucks and light duty application dates to 1992, with the introduction of the EURO 1 standard. The actual regulations decisions are undertaken by the European Parliament and Council, with the knowledge and data provided by the advisory organ, which is the European Environmental Agency (EEA) [3]. In US, instead, the current Harmonized National Program is composed by three legal authorities: NHTSA (National Highway Traffic Safety Administration) which administrates the CAFE standard, EPA (Environmental Protection Agency) which set the maximum pollutants tolerated level and the CARB (California Air Resource Board) which historically focus is related to more stringent standards proposed for California [2]. It is important to underline that there are different regulations for fuel consumption and pollutant emissions. The fuel burnt directly relates to the dioxide carbon (CO_2) emission, the principal GHG gas. The cars, according the European commission, still contributes for around 12% of CO_2 production [4]. Currently, the standards requirements are becoming more severe both in terms of tolerated emissions of GHG and in terms of pollutants, such as CO, NO_x, particulate matters (PM). For example, concerning the CO_2 generation, in EU, for MY 2021 the acceptance threshold will be set at 95 grams per kilometre as average for the fleet [3]. Indeed, in US, the vehicles target for MY 2025 will be 163 grams per mile, equivalent to 101 grams per kilometres [2]. To meet these requirements, the most promising solution is represented by the electrifications which would allow to switch to a new concept of more sustainable transportation. This paradigm shift will be, eventually, completed with a market dominated by EVs. In fact, the electrification has become a promise alterative with the development of the power electronics technologies which allow to get full advantage of both DC and AC systems introduced during the early 1900s by Edison and Tesla [1]. Nevertheless, some limitations particularly related to the batteries know-hows, as power density and cost, result in a transition phase likely dominated by HEVs. These types of vehicles are characterized by higher value of efficiency compared with conventional ones. On the historical side it is interesting to notice that the introduction of the concepts of EV and HEV is not recent. By 1900 the electric cars produced in U.S. were almost the double as number compared to the gasoline ones. As matter of fact, during the first National Automobile Show in New York City, the EV was indicated as the preferred candidate for the mass production. For instance, the first car manufactured by the German pioneer Ferdinand Porsche was the Lohner Electric Chaise (Figure 1.2) [5]. This engineering masterpiece was propelled by two electric motors and a lead battery with an output voltage of 40 V, providing 2.5 horse power [6]. Instead, the second vehicle built by Ferdinand Porsche was hybrid. However, the improvement introduced in the internal combustion engine (ICE) technology by other innovators of the 19^{th} century as Rudolf Diesel, Nikolaus Otto, Karl Benz and James Atkinson creates a large gap between the engine-based propulsion and the electrified one. Starting from 1908, when Henry Ford launched the mass production of the Model T, this discrepancy has been unbridgeable for almost one century up to 1997, once Toyota sold in the Japanese market the first modern hybrid car, the Toyota Prius (Figure 1.3). This date can be identified as the initial point of the paradigm shift which we expect will radically change the concept of transportation in the next decades [1].

Figure 1.1 Cars wait in long lines during the gas shortage. (Library of Congress Prints and Photographs Division, U.S. News & World Report Magazine Photograph Collection, Warren K. Leffler)

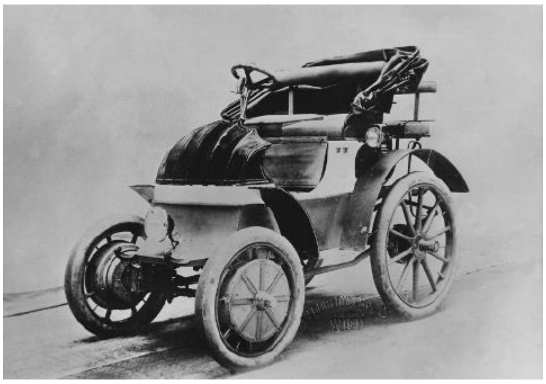

Figure 1.2 Lohner-Porsche-1898

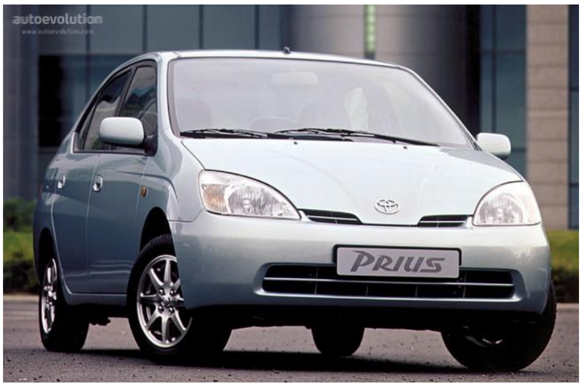

Figure 1.3 Toyota Prius-1997

1.2 Electrification Degree

The HEV represents an intermediate solution between the conventional and the battery electric vehicles (BEVs). A powertrain is defined hybrid if at least two different energy sources are used for the propulsion [7]. HEVs are usually classified according the degree of electrification which defines the ratio between the electric and the total vehicle power. Different electrification degrees result in a different dimensioning of the electrical components, particularly motor generator unit (MGU) and battery. Furthermore, the gain in terms of fuel economy is different. In the literature [1, 8], typically, the powertrains are classified as reported by following according a crescent degree of electrification:

- Start-stop Hybrid: they are usually equipped with a small electric machine which acts as a starter for the ICE avoiding the fuel consumption during the idle periods. The cost associated with the electrification is almost negligible, resulting in a typical improvement of 2-3 % on the fuel economy side. The largest part of the vehicle currently manufactured has this functionality.
- Micro Hybrid: as for the Start-stop hybrid they are characterized by a contained gain in terms of fuel burnt and usually the electrification is not directly related to the propulsion but to the accessories, such as electric pumps or electric activated air conditioning units.
- Mild Hybrid: they usually provide improvement of around 10% in terms of fuel consumption and they are characterized by some important functionalities as the regenerative breaking, which allows to recover the kinetic energy during breaking operation to charge the battery. They might use some electric power for the propulsion and dependently on the electric requirements they can be produced either as high or as low voltage systems. The crescent electric demand generation and the necessity of a starter to crank the thermal machine has led in some cases to the presence of a reversible machine accomplishing both the tasks.
- Full Hybrid: in this case the electric machines directly contribute to the propulsion leading to more evident and remarkable advantages in terms of fuel consumption, typically comprised between 20 and 50%. This benefits amount is strongly connected with the type of powertrain architecture and with the mission.

- Plug-in Hybrid Vehicles (PHEVs): the major difference between HEV and PHEV is related to the dimensions of the battery system. In fact, the PHEV can be directly plugged into the electric grid increasing the advantages in terms of energy price. They represent a very attractive alternative for a use characterized by frequent short distance travels and infrequent long distance journeys.
- Battery Electric Vehicles (BEVs): the vehicle is in this case entirely propelled by electric machines. Consequently, the crucial characteristic is the absence of the ICE. Today's more stringent limitations, obstructing a massive diffusion of these vehicles' category, are related to the limited electric range and in general to the actual battery technologies.

It is evident that an increase in the electrification level allows to get crescent reduction in the amount of fuel burnt. However, it is interesting to acknowledge some researches which have shown that fixing the component dimensions there is some local maxima of the fuel economy as function of the electrification level. This trend is basically related to the possibility of fully exploit the advantages of each powertrain component. Nevertheless, the global minimum of fuel consumption is for the BEV category, with all the limitations of the actual know-how [9]. In general, the most significant benefits of the HEV are related to the improved efficiency and to the quicker acceleration offered by the MGUs. In fact, differently from the ICE, which has usually an averaged efficiency below 30%, they can work with a reduced amount of losses. Nowadays, electric machines used for propulsion applications are either induction motors or permanent magnet machines (PM). The first are simple to build and robust but their efficiency is lower, while the second are characterized by lower losses, higher torque capability and power density. However, the PM motors have limitations related to the speed range and to the cost of the permanent magnets which are rare materials. Important improvements are expected in the next years related to the motor technologies to fully complete the paradigm shift. An interesting solution seems to be represented by the Switched Reluctance machine (SRM). Their cost and robustness, together with the wide speed range, would allow them to be a perfect candidate if new solutions would be introduced to solve issues as the torque ripple and acoustic noise [1, 5].

1.3 Hybrid Powertrain Architectures

1.3.1 Series Powertrains

In a series HEV architecture the ICE is decoupled from the transmission and consequently does not contribute directly to generate the mechanical power flowing through the differential (Figure 1.4). Because of this inherent characteristic, this hybrid topology can be considered as an electric architecture with an on-board device to charge the battery. In fact, the engine is connected to a generator and it is used to avoid charge depletion of the storage unit below a certain threshold. Usually the battery is maintained around a SOC level comprise between 65 and 75%. Since the ICE is not connected to the driving wheels, this arrangement offers the possibility to preserve its working points as close as possible to the Optimum Operating Line (OOL), space of best torque-speed combination for the fuel economy [7]. The series architecture represents the simplest solution for HEV design and different researches have been conducted searching for the optimal control strategy [10, 11]. However, the largest limitation is related to the multiple energy conversions required from mechanical to electrical power with the related losses. Furthermore, the system sizing represents a restriction because the electrical components needs to be chosen big enough to ensure the achievement of the power demand [5]. Due to the discussed limits, together with the simple design and control, the series hybrid powertrain has found applications only in trucks and urban buses [10, 12].

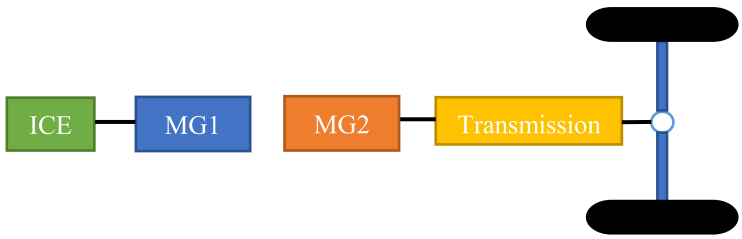

Figure 1.4 Schematic representation of a series architecture

1.3.2 Parallel Powertrains

In the parallel powertrain architecture both ICE and MGU contribute directly to the propulsion. Indeed, the name parallel derives from the fact that the electrical and the mechanical power sum up together. Contrarily to the series arrangement there is no need for two electric machines. The system efficiency is also higher since less energy conversions are required. Furthermore, both ICE and MGU can be downsized obtaining the same performances of the series counterpart, up to the point in which the battery is fully discharged [5]. The higher flexibility in operations is associated also with the variety of possible arrangements. Usually the parallel architectures are categorized in 4 groups, from P1 to P4 as reported in Figure 1.5. In the P1 configuration the electric machine is placed before the engine. The principal advantages are related to the integrated function of the MGU which starts the engine and power the accessories. The energy recovered in braking operations is usually contained and generally this architecture has been used in market applications with a contained electrification level. A more effective contribution from the electric side, both in propulsion and recovering operations, is obtained with the P2 arrangement, where the MGU is placed after the ICE. Alternatively, in the P3 architecture the electric machine is directly coupled to the differential and mounted after the transmission. In all these configurations ICE and MGU torque are coupled before the differential. Instead, in the P4 arrangement each propulsion unit is mounted on a different axle, generating an architecture known as trough-the-road. The most important benefit of this choice regards the All-Wheel Drive (AWD) design [13]. As for all the different hybrid categories, to fully exploit the advantages offered by the parallel powertrains the adopted control strategies is fundamental. Usually at low speed only the electric motor is used, while at higher speeds the ICE is turned on regulating the power flow towards battery and output to reach the best efficiency [7]. Different studies have been conducted in this direction searching for the best control algorithm [14, 15]. In the market, currently, it is possible to find many examples of vehicles with a parallel architecture as the Honda Civic Hybrid, the BMW Active Hybrid (model 3 and 5), Chevrolet Impala Hybrid, Audi Q5 Hybrid and Porsche Cayenne S Hybrid [13].

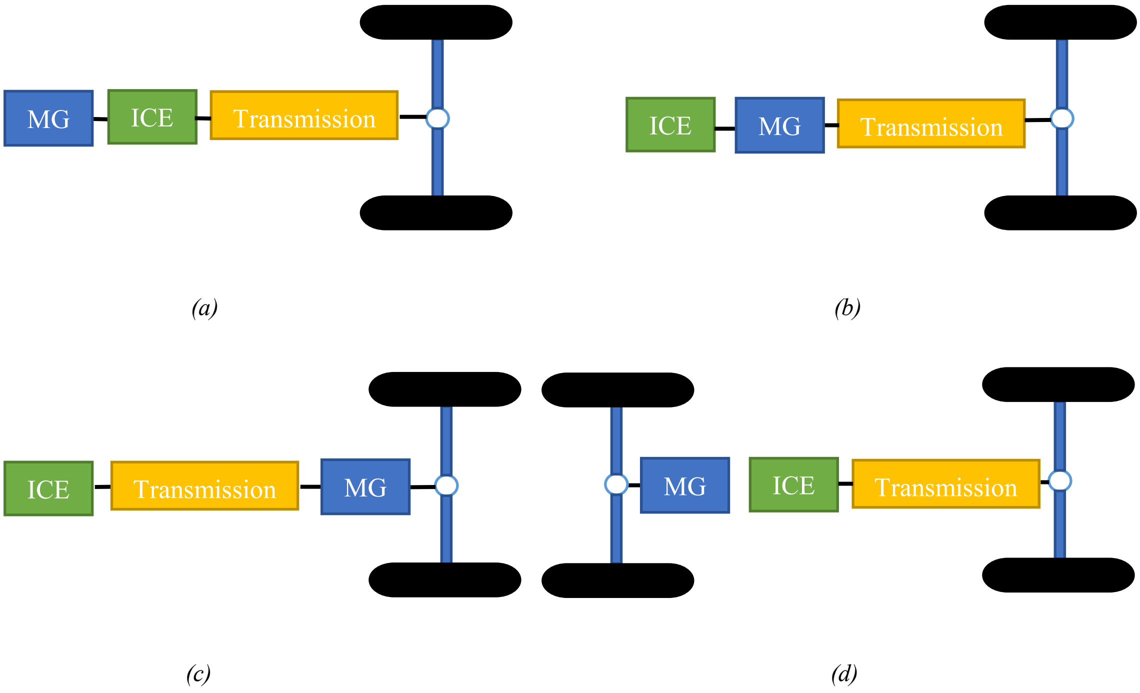

Figure 1.5 Schematic representation of parallel architectures, (a) P1, (b) P2, (c) P3, (d) P4

1.3.3 Series-Parallel Powertrains

The series-parallel architecture offers the advantages of both series and parallel configurations with an increase in the powertrain complexity and cost. A mechanical link, as a clutch, is used to switch between different operating modes. As for the series arrangement two MGUs are present, one acting typically as generator and starter and the other as electric motor [5, 7]. The series-parallel powertrain can be found in some market applications as Hyundai Sonata Hybrid, Kia Optima Hybrid and Honda Accord Hybrid [13].

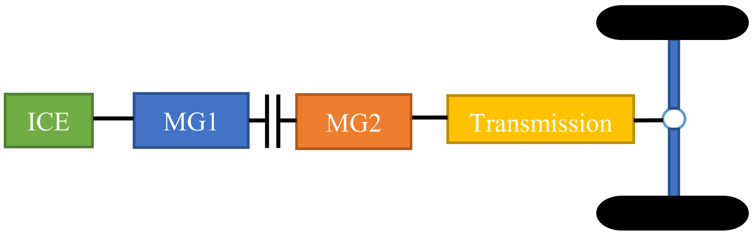

Figure 1.6 Schematic representation of series-parallel architecture

1.3.4 Power split Powertrains

Power split powertrains architectures use devices as Planetary Gear sets (PGs) to realize the power split function. The device decouples the engine from the output shaft and divides its power in two different paths, one electric and one mechanical. Thus, the ICE torque and speed can be controlled through the continuous variable transmission (CVT) such that the operating point are distributed in more favourable zones in terms of fuel consumption and pollutants emission [16]. Since the ICE is controlled using the electric machines this type of transmission is known as electrical continuously variable transmission (e-CVT) [17]. The first power split vehicle, the Toyota Prius I generation, has been introduced in the Japanese market by Toyota in 1997. This transmission is also known as Toyota Hybrid System (THS). As shown in Figure 1.7, the engine is connected to the planetary carrier, the electric machine generally working as generator is attached to the sun gear and the other MGU is coupled first to the ring gear and then to a reduction gear [13].

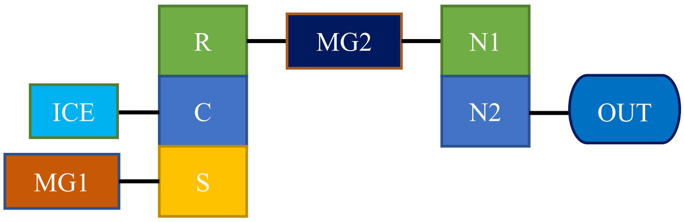

Figure 1.7 Schematic representation of the Toyota Prius I generation (THS) transmission

Starting with the II generation of the Prius, manufactured between 2004 and 2009 and subsequently with the III generation, appeared for the first time in 2010, the THS has been renamed Hybrid Synergy Drive (HSD) in a patent granted also to Nissan and Ford. In addition to the improvement related to the powertrain components the main differences introduced with the HSD are the addition of a second PGs and the removal of the chain connected to the final drive [13, 18, 19].

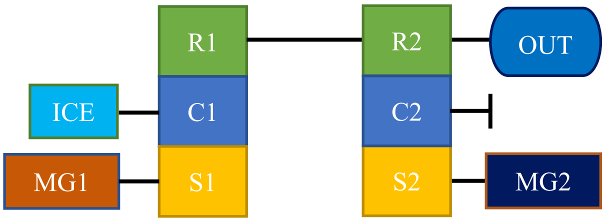

Figure 1.8 Schematic representation of the Hybrid Synergy Drive (HSD) transmission

Depending on the position of the powertrain components, the power split architectures are classified in input-split, output-split and compound split. In the input-split powertrain one of the two electric machine is collocated with the output shaft while the other MGU is neither directly connected to the engine, nor to the output. Contrarily, for the output-split design one electric machine is collocated with engine. Moreover, using at least two PGs it is possible to realize the so-called compound split architecture with the two MGUs both decoupled from engine and output shaft [17, 20]. Historically, due to the advantages connected with the power split functionality, this type of hybrids vehicles has been the most diffused world-wide. In 2017 the best seller of the HEV categories was the Toyota Prius with 210.000 units sold (31% in U.S. and 7.8% in Europe), followed by the Toyota C-HR crossover and the Prius C, respectively with 190.000 and 149.000 sales units [21]. All these models are equipped with the e-CVT transmission. Other examples of vehicles which have adopted the power split architecture are Toyota Camry Hybrid, Ford Fusion Hybrid, Ford C-Max Hybrid, Ford Escape Hybrid and Lincoln MKZ Hybrid. In some SUVs applications, as Toyota Highlander and Lexus RX450h, a third electric machine has been added to the rear axle to exploit the benefits of the AWD configuration. In other models, instead, as Lexus GS450h and Lexus LS600 the second PGs has been substituted with a Ravigneaux gear [13].

1.3.5 Multimode Powertrains

The addition of clutches on the power split powertrains improves greatly the transmission flexibility, allowing to switch between different operating modes. One of the first multimode power split powertrain has been introduced by General Motors which patented the Allison two-mode hybrid system (Figure 1.9) in 2005 [22].

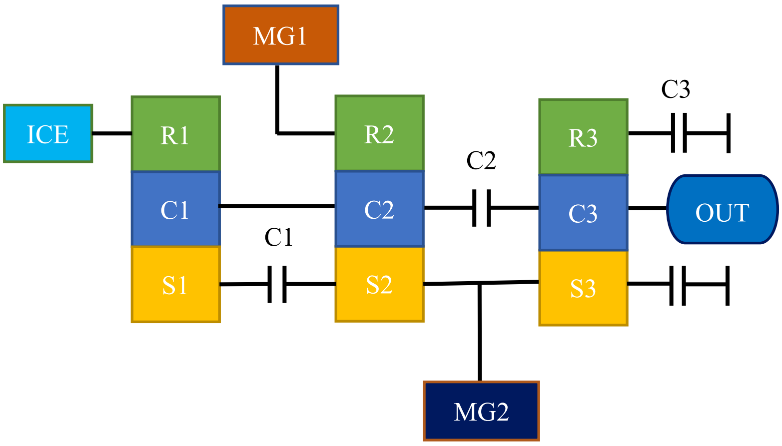

Figure 1.9 Schematic representation of the GM Allison two-modes transmission

The transmission of the Allison can achieve with its three PGs two continuous variable transmission modes and four fixed-gear ratio modes. The first CVT mode is the input-split, achieved engaging the clutch C3. This mode is usually selected for low vehicle speeds and it is interesting to note that to control the engine operations, MG1 is used as speed coupler while MG2 is designed to fulfill the torque coupling function. Differently, the second CVT mode, the compound split, is realized engaging the clutch C1. This mode is the preferred for highest output request in terms of torque and speed. Furthermore, the compound-split mode allows to reduce the torque and speed demand to the electric machines, allowing to decrease the system dimensions and consequently the cost. Both the two CVT modes allow to cover a wide range in terms of torque and speed maintaining the ICE operating points in the best region for the fuel consumption. Apart from these two modes, the Allison transmission can realize four fixed gear ratio modes engaging at least two connections. The 1st fixed gear ratio is realized engaging the clutches C3 and C2 and it is typically used, when at low speed, there is a transition to higher torque demand. In fact, when the speed is low, the mode usually preferred is the input-split, while the transition from this last to the 1st fixed gear ratio only requires the engagement of the clutch C2. The 2nd fixed gear ratio, typically, completes the transition process towards the compound split mode. Thus, these first two fixed gear ratio modes can be interpreted as auxiliary modes allowing a smooth transition between the two CVT arrangements. The 3rd fixed gear ratio mode is reached engaging both clutches, C1 and C2, locking together the three PG sets and in a 1:1 ratio between input and output. Finally, the 4th fixed gear mode is selected at high speed, engaging the clutches C1 and C4, while the engine propels the vehicle. The operative modes of the GM-Allison are summarized by following in the Table 1.1 [13, 23].

	C1	C2	C3	C4
Input-split			o	
Compound-split	o			
1st Fixed gear		o	o	
2nd Fixed gear	o		o	
3rd Fixed gear	o	o		
4th Fixed gear	o			o

Table 1.1 Operative modes of the GM two-modes Allison transmission

Another example of multimode e-CVT application is the 1st Generation of the GM Chevrolet Volt, appeared for the first time in the market in the last part of 2010. The Volt is a PHEV and differently from the THS has an output-split configuration. Its powertrain, named 4ET50, is below represented in the Figure 1.10, while the four possible operative modes are reported in the Table 1.2. The first two modes are purely electric, with the possibility of use either one or both MGUs. Engaging the Clutch C1 the vehicle is propelled only by the MG2, while engaging the clutch C2 the two MGUs are involved in the propulsion. Instead, the two HEV modes are a series and an output mode. The first is achieved closing both the clutches C1 and C3, while the second is accomplished with the clutches C2 and C3. Clearly the strategy for the battery management is different for the two modes types being the storage unit depleted by the electric modes and maintained around a stable value in Charge Sustaining (CS) operations, when hybrid modes are selected. Some analysis referred to the first generation of Chevrolet Volt have highlighted the improved fuel economy and the reduced number of components required in comparison with a series transmission [24, 25].

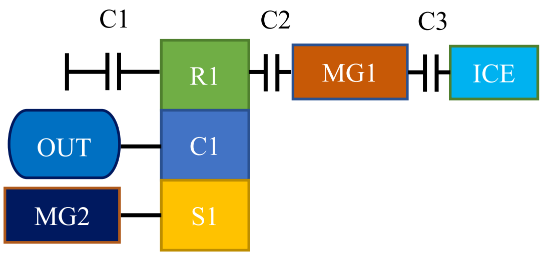

Figure 1.10 Schematic representation of the GM Chevrolet Volt I generation

	C1	C2	C3
EV (MG2 only)	o		
EV (2 MGUs)		o	
Series	o		o
Output-split		o	o

Table 1.2 Operative modes of the GM Chevrolet Volt I generation

During February 2015, at the SAE vehicle electrification conference, in Los Angeles, GM presented the II generation of the Chevrolet Volt. Differently from its predecessor, the Volt MY 2016 CVT transmission, defined an engineering work of art, is equipped by two PGs and three clutches (Figure 1.11). The motor has been downsized and improved while the performance has been enhanced allowing to reach in 2.6 seconds the speed of 30 mph starting from still. The total number of achievable modes for the II generation of Volt is five, with two charge depleting modes and three charge sustaining ones (Table 1.3). The first EV mode is achieved engaging the clutch C2. In this case the vehicle is propelled only by one MGU, while the CVT works as a reduction gear. To achieve the second EV mode, for which both the MGUs contribute to the propulsion the clutch C3 is loaded. C3 is a clutch of the one-way type preventing the ICE from spinning backwards. Maintaining close the clutch C2 and opening simultaneously the clutches C1 and C3, the low extended range (ER) HEV mode is realized. In this condition, the engine power is divided among the output and MGA, which acts as starter. Referring to the fixed ratio extended mode it is realized engaging all the clutches. The MGA is consequently turned off while the engine power is fully used through its fixed connection with the output. The second electric machine, MGB, might be used either for giving extra boost, or to charge the battery with the scope of maintaining the engine as close as possible to its OOL. Finally, engaging only the clutch C1 the high extended range mode is realized. This mode allows to reach a higher gear ratio still allowing the effective control of the engine working points [26].

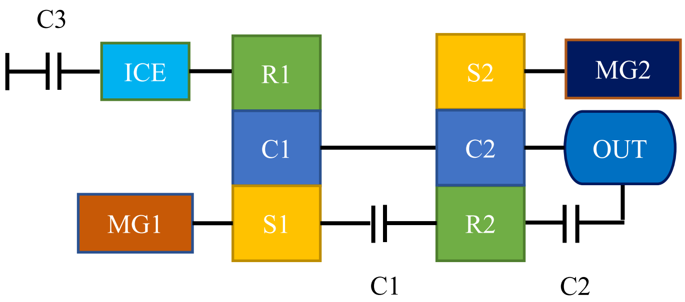

Figure 1.11 Schematic representation of the Chevrolet Volt II generation

	C1	C2	C3
EV (MG2)		o	
EV (2 MGUs)		o	o
Low ER		o	
Fixed ratio ER	o	o	
High ER	o		

Table 1.3 Operative modes of the GM Chevrolet Volt II generation

Another case, coming from the actual market application is the one of the Chrysler Pacifica Hybrid MY 2017. The transmission of this minivan identified either as ‘e-flite’ or as ‘Si-EVT’ is equipped with two PGs and a clutch enabling two operative modes (Figure 1.12). The first is a charge depleting electric mode, achieved engaging the clutch C1. In this arrangement either both the MGUs, or only the large machine, can power the vehicle. Alternatively, during deceleration phases, this mode is the one preferred due to the regenerative opportunities. Instead, disengaging the clutch, the charge depleting input-split hybrid mode is realized. Thus, the engine power is used to directly propel the vehicle or alternatively to spin up the generator [27, 28].

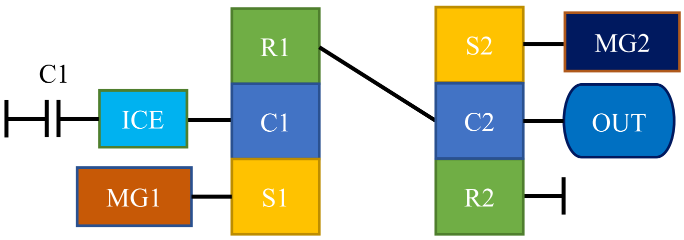

Figure 1.12 Schematic representation of the Chrysler Pacifica

	C1
EV (2 MGUs)	o
Input-split	

Table 1.4 Operative modes Chrysler Pacifica

Chapter 2: Design Tool structure

The focus of this chapter is to present the vehicle model implemented in the proposed design tool (ATDT) and its logical structure. First, the model of the road load and of the powertrain components are presented. Subsequently, the expressions of the nodes torque and speed are derived both for transmissions with single and double PGs arrangement. To manage the large dimensions of the candidate pool, an automatic state space model is introduced with the related criteria and rules. Furthermore, the reasons behind the choices and the hypothesis adopted are explained. Finally, it is discussed the method implemented to generate the design topologies though the combination of the operative modes.

2.1 Road load Model

The road load is modelled as sum of three main contributions: the rolling resistance F_{roll}, the air drag resistance F_{air} and the gravity resistance F_{grade} acting when a road slope is present (Equation 2.1).

$$F_{road} = F_{roll} + F_{air} + F_{grade} \tag{2.1}$$

The three components are reported in the following equation, where m_v is the vehicle mass, μ is the rolling resistance coefficient, g is the acceleration of gravity, ρ is the air density, A_f is the vehicle frontal area, C_d is the drag resistance coefficient, v is the vehicle linear speed and α is the road slope angle.

$$F_{roll} = \mu\, m_v\, g \tag{2.2}$$

$$F_{air} = \frac{\rho\, A_f C_d v^2}{2} \tag{2.3}$$

$$F_{grade} = m_v\, g\, \sin(\alpha) \tag{2.4}$$

It should be underlined that in this research the road slope angle is not considered. Furthermore, clearly, in the real case, also other resistance forces, as the side ones, are present. The overall resistance contribution is modelled with the coast-down coefficients, R_{LA}, R_{LB}, R_{LC} (Equation 2.5).

$$F_{road} = R_{LA} + R_{LB}v + R_{LC}v^2 \tag{2.5}$$

For details about the experimental procedures followed to detect these quantities it is possible to refer to Karlsson [29]. Finally, the resistance load torque can be computed as stated in the Equation 2.6, where r_{dyn} is the wheel dynamic radius, I_v is the vehicle inertia, a is the driving cycle acceleration and K is the final drive ratio [30].

$$T_{load} = \frac{F_{road}r_{dyn} + \dfrac{I_v\, a}{r_{dyn}}}{K} \tag{2.6}$$

To compute the instantaneous value of the acceleration, continuous derivative of the velocity imposed by the driving cycle, the forward difference approximation is used, as reported in the Equation 2.7, where v is the instantaneous velocity and Δt is the time interval.

$$a(i) = \frac{v(i+1) - v(i)}{\Delta t\ K} \tag{2.7}$$

The parameters used to obtain the results presented in this dissertation are summarized in Table 2.1.

Parameter	Unit	Value
$\boldsymbol{m_v}$	kg	2248
$\boldsymbol{R_{LA}}$	lb	35.530
$\boldsymbol{R_{LB}}$	lb/mph	0.327
$\boldsymbol{R_{LC}}$	lb/mph^2	0.023
$\boldsymbol{r_{dyn}}$	m	0.358
$\boldsymbol{I_v}$	$kg\ m^2$	309.598

Table 2.1 Vehicle parameters used for the simulation

2.2 Powertrain components model

In this paragraph we present the model implemented for the four principal powertrain components: the MGUs, the ICE and the battery. In the current version of the tool the size of the machines is an input-data and consequently, they are not subjected to any optimization procedure. However, it is important to underline that a future objective is to implement a strategy capable to select the best candidates also on different range of components dimensions. Clearly, these initial data together with the geometrical sizes of the PGs have a strong impact on the final solution. Regarding the research presented in this thesis, both the ICE and MGUs data are implemented as experimentally derived look-up tables. In fact, this choice allows the use of a matrix approach with great advantages in terms of computational speed. The map used to model the ICE to obtain the results presented in this thesis is reported in Figure 2.1. The amount of fuel injected is measured as function of the ICE torque and speed. Furthermore, the map can be eventually manipulated to easily obtain the efficiency values, whenever required by the control strategy, as for the case of the PEARS algorithm. The efficiency is obtained through the Equation 2.8, where T and ω are the engine torque and angular speed, $\dot{m_{fuel}}$ is the injected fuel flow rate and LHV is the fuel lower heating value.

$$\eta_{ENG_i} = \frac{P_{OUT_i}}{P_{IN_i}} = \frac{T_i\ \omega_i}{\dot{m_{fuel_i}} LHV_i} \tag{2.8}$$

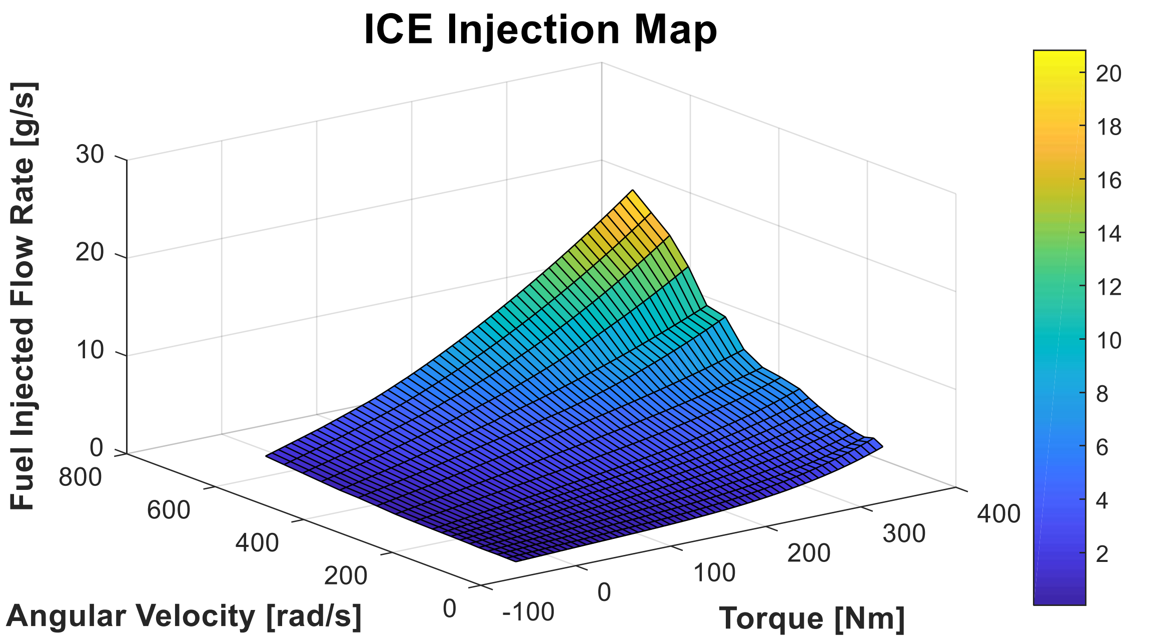

Figure 2.1 ICE fuel injected map

Instead, for the MGUs, an example of map is reported in Figure 2.2. As can be observed, the losses, mainly related to mechanical dissipation and electro-magnetic phenomena, are again measured as function of the machine torque and speed. As for the ICE, also in this case the data can be easily rearranged to derive the efficiency map (Equation 2.9).

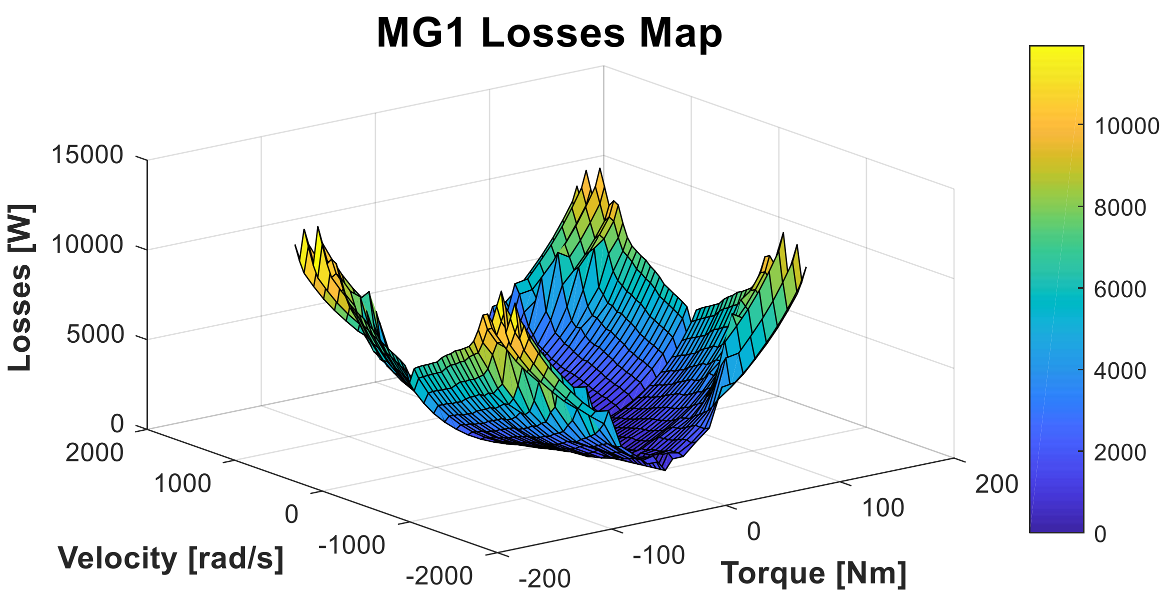

Figure 2.2 MGU losses map

$$\eta_{MGU_i} = \frac{P_{OUT\,i}}{P_{IN\,i}} = \frac{T_i\ \omega_i}{T_i\ \omega_i + P_{loss_i}} \tag{2.9}$$

To model the battery a simple equivalent circuit model is adopted (Figure 2.3). In fact, as for the other powertrain components, at this stage of the design process is required a model providing fast results with a good level of approximation. The choice is the same made by other researchers in the field of the powertrain design [31]. Both the battery internal resistance and the open circuit voltage are function of the State of Charge (SOC), temperature and State of Health (SOH). As described in the following equations, the current flowing in the battery I_b (Equation 2.12) can be easily computed passing though the determination of terminal voltage U_0 (Equation 2.10) and battery power P_{BATT} (Equation 2.11).

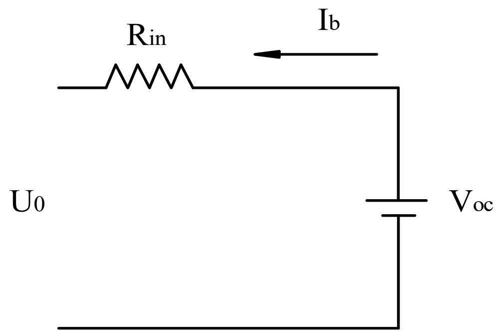

Figure 2.3 Battery Equivalent Circuit

$$U_0 = V_{OC} - R_{in} I_b \tag{2.10}$$

$$P_{BATT} = U_0 b = V_{OC} I_L - R_{in} I_b^2 \tag{2.11}$$

$$I_b = \frac{V_{OC} - \sqrt{V_{OC}^2 - 4 R_{in} P_{BATT}}}{2\ R_{in}} \tag{2.12}$$

Similarly to the previous modelled components, it is useful to derive the relation describing the battery efficiency. This last has different expressions depending on the operative conditions of charging and discharging (Equations 2.13 and 2.14).

$$\eta_{batt_{charg}} = \frac{V_{OC}\, I_b}{P_{BATT}} = \frac{V_{OC}\, I_b}{V_{OC} I_L - R_{in} I_b^2} \tag{2.13}$$

$$\eta_{batt_{discharg}} = \frac{P_{BATT}}{V_{OC}\, I_b} = \frac{V_{OC} I_L - R_{in} I_b^2}{V_{OC}\, I_b} \tag{2.14}$$

Despite the dependencies previously discussed, in this dissertation to obtain the battery efficiency and parameters, we consider the open circuit voltage and the internal resistance as constant parameters regarding temperature, SOC and SOH. In fact, all the candidates are tested considering the same conditions of battery wear and an average usage temperature of 30°. Furthermore, the dependency by the SOC can be neglected without strongly compromising the results since a Charge Sustaining (CS) strategy is implemented for the battery management system. Finally, the assumption is even justified by the independency of the battery parameters from the output request in terms of torque and speed. Consequently, to perform our analysis, we use values averaged over the experimental results (Table 2.2).

Parameter	Unit	Value
$\boldsymbol{V_{OC}}$	V	355
$\boldsymbol{R_{in_{charging}}}$	Ω	0.1158
$\boldsymbol{R_{in_{discharging}}}$	Ω	0.2390

Table 2.2 Battery average parameters

Under this hypothesis the battery efficiency can be represented as only function of the battery power P_{batt}, which is positive or negative depending respectively on the discharging or charging conditions (Figure 2.4).

To conclude this paragraph dedicated to the model of the components, in the Table 2.3 the more relevant powertrain parameters are resumed. They are representative of a typical mini-van application. We have chosen to use this data which were the most complete set available during the simulation activity. However, the implementation of a specific market vehicle powertrain is beyond the purpose of this research. In fact, once the tool is proven to provide good quality results in terms of topology evaluation the components input data can be easily modified.

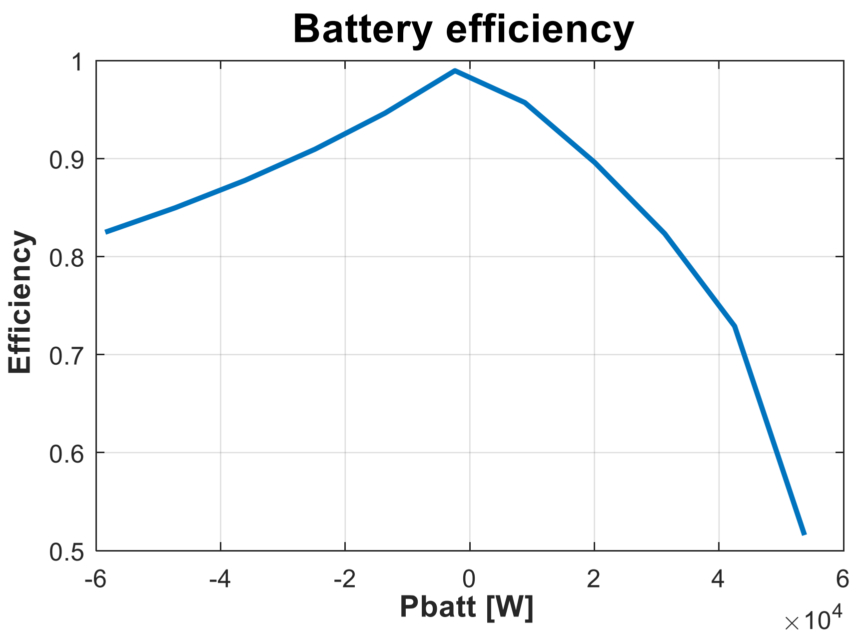

Figure 2.4 Battery Efficiency plot

Components	Parameters	Value
ICE	$Capacity$	3.6 L
	P_{max}	188 kW @5800 rpm
	T_{max}	320 Nm @4400 rpm
	LHV	43700 J/g
	ρ_{fuel}	737 g/l
MG1	P_{max}	60 kW
	T_{max}	123 Nm
	n_{max}	14500 rpm
MG2	P_{max}	85kW
	T_{max}	317 Nm
	n_{max}	14500 rpm

BATTERY	$P_{dischar g_{max}}$	59 kW
	$P_{char g_{max}}$	107 kW
	V_{max}	402 V
	I_{max}	300 A
	$Energy_{max}$	64.26 MJ

Table 2.3 Powertrain components main parameters

2.3 PGs Manual Model

The PG device, core element of the studied transmission, is a two DOF dynamic system. Its ring, carrier and sun node's accelerations and speeds are subjected to the kinematic constraint:

$$\omega_s r_s + \omega_r r_r = \omega_c (r_r + r_s) \tag{2.15}$$

To easily derive the torque and speed relations of this mechanical device it is common to use the Benford lever analogy. This approach is particularly beneficial when compound PGs are used [32].

Regarding the power split device dynamic, as matter of example, the free body diagram of one of the most popular market applications, the Toyota Prius MY 2004 (THS) is reported below in Figure 2.6 followed by the node's dynamic equations. $I_{MG1}, I_{MG2}, I_{ICE}, I_S, I_R, I_C$ are respectively the inertia of the MGUs, ICE, sun, ring and carrier, T_f is the conventional braking torque, F is the node force, while S and R are the sun and ring radii. It should be observed that to perform a fast design analysis the pinion inertia is considered negligible [31].

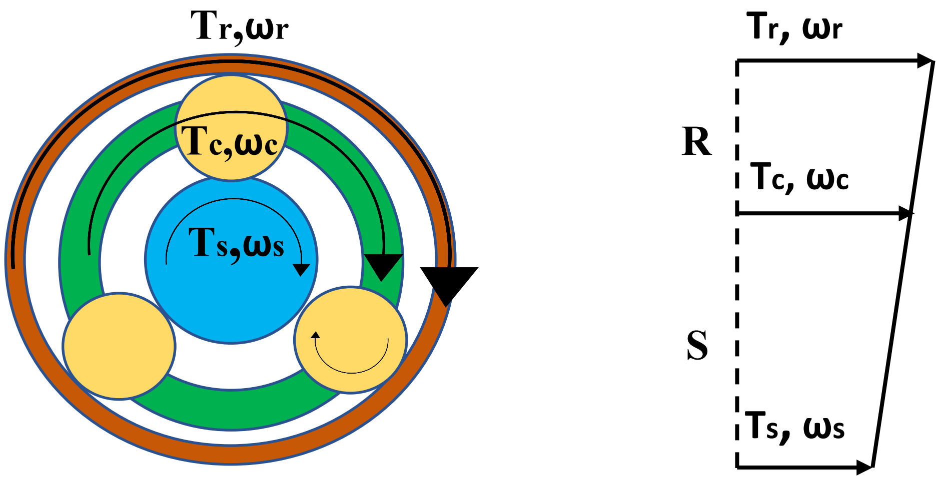

Figure 2.5 Planetary Gear set and lever diagram

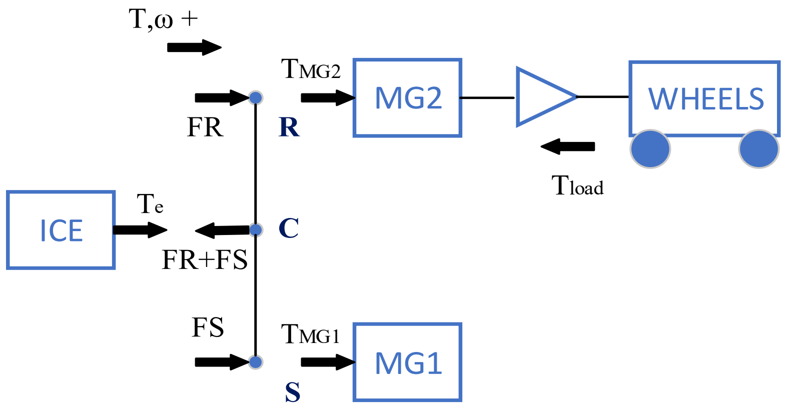

Figure 2.6 Free body diagram Toyota Prius MY 2004

$$\dot{\omega_{MG1}}(I_{MG1} + I_S) = FS - T_{MG1} \tag{2.16}$$

$$\dot{\omega_E}(I_E + I_C) = T_E - FS - FR \tag{2.17}$$

$$\dot{\omega_r}\left(\frac{R_{tire}^2}{K} m_v + I_{MG2}K + I_r K\right) = (T_{MG2} + FR)K - T_f - \mu m_v g R_{tire} - \frac{\rho\, A_f C_d \left(\frac{\omega_r}{K}\right)^2 R_{tire}^3}{2} \tag{2.18}$$

This system of equations can be conveniently reported in matrix form (Equation 2.19).

$$\begin{bmatrix} I_S + I_{MG1} & 0 & 0 & -S \\ 0 & I_C + I_E & 0 & R+S \\ 0 & 0 & \frac{R_{tire}^2}{K} m_v + I_{MG2}K + I_r K & -KR \\ S & -(R+S) & R & 0 \end{bmatrix} \begin{bmatrix} \dot{\omega}_{MG1} \\ \dot{\omega}_E \\ \dot{\omega}_r \\ F \end{bmatrix} = \begin{bmatrix} T_{MG1} \\ T_E \\ (T_{MG2} + FR)K - T_f - \mu m_v g R_{tire} - \frac{\rho \, A_f C_d \left(\frac{\omega_r}{K}\right)^2 R_{tire}^3}{2} \\ 0 \end{bmatrix} \tag{2.19}$$

Despite the great diffusion of the first model of the Prius, nowadays, the market is focusing on powertrains characterized by multiple power split devices, which allow to fully exploit the advantages of the transmissions. As a matter of fact, Zhuang et al have made some comparative analysis among the triple and the double PGs solutions. They have demonstrated how increasing the number of power-split devices up to three permits to obtain some qualitative advantages both in terms of efficiency and performances. However, the quantitative study has underlined only considerable benefits on the acceleration side. Consequently, considering the higher cost of the transmission the three PGs solution is suggested only for the case of heavy-duty applications [33]. For this reason, in this dissertation, we focus on powertrain equipped with a double PGs arrangement. Consequently, as matter of example, by following it is proposed the free body diagram of another diffused market application characterized by a double power split device powertrain, the Toyota Prius MY 2010 [34]. The system of equations describing the nodes dynamic is opportunely directly reported in matrix form. This compact arrangement is crucial in understanding the automatic model rules derivation.

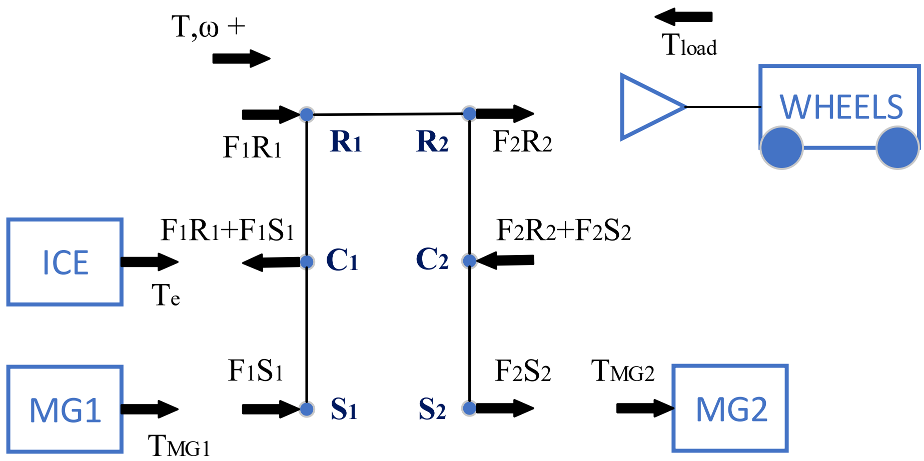

Figure 2.7 Free body diagram Toyota Prius MY 2010

$$A_o \dot{\Omega}_o = T_o$$

$$A_o = \begin{bmatrix} I_{OUT}+I_{R2} & 0 & 0 & 0 & 0 & 0 & 0 & -R_2 \\ 0 & I_{C1}+I_E & 0 & 0 & 0 & 0 & R_1+S_1 & 0 \\ 0 & 0 & I_{MG1}+I_{S1} & 0 & 0 & 0 & -S_1 & 0 \\ 0 & 0 & 0 & I_{MG2}+I_{S2} & 0 & 0 & 0 & -S_2 \\ 0 & 0 & 0 & 0 & I_{R1} & 0 & -R_1 & 0 \\ 0 & 0 & 0 & 0 & 0 & I_{C2} & 0 & R_2+S_2 \\ 0 & R_1+S_1 & -S_1 & 0 & -R_1 & 0 & 0 & 0 \\ -R_2 & 0 & 0 & -S_2 & 0 & R_2+S_2 & 0 & 0 \end{bmatrix} \quad (2.20)$$

$$\dot{\Omega}_o = [\dot{\omega}_{OUT} \quad \dot{\omega}_{ENG} \quad \dot{\omega}_{MG1} \quad \dot{\omega}_{MG2} \quad \dot{\omega}_{R1} \quad \dot{\omega}_{C2} \quad F_1 \quad F_2]^T$$

$$T_o = [T_{LOAD} \quad T_E \quad T_{MG1} \quad T_{MG2} \quad 0 \quad 0 \quad 0 \quad 0]^T$$

2.4 Number of design candidates

Being the purpose of this study to effectively evaluate a large number of design candidates, it is obviously impossible to manually derive all the equations for each case. Consequently, an automatic model is indispensable.

Previously, it is necessary to define the technical vocabulary adopted along the whole thesis. We refer to the term configuration to identify a specific position of the powertrain components (ICE, MG1, MG2 and Output). Instead, the word topology, identifies a configuration with defined clutches and permanent connections location. In other words, each topology represents a design candidate. For a double PGs, the number of unique configurations is obtained considering the combinations of the four powertrain components over the six PGs nodes ($P_{6,4} = 360$). Nevertheless, both having three powertrain components or two electric machines on the same PGs would reduce the design flexibility. Consequently, under these assumptions, the design space design space is reduced first to 216 ($C_{2,4}\, P_{2,3} P_{2,3} = 216$) and finally to 144 candidates ($C_{1,2}\, C_{1,2}\, P_{2,3} P_{2,3} = 144$) [35]. Previously P and C are used to distinguish the combinations whenever is important or indifferent the elements order ($P_{k,n} = \frac{n!}{(n-k)!}$, $C_{k,n} = \frac{n!}{k!\,(n-k)!}$). As already stated in the initial part of the dissertation, adding clutches allow to reach multimode operations. For a double PGs arrangement, the total number of DOF is equal to four. Consequently, to be the vehicle drivable maximum three clutches can be simultaneously engaged. In fact, this choice allows to preserve the DOF related to the differential in output. For this reason, in this research activity, we decide to investigate transmissions with maximum three clutches. In fact, adding more clutches would even enhance the usage flexibility by increasing the number of possible modes but at the same time it would lead to higher powertrain complexity which in turns decreases its reliability. Furthermore, the II generation of the Chevrolet Volt is equipped with three clutches, which ensures the feasibility of the choice. For the studied arrangements the total maximum number of clutches is sixteen (Figure 2.8). This quantity can be derived with the relation reported in the Equation 2.21.

$$N_{clutches} = C_2^{3n} + (3n - 1) - 2n \tag{2.21}$$

In the previous expression n represents the number of power split devices and C stays for the number of clutches. The first part of the relation is referred to the number of possible clutches among the PGs nodes, while the second term adds the ground clutches for the six nodes, except for the output. Finally, in the last part the redundant clutches are removed. In fact, locking two nodes sticks the whole device to behave as rigid body.

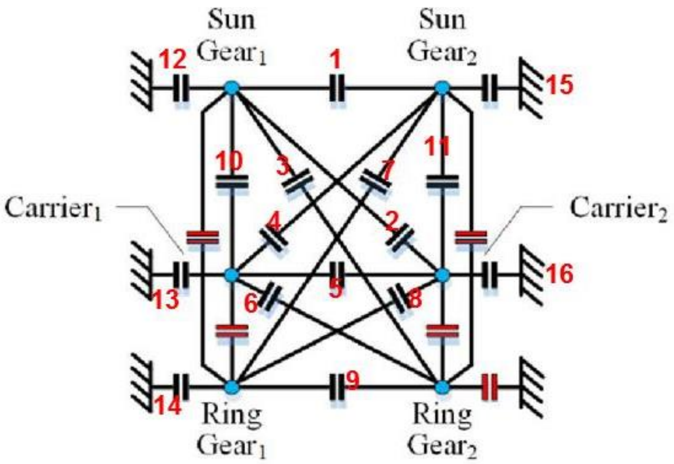

Figure 2.8 Possible clutches for a double PGs arrangement

2.5 PGs Automatic Model

To screen all the possible transmission candidates an automated dynamic model of the PGs has been developed by Lui, Zhang et al. [34, 35, 36]. Alternatively, another model is present in literature and has been derived by Bayrak using the bond graph technique [37]. However, in this study the dynamic approach is adopted since “using the graph theory as auto-generation is more complex as all the unique mode graph have to be drawn before composing a multi-mode design” [38]. The adopted state space model has been formulated extrapolating some general rules from the system dynamic equations of the possible design candidates. As first, it is crucial to recognize that the dynamic relations can be always rearranged in a matrix form, according a structure analogous to the one reported in the Equation 2.22. This consideration is general and independent by the number of power split devices.

$$A_o\dot{\Omega}_o = \begin{bmatrix} J & D \\ D^T & 0 \end{bmatrix} \begin{bmatrix} \dot{\Omega} \\ F \end{bmatrix} = \begin{bmatrix} T \\ 0 \end{bmatrix} = T_o \tag{2.22}$$

1-Initialize the matrix A_0

The matrix A_0 constitutes the dynamic link between the generalized acceleration vector $\dot{\Omega}_o$ and the component torque T_o. For the case of a double PGs device, it is an 8x8 matrix formed by four recognisable parts.

J is a *6x6* diagonal matrix containing the inertia properties. The first four elements refer respectively to the sum of the inertia of vehicle, ICE, MG1, MG2 and the respective epicyclic gears to which they are connected. Instead, the last two entries are filled with the inertia of the PG nodes which are not linked with any of the powertrain component.

D is a *6x2* matrix representing the different connections among the four powertrain components and the PGs nodes. Each column identifies a single power split device. The coefficient entering the matrix are:

- $-r_s$ if the component is connected to the sun gear;
- $-r_r$ if the component is connected to the ring gear;
- $r_s + r_r$ if the component is connected to the carrier;

2-Transform matrix definition

Two auxiliary transformation matrixes are introduced to describe the clutch state.

M is an *8x8* identity matrix. When two nodes j and k are connected, with $j < k$ we apply the relations reported at the Equations 2.23 and 2.24.

$$A_o\dot{\Omega}_o = \begin{bmatrix} J & D \\ D^T & 0 \end{bmatrix} \begin{bmatrix} \dot{\Omega} \\ F \end{bmatrix} = \begin{bmatrix} T \\ 0 \end{bmatrix} = T_o \tag{2.23}$$

$$\begin{gathered} j^{th}row = j^{th}row + k^{th}row \\ k^{th}row = [\,] \end{gathered} \tag{2.24}$$

The final dimensions of the *M* matrix are *(8-n) x8,* where *n* is the number of clutches simultaneously engaged. Being 3 the number of controllable powertrain components, to have a feasible solution, which means a drivable vehicle, *n* should be a number between 1 and 3.

The matrix *P* is built following a similar logic. The difference is that in this case only the row deletion process of the Equation 2.24 is performed.

3-Formulation of the system dynamic equation

The transitions matrixes, defined at the previous step, are used to derive the updated powertrain dynamic matrixes after the definition of the clutch status.

$$A = MA_oM^T \qquad T = MT_o \qquad \dot{\Omega} = P\dot{\Omega}_o \qquad A\dot{\Omega} = T \tag{2.25}$$

4-Build the A^* matrix

To obtain the state space model correlating the input torque signals to the output state acceleration the matrix A should be inverted. Even if not every part of the inverse of A is useful, the procedure adopted always ensure the invertibility of the A matrix. Therefore, after the inversion, it follows an elimination procedure which can be basically divided in two different cases. In fact, if considering the clutch status there is no component collocation the rows not connected with any powertrain component are deleted. On the other hand, if there is component collocation, the rows referred to the collocated components are duplicated, while, once again, the ones not carrying any link are removed. This step ends up with a state space model in the form reported below (Equation 2.26).

$$\begin{bmatrix} \dot{\omega}_{out} \\ \dot{\omega}_{ICE} \\ \dot{\omega}_{MG1} \\ \dot{\omega}_{MG2} \end{bmatrix} = A^* \begin{bmatrix} T_{load} \\ T_{ICE} \\ T_{MG1} \\ T_{MG2} \end{bmatrix} \tag{2.26}$$

5-Refinement of the A^* matrix

Before defining the operating modes, the matrix A^* needs to be refined. Being each row representative of a powertrain components if three entries over four are null the whole row is deleted. In fact, in this case it means that the specific component has not connections with the powertrain itself. As far as the 3th and the 4th row, which refer to the electric machines, if the 1st and the 2nd elements are both null it signifies that they are not connected neither with the vehicle, nor with the engine. Consequently, they are eliminated being their working conditions irrelevant both for the output and for the other components.

6-Mode definition

The modes are defined according the A^* matrix, which rows are re-called as reported in the Equation 2.27.

$$A^* = \begin{bmatrix} V_{VEH} \\ V_{ENG} \\ V_{MG1} \\ V_{MG2} \end{bmatrix} \qquad V_{veh} = [C_{VEH} \quad C_{ENG} \quad C_{MG1} \quad C_{MG2}] \tag{2.27}$$

Primary, if the 1st row of the A^* matrix is full of zero, the represented mode is considered infeasible since the vehicle cannot be powered by any of the powertrain components. Secondly, if two modes have the same dynamic and consequently the same A^* matrix they are identified as redundant and only one of them is kept during the analysis. This consideration is fundamental in speeding up the operation of the design tool. Then, the type of mode is identified according to the A^* matrix properties as reported in the table below, exhaustively discussed by Zhang et al [35]. The number of the system DOF is identified through the rank of the matrix. It should be noticed that six additional auxiliary matrixes are defined to shortly identify the criteria of the mode classification:

$$M_{VE} = [V_{VEH}, V_{ENG}],\ M_{VMG1} = [V_{VEH}, V_{MG1}],\ M_{VMG2} = [V_{VEH}, V_{MG2}],\ M_{EMG1} = [V_{ENG}, V_{MG1}],\ M_{EMG2} = [V_{ENG}, V_{MG2}],\ M_{MG1\,MG2} = [V_{MG1}, V_{MG2}].$$

Their respective ranks are identified as $r_{VE}, r_{VMG1}, r_{VMG2}, r_{EMG1}, r_{EMG2}, r_{MG1MG2}$.

N°	Mode Type	Criteria
1	Series Mode	$DOF=2, C_{ENG}=0, V_{ENG}\neq 0, C_{MG1}C_{MG2}=0,$ $C_{MG1}^2+C_{MG2}^2\neq 0$
2	Compound split (3DOF)	$DOF=3$
3	Compound split (2DOF)	$DOF=2, C_{ENG}\neq 0, C_{MG1}C_{MG2}\neq 0, r_{VMG1}=2,$ $r_{VE}=2, r_{VMG2}=2, r_{EMG1}=2, r_{EMG2}=2$
4	Input split	$DOF=2, C_{ENG}\neq 0, r_{VMG1}r_{VMG2}=2,$ $C_{MG1}C_{MG2}\neq 0$
5	Output split	$DOF=2, C_{ENG}\neq 0, r_{EMG1}r_{EMG2}=2,$ $C_{MG1}C_{MG2}\neq 0$
6	Parallel EVT (ICE+1MG)	$DOF=2, C_{ENG}\neq 0, C_{MG1}C_{MG2}=0,$ $C_{MG1}^2+C_{MG2}^2\neq 0$
7	Parallel EVT (ICE+2MGs in serial)	$DOF=2, C_{ENG}\neq 0, C_{MG1}C_{MG2}\neq 0, r_{MG1MG2}$ $=1$
8	Engine only (Fixed Gear)	$DOF=1, C_{ENG}\neq 0, C_{MG1}^2+C_{MG2}^2=0$
9	Parallel with Fixed Gear (ICE+2MGs, 2DOF)	$DOF=2, C_{ENG}\neq 0, r_{VE}=1, C_{MG1}C_{MG2}\neq 0$
10	Parallel with Fixed Gear (ICE+2MGs, 1DOF)	$DOF=1, C_{ENG}\neq 0, C_{MG1}C_{MG2}\neq 0$
11	Parallel with Fixed Gear (ICE+1MGs, 2DOF)	$DOF=1, C_{ENG}\neq 0, C_{MG1}C_{MG2}=0,$ $C_{MG1}^2+C_{MG2}^2\neq 0$
12	EV (2MGs, 2DOF)	$DOF=2, C_{ENG}=0, V_{ENG}(2)=0$
13	EV (2MGs, 1DOF)	$DOF=1, C_{ENG}=0, V_{ENG}(2)=0,$ $C_{MG1}C_{MG2}\neq 0$
14	EV (1MG, 1DOF)	$DOF=1, C_{ENG}=0, V_{ENG}(2)=0,$ $C_{MG1}C_{MG2}=0, C_{MG1}^2+C_{MG2}^2\neq 0$

Table 2.4 Criteria for the modes classification

2.6 Operative modes

In this paragraph each of the fourteen operative modes achievable with a double PGs arrangement is described. More details can be found in [39].

Mode 1: Series Mode

As discussed in the 1st Chapter, in a series mode the ICE is not directly connected with the output shaft, which means that it can be used only to provide power through the MGU and consequently to charge the batteries. This peculiarity allows to control flexibly the ICE operating points to be as close as physically possible the OOL. However, on the other hand, since the vehicle is only directly powered by an electric machine the efficiency may be poor due to the multiple energy conversions between mechanical and electrical power. Another advantage related to this type of mode is referred to the capability to drive the vehicle reversely without the need of a mechanical reverse gear.

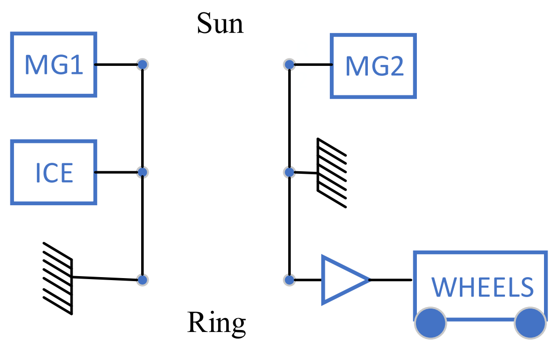

Figure 2.9 Example of series mode

Mode 2: Compound split (3DOF)

For this mode only three speed relations can be written. This explains the reason why the number of DOF is three as the number of governable components. Fundamentally, using this arrangement, the speeds of ICE and of one of the MGU, as well as the output one, are controllable. However, there is no flexibility allowed on the torque control when the components accelerations are determined. This conclusion can be achieved going through the dynamic equations of the system. Since this mode is difficult to be controlled in a real application, is not considered in this analysis.

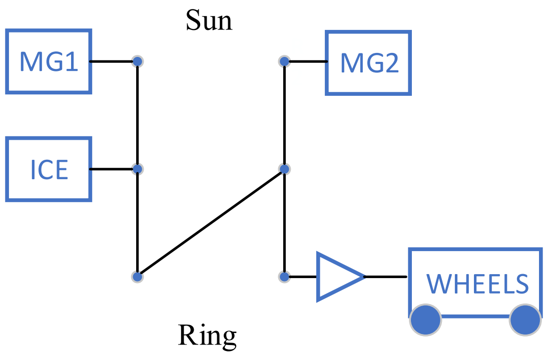

Figure 2.10 Example of compound split (3DOF) mode

Mode 3: Compound split (2DOF)

In this case, the ICE power is divided between the wheels and the MGUs. This mode has typical applications as high speed EVT mode and it has been used in vehicles as the II generation of the Chevrolet Volt.

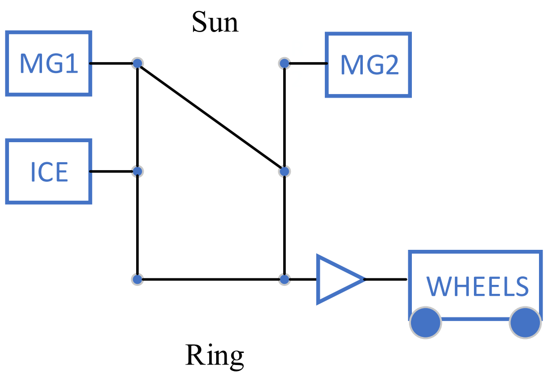

Figure 2.11 Example of compound split (2DOF) mode

Mode 4: Input split

This mode is one of the most popular in commercial vehicles. For example, it is enabled both in the II generation of Chevrolet Volt and in the Toyota powertrains. In fact, it offers high level of flexibility since the ICE is decoupled from the final drive increasing the efficiency performances. Moreover, one MGU is connected to the output through a fixed gear ratio providing an effective assistant during manoeuvres as vehicle launching or, in general, when torque picks are requested.

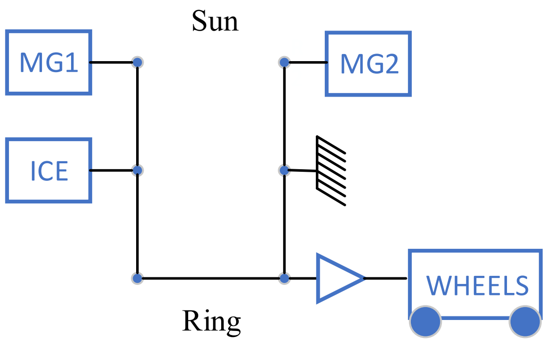

Figure 2.12 Example of input split mode

Mode 5: Output split

In this architecture the ICE speed is always constrained to an MGU. Similarly, to the previous cases being the engine decoupled from the output, the control of the engine performances is optimized.

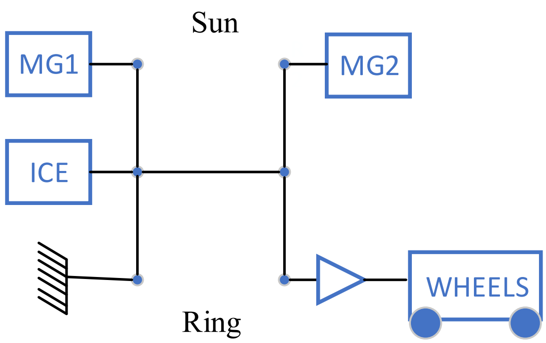

Figure 2.13 Example of output split mode

Mode 6: Parallel EVT (ICE+1MG)

For this mode only one of the two MGUs is turned on. Although it offers as the other modes the possibility to control the ICE speed independently from the output one, it does not allow the control of the ICE torque when the speed is assigned. The reasons behind are the same explained for the case of the three DOF arrangement. Therefore, this mode is not diffused. In addition, when the fuel is cut the speed is not controllable at all. This architecture might find applications as bridge mode when clutches engaging and disengaging operations are required to switch between various working conditions.

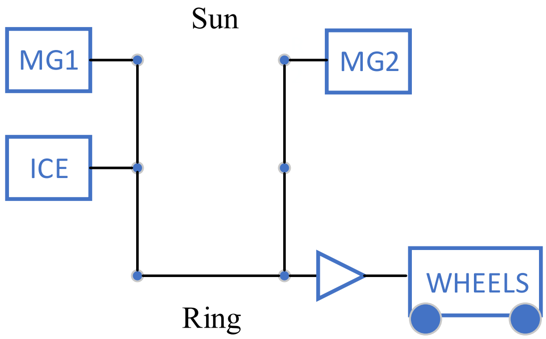

Figure 2.14 Example of parallel EVT mode (ICE+1MG)

Mode 7: Parallel EVT (ICE+2MGs in serial)

In this case, the two MGUs are connected in series. Also, for this mode when the fuel is cut the speed is not controllable. Although this mode is physically realizable, it is not currently adopted for any real application.

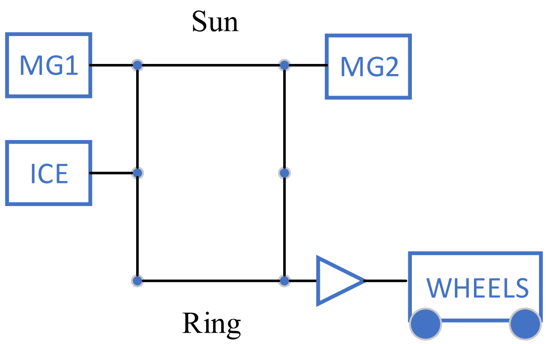

Figure 2.15 Example of parallel EVT mode (ICE+2MGs in serial)

Mode 8: Engine only (Fixed Gear)

For this mode both MGUs are disabled, and the vehicle is only powered by the ICE. This last is connected to the output by a fixed gear ratio. The powertrain behaviour is the same as the one of the conventional vehicles.

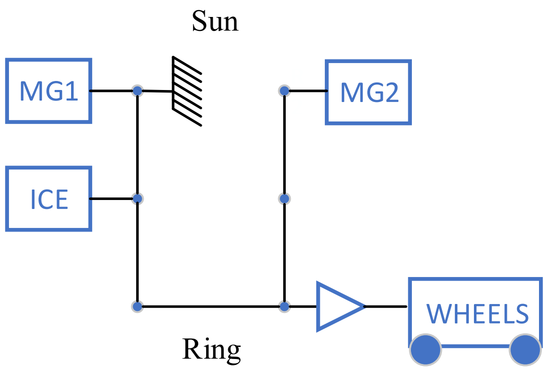

Figure 2.16 Example of engine only mode (Fixed Gear)

Mode 9: Parallel with Fixed Gear (ICE+2MGs, 2DOF)

In this mode the ICE is directly connected to the final drive which limits the control possibilities on the thermal component side. As regards the electric machines, instead, their speed could be efficiently manipulated towards higher performances. There is still no application of this mode on vehicle on the market.

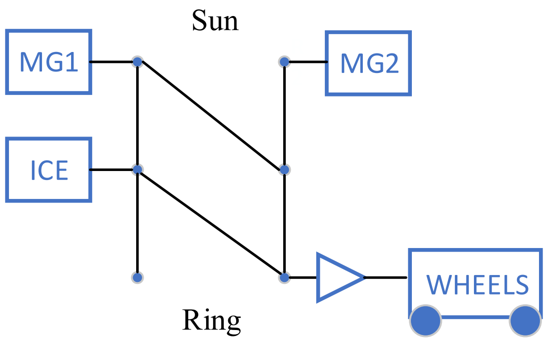

Figure 2.17 Example of parallel mode with fixed gear (ICE+2MGs, 2DOF)

Mode 10: Parallel with Fixed Gear (ICE+2MGs, 1DOF)

For this mode all the speeds, both of MGUs and of the ICE, are rigidly constrained to the output one. Since both thermic and electric part contribute to the propulsion, the motor generator unit torque is selected according the driver demand and the necessities in terms of ICE torque. In fact, this last is adjusted to optimize the component efficiency, since the two electric machines can flexibility either provide or consume power depending on the working conditions.

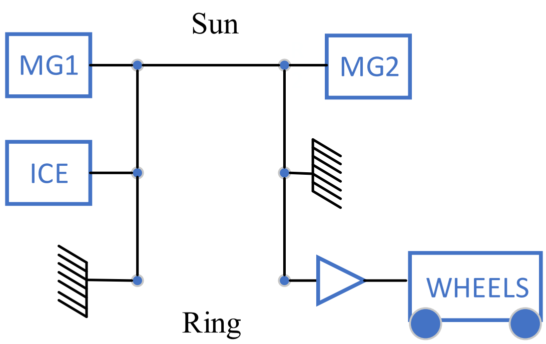

Figure 2.18 Example of parallel mode with fixed gear (ICE+2MGs, 1DOF)

Mode 11: Parallel with Fixed Gear (ICE+1MGs, 2DOF)

This mode is similar to the mode number ten. In fact, the component speeds are proportional to each other with the possibility of choosing the ICE torque to enhance the efficiency. The main difference compared to the previous mode is only related to the deactivation of one of the two electric machines.

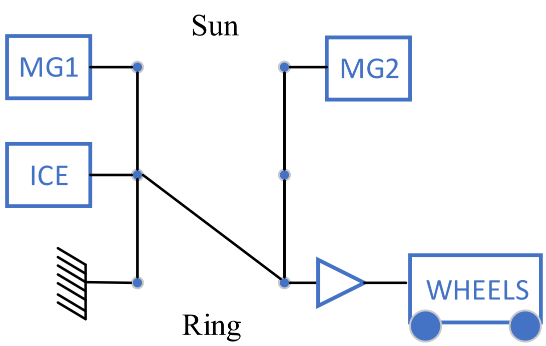

Figure 2.19 Example of parallel mode with fixed gear (ICE+1MGs, 2DOF)

Mode 12: EV (2MGs, 2DOF)

In this mode, as for all the EV cases, the ICE is disabled and directly connected to a ground clutch. This arrangement gives the possibility to select the speed of the two electric machines reducing the losses.

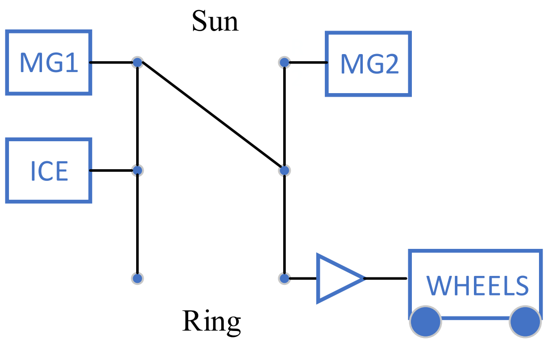

Figure 2.20 Example of EV mode (2MGs, 2DOF)

Mode 13: EV (2MGs, 1DOF)

Differently from the previous case, in this mode the speeds of the electric machines are directly coupled to the output one. The torque provided by both can be controlled to increase the mode efficiency. Moreover, the superimposition of the torques to the final drive allows to reach better performances during some working condition as in the case of launching operations. As matter of example, this mode can be found in the II generation of the Chevrolet Volt.

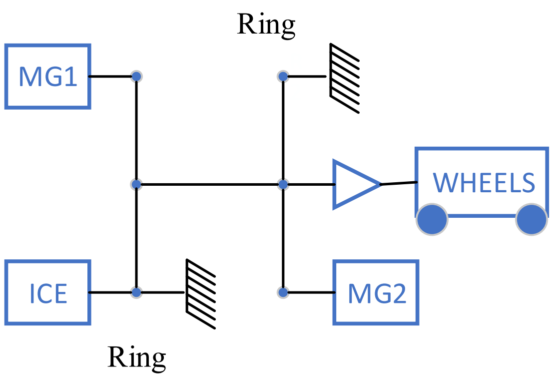

Figure 2.21 Example of EV mode (2MGs, 1DOF)

Mode 14: EV (1MG, 1DOF)

In this mode only one MGU is used to propel the vehicle while the other powertrain components are grounded or disabled.

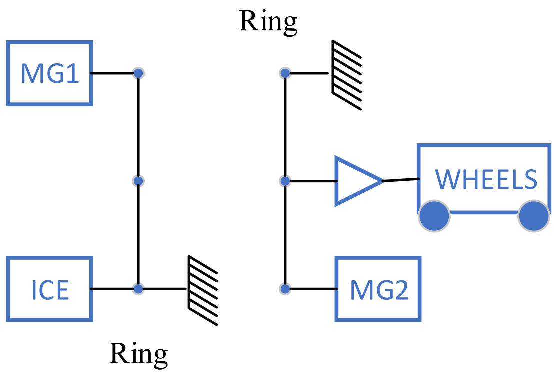

Figure 2.22 Example of EV mode (1MG, 1DOF)

2.7 Generation of the design candidates

2.7.1 Modes combination

After having identified through the A^* matrix properties the possible operative modes of the transmission, in this paragraph we discuss the procedures allowing to generate the complete set of design candidates. After the automatic model processes, we only keep the unique A^* matrix, but at the same time we save all the nodes connections realizing the same operative mode. In fact, they have a different impact for the following operations. To store the results for all the design achieving a defined mode, we use a binary vector, identifying with the numbers "1" and "0" respectively the clutch engaged and disengaged status. As matter of example the set of vectors X^n is reported in the Equation 2.28, where n identifies the studied mode and m is referred to all the topologies realizing the same operating conditions.

$$X^n = \{x_1^n, x_2^n, \dots, x_m^n\} \tag{2.28}$$

At this stage it is possible to select in the tool the maximum number of clutches and the minimum amount of operative modes we require to the topology. As already mentioned, in this dissertation we consider transmissions with maximum three clutches and a minimum number of two operative modes. Consequently, we couple all the modes generated though the previous steps, and if the produced results meet the clutch constraint the topology data are stored. Clearly, when it is possible, the clutches are substituted with permanent connections with a reduction in the transmission cost and complexity. To pair the operative modes, we accomplish binary operations, allowing to obtain the vectors C_{clu}, C_{per} and C_{all} respectively identifying the location of clutches, permanent connections and the set union of the two [40].

$$C_{clu} = (x_j^h \oplus x_i^k) \tag{2.29}$$

$$C_{all} = x_j^h \vee x_i^k \tag{2.30}$$

$$C_{per} = C_{clu} \oplus C_{all} \tag{2.31}$$

The size of the columns of this vector is sixteen, which is the total maximum number of clutches, as identified in the previous paragraph.

2.7.1 Analysis function

Once all the feasible design candidates are generated though the mode combination, we apply a technique called "Analysis function". This procedure allows to identify all the other operative modes realized by the screened topology. Theoretically, the maximum number of achievable modes by the types of powertrain studied is 2^3, being "2" the number of power split devices and "3" the maximum number of clutches. However, if no clutch is engaged the DOF number is larger than the number of controllable powertrain components. This consideration decreases the maximum number of operative modes to seven. In Figure 2.24 there is a conceptual graphical representation of the explained procedures [41]. Finally, since in the current version of the tool the candidates are uniquely ranked according to the fuel consumption value, if different topologies realize the same operative modes, only one of them is analysed with the implemented control strategy to determine the fuel consumption.

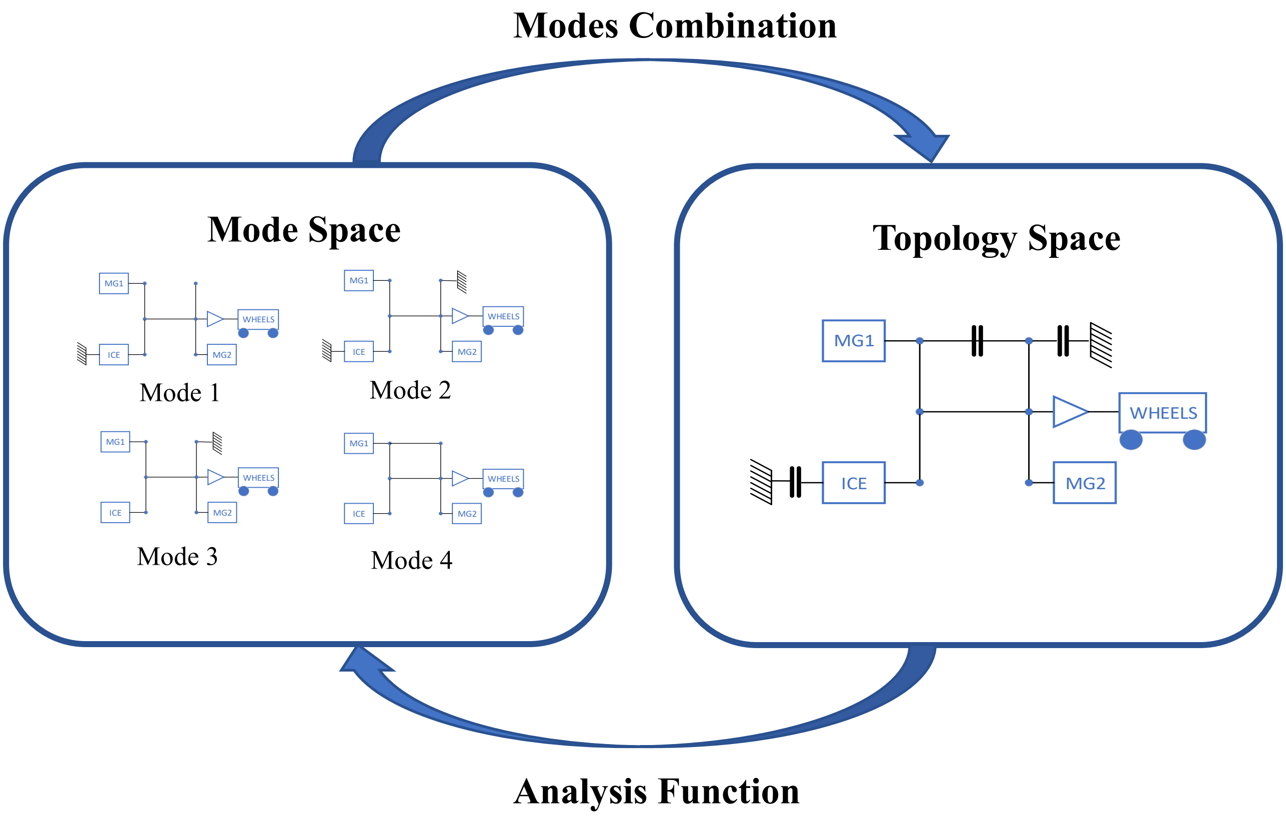

Figure 2.23 Generation of the design candidates

Chapter 3: Design Candidates Selection

After having identified all the possible design candidates, the best ones should be selected based on the base of the design requirements. In this dissertation the topologies are only ranked according the estimated fuel consumption values. Consequently, the choice is strongly associated with the Energy Management Strategy (EMS) adopted both to select the operating mode and the operating conditions in terms of power split. In this chapter at first, the energy management problem is recalled together with the universally accepted control strategies. After having explained the reasons making them not suitable for the design activity, the PEARS algorithm logic (Power-Weighted analysis for Rapid Sizing) is presented. This strategy has been designed ad hoc to deal with the topologies selection and it has been extensively studied during the previous years. However, it has been shown that, in some cases, it can produce results far from the global optimum. To overcome the limitations of the PEARS, another strategy called SERCA (Slope weighted Energy-based Rapid Control Analysis) is introduced. After some robustness and consistency analysis, it is proposed a new methodology, called SERCA$^+$, which enhances the strength of both PEARS and SERCA. The widespread study of the multimode extension and the introduction of the SERCA$^+$ represent the main contributions of this research.

3.1 Energy Management Problem

The energy management problem for HEV powertrains involves the definition of a proper sequence of control variable $u(t)$ (Equation 3.1) leading to the minimization of the instantaneous performance index (Equation 3.2). In the analysed problem, when dealing with multiple DOF, the control variable is generally function of the battery power and of the power split selected.

$$u(t) \in R^m \qquad u(t) = \{P_{batt}(t),\ \rho_1(t), .., \rho_{m-1}(t)\} \tag{3.1}$$

$$J\left(x(t_0), u(t), x(t_f)\right) = \Phi\left(x(t_0), x(t_f)\right) + \int_{t_0}^{t_f} L(x(t), u(t), t)\, dt \tag{3.2}$$

The first part of the cost function $\Phi(*)$ identifies the cost linked to the final value of the state variable $x(t)$, while $L(*)$ denotes the instantaneous cost. In this work the final cost is set equal to zero since a CS strategy for the battery management is implemented. Regarding the state variables adopted in the HEV control problem the vehicle can be studied as a dynamic system with two decoupled states, which are the vehicle speed and the battery SOC. Being these two states mutually independent, the battery SOC is used as state variable while the vehicle speed is separately controlled. Moreover, phenomena as speed transients, involving higher order dynamic models are ignored since they affect the fuel consumption only to a minor extend.

$$x(t) \in R \qquad x(t) = SOC \tag{3.3}$$

The problem is subjected to the following constraints:

- Initial and terminal value of the state

$$x(t_0) = x(t_f) = x_0 \tag{3.4}$$

- Instantaneous restriction on the battery SOC

$$x_{min} \leq x(t) \leq x_{max} \tag{3.5}$$

- Instantaneous restriction on the control variable

$$u(t) \in U(t) \tag{3.6}$$

Clearly the powertrain components torque and speed should be within the allowed physical limits, while at the same time the power supplied should satisfy at least the driving cycle requirement (Equation 3.7).

$$P_{MG1}(t) + P_{MG2}(t) + P_{ICE}(t) \geq P_{OUT}(t) \tag{3.7}$$

- Dynamic of the system

$$\dot{x}(t) = f\big(x(t), u(t)\big) \tag{3.8}$$

This equation traces the evolution of the battery SOC as function of the control variable and it depends by the battery model adopted for the investigation. According to the one implemented in this thesis work and reported in the Chapter 2, the evolution of the system dynamic is described in the Equation 3.9 [42].

$$\dot{x}(t) = -\frac{1}{Q_{nom}} \frac{V_{oc}(x) + \sqrt{V_{oc}(x)^2 - 4R_o(x)\, P_{batt}(t)}}{2\, R_o(x)} = f(x, P_{batt}) \tag{3.9}$$

3.2 Dynamic Programming

The Dynamic Programming (DP) is a numerical optimization method based on the Bellman's principle [43]. To apply this control strategy both time and the state variable need to be gridded. Consequently, the general continuous time-variant model of the Equation 3.8 is discretized as reported in the Equation 3.10 [44].

$$x_{K+1} = F_K\,(x_K, u_K),\;\; t = t_K \;\;\; with\; k = 0, 1, \ldots, N-1 \tag{3.10}$$

The objective is to find the optimal control strategy π (Equation 3.12) minimizing the discretized cost function J (Equation 3.11).

$$J_0(\pi) = \phi(x_N) + \sum_{0}^{N-1} L(x_K, u_K, t_K) \tag{3.11}$$

$$\pi^* = \arg\min_{\pi}\; J_0(\pi) \tag{3.12}$$

The algorithm minimizes the cost to go from each time step up to end of the discretization horizon. Since each possible alternative is analysed, this numerical method guarantees the global optimality within an approximation defined by the discretization step. The optimal cost to go is calculated moving from the last instant of the optimization process up to its initial point (Equations 3.13 and 3.14) [42].

$$J_N^*(x) = \phi(x_N), \quad t = t_N \tag{3.13}$$

$$J_K^*(x) = J_{K+1}^*(x) + min_{u_k \in U_k} L(x_K, u_K, t_K), \quad t = t_k$$
$$with \quad k = N-1, N-2, \ldots, 0 \tag{3.14}$$

Nevertheless, DP cannot be applied for the design analysis. In fact, while the cost dependency by the final time is linear, the computational burden increases exponentially with both number of states and number of inputs [45]. Consequently, the computation weight increases by a large extend when increasing the number of analysed topologies. This problem is well known in literature as curse of dimensionality [46]. In general, it is worth to underline that the DP algorithm is not used in real applications for the HEV control. In fact, this strategy cannot be applied in real-time conditions since, to reach the optimal solution, it is requited the aprioristic overall knowledge of the driving cycle. This is the reason why other approaches as Stochastic Dynamic Programming (SDP) has been introduced. In fact, SDP permits to account for casual system perturbations. However, the results quality is strongly correlated with the random process model. The more sophisticated approaches existing in literature uses a random Markov chain process to derive the future power demand as function of both current output and vehicle velocity [47, 48]. Nowadays, DP is mostly used as benchmark for the other control strategies and to derive some practical rules implemented in the real controller which is typically a rule-based type. Similarly, in this research DP is used to define the quality of the results derived with other strategies.

3.3 Pontryagin's Minimum Principle

The Pontryagin's minimum principle (PMP) is an analytical optimization algorithm which has been proven to achieve optimal performances for the HEV energy management problem if the battery efficiency is a concave function of the battery SOC [49]. The method consists in the minimization at each time step of the Hamiltonian function. This last is defined for the HEV management problem as reported in the Equation 3.15, where $f(*)$ is the system dynamic (Equation 3.9), $\lambda(t)$ is the co-state function (Equation 3.16) and $m_f(*)$ is the instantaneous fuel consumption.

$$H\big(x(t),\, P_{batt}(t), t,\, \lambda(t)\big) = -\lambda(t) f\big(x(t),\, P_{batt}(t)\big) + m_f\, \left(P_{batt}, P_{req}(t)\right) \quad (3.15)$$

$$\dot{\lambda}(t) = -\frac{\partial H\,\big(x(t),\, P_{batt}(t), t, \lambda(t)\big)}{\partial x} \quad (3.16)$$

The input control signals satisfying both the equations belongs to the family of the so-called extremal solution, but it might not be optimal. In fact, the two conditions are necessary but not sufficient. In the more general formulation, it is not even possible to prove analytically the solution existence. However, for the HEV energy management problem it should reasonably exist a solution leading to the cost function minimization. To apply the strategy, it is often convenient to introduce some simplifications on the state variable equation. First it can be rewritten considering that the fuel consumption does not depend on the SOC (Equation 3.17).

$$\dot{\lambda}(t) = -\lambda(t)\frac{\partial f\big(x(t), u(t)\big)}{\partial x} \quad (3.17)$$

It can be noticed as the co-state can be approximated as a constant function if the dependency by the system dynamic equation regards the state variable is neglected. Physically it means that the co-state variation can be approximated as null if open circuit voltage and internal resistance are considered independent variables from the SOC. In this case, the constant co-state value needs an off-line tuning procedure being one of the two boundary constraints enforced at the end of the optimization horizon [42, 45]. Although the computational request is considerably lower than for the DP, the PMP cost does not suit the design activity. Moreover, the tuning of the parameters introduces heuristic procedure of error and trial which are not desirable for this research.

3.4 Equivalent Consumption Minimization Strategy

The Equivalent Consumption Minimization Strategy (ECMS) has been introduced by Paganelli et al in 1999 [50, 51]. It belongs to the category if the instantaneous optimization methods, being required at each discretized time step the minimization of a properly defined cost function. This function is an equivalent virtual fuel consumption obtained summing up the actual fuel burnt, and a virtual cost referred to the battery usage (Equation 3.18).

$$m_{feq}(t) = m_f(t) + m_{batt}(t) = m_f(t) + \frac{s}{Q_{LHV}} P_{batt}(t)\, p(x) \tag{3.18}$$

The basic idea behind this method is that for propelling HEVs, except for the plug-in case, the expense derives entirely from the fuel while the battery is only used as energy buffer to increase the efficiency. In the definition of the battery virtual cost, $p(x)$ is a corrective factor, which is helpful for reaching CS conditions. In fact, this term reduces or increases the electric power cost depending on the instant value of the SOC consequently leading to a smoother profile around the target value. The other relevant term related to the battery cost is the so called s factor. This equivalence factor role is to make the energy power comparable with the actual fuel burnt. When the battery is discharged, it is considered the cost of the future charging operation of the battery while in the opposite case, when the battery is charged, the cost of the future usage is counted. Practically the s parameter is dependent by the powertrain components efficiencies and by the power flow direction. This is the reason why there is a built-in asymmetry for the s definition, which ponders the battery consumption, according to the different operating conditions. An example of s factor for charging and discharging conditions is reported in the Equations 3.19 and 3.20 [42].

$$\begin{gathered} s_{dis} = \frac{1}{\eta_{EM,dis}\,(P_{EM})\eta_{batt,dis}(P_{EM})\overline{\eta_{ch}}} \\ \overline{\eta_{dis}} = \frac{1}{T}\left[\int \eta_{batt,dis}\,\eta_{EM,dis}\eta_{coupling}dt\right] \Delta t \end{gathered} \tag{3.19}$$

$$\begin{gathered} s_{ch} = \frac{\eta_{EM,ch}\,(P_{EM})\,\eta_{batt,ch}(P_{EM})}{\overline{\eta_{dis}}} \\ \overline{\eta_{ch}} = \frac{1}{T}\left[\int \eta_{ICE}\,\eta_{batt,ch}\eta_{EM,ch}\eta_{coupling}dt\right] \Delta t \end{gathered} \tag{3.20}$$

Although ECMS has been extensively used as HEV energy management strategy it cannot be applied for the design activity. In fact, the quality of the results is intimately connected with the offline parameters tuning. Furthermore, the s factor depends by the different mode selected which is in contrast with the scope of this research, aiming to find an effective and precise way to analyse a huge design space of multi-mode powertrains without any procedure of parameters tuning.

3.5 Power-weighted Efficiency Analysis for Rapid Sizing (PEARS)

To accomplish the difficulties related to the use of the well-known control strategies, a new algorithm called Power-weighted Efficiency Analysis for Rapid Sizing (PEARS) has been introduced for the design activity by Zhang et al [52]. The basic idea behind this technique is that to minimize the fuel consumption, each component should work as close as possible to its best efficiency region. The steps describing the algorithm procedures are reported by following.

STEP 1: Discretization of the driving cycle

As initial stage, the analysed driving cycle is discretized according the two independent variables of vehicle speed and road load torque. The choice of the torque as parameter, differently from the acceleration, allows to take into consideration the eventual presence of a road slope grade without increasing the number of used variables. The entrances of this 2-D matrix refer to the frequencies of occurrence of the torque speed cells for the analysed driving cycle. Organizing the driving cycle points as probability function allows, adopting a statistical approach, to speed up the algorithm procedures which is one of the crucial requirements. The number of points used for the discretization of torque and speed is a compromise between the results precision and the computational burden. Afterwards, the analysis of the transmission operating modes is carried separately for EV and HEV modes.

STEP 2.1: EV Mode Analysis

For each possible torque-speed cell with a frequency of occurrence larger than zero the EV modes are analysed according the efficiency definition reported in the Equation 3.21. P_{EV}^{in} refers to the power flow entering the system and it corresponds to the battery power for the positive acceleration case. On the contrary, it denotes the differential power for the regenerative breaking case. On the other hand, P_{EV}^{loss} considers all electrical path losses summing up the motor generator units and the battery ones. For modes with one DOF all the possible torque combinations (T_{MG1}, T_{MG2}) are examined, meanwhile for modes with two DOF also all the possible speed groupings are considered $(\omega_{MG1}, \omega_{MG2})$. The mode with highest efficiency is recorded together with the value of the electrical battery consumption (Equation 3.22).

$$\eta_{EV} = 1 - \frac{P_{EV}^{loss}}{P_{EV}^{in}} \tag{3.21}$$

$$\eta_{HEV}^{*}|_{\omega_{out},\dot{\omega}_{out}} = max[\eta_{EV}\ (\omega_{ICE}, T_{ICE})]|_{\omega_{out},\dot{\omega}_{out}} \tag{3.22}$$

STEP 2.1: HEV Mode Analysis

The HEV modes are evaluated using the normalized efficiency definition of the Equation 3.23. The power flow is separated in three contributions (Figure 3.1):

1. P_{ICE1} is the power flowing from the engine to the generator and finally to the battery;
2. P_{ICE2} is the power fraction coming from the engine and moving towards the generator ultimately arriving to the motor;
3. P_{ICE3} is the power that from the engine directly reaches the differential.

$$\eta_{HEV}(\omega_e, T_e) = \frac{P_{ICE1}\,\eta_G \eta_{batt} / \eta_{ICEmax}\,\eta_{Gmax}}{P_{fuel} + \mu P_{batt}} + \frac{P_{ICE2}\,\eta_G \eta_M / \eta_{ICEmax}\,\eta_{Gmax}\,\eta_{Mmax}}{P_{fuel} + \mu P_{batt}} + \frac{P_{ICE2} / \eta_{ICEmax} + \mu P_{batt} \eta_{batt} \eta_M / \eta_{Mmax}}{P_{fuel} + \mu P_{batt}} \tag{3.23}$$

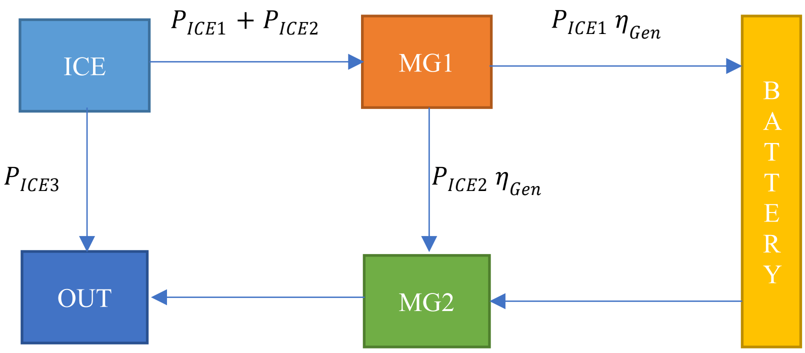

Figure 3.1 Schematic representation power flow PEARS algorithm

In the efficiency equation μ is a bit which has a unitary value when the battery power is used to assist the propulsion, while it is null when only the ICE is contributing to satisfy the power demand. η_{ICEmax}, η_{Mmax}, η_{Gmax} are the highest possible efficiencies respectively for engine, motor and generator. It is worth to recall that in the whole dissertation the subscript M and G are used to label the electric machines working correspondingly as motor and as generator. Furthermore, it is crucial to notice the choice to normalize the efficiency regarding the engine, which is the least efficient component. A different choice would likely lead to cases in which the engine is infrequently preferred [35]. Similarly to the EV case, also for the HEV analysis, the best mode is selected on the base of the highest efficiency value obtained by sweeping all the possible combination of torque and speed of the engine (T_{ICE}, ω_{ICE}) within the machine physical value. The three power flow contributions are computed according the Equations 3.24, 3.25 and 3.26, while the relation 3.27 is applied to calculate the fuel injected. Finally, the best efficiency (Equation 3.28) and the related power split are recorded [53].

$$P_{ICE2} = \frac{P_M}{\eta_M \eta_G} \tag{3.24}$$

$$P_{ICE1} + P_{ICE2} = P_G \tag{3.25}$$

$$P_{ICE} = P_{ICE1} + P_{ICE2} + P_{ICE3} \tag{3.26}$$

$$P_{fuel} = \frac{P_{ICE}}{\eta_{ICE}} \tag{3.27}$$

$$\eta^*_{HEV}|_{\omega_{out}, \dot{\omega}_{out}} = max[\eta_{EV}\ (\omega_{ICE}, T_{ICE})]|_{\omega_{out}, \dot{\omega}_{out}} \tag{3.28}$$

STEP 3.1: Modes efficiencies matrix initialization

After having analysed all the achievable modes for the design candidate, the modes to be selected and the shifting strategy are defined. For each torque-speed cell the results are organized reporting the best modes and their difference according the structure shown in Table 3.1.

Torque-speed cell	*Best* $\boldsymbol{\eta_{EV}}$		*Best* $\boldsymbol{\eta_{HEV}}$		$(\boldsymbol{\eta_{HEV}} - \boldsymbol{\eta_{EV}})$
$\boldsymbol{j-1}$	…	…	…	…	…
$\boldsymbol{j}$	$Best\ EV^j$	$\eta_{EV}^{best,i}$	$Best\ HEV^j$	$\eta_{HEV}^{best,i}$	$\eta_{HEV}^{best,i} - \eta_{EV}^{best,i}$
$\boldsymbol{j+1}$	…	…	…	…	…

Table 3.1 Example of efficiency matrix PEARS algorithm

STEP 3.2: EV mode selection

For each torque-speed combination the best EV modes is selected. If for the analysed transmission, there are driving cycle points in which none of the available EV modes satisfies the output request, the best HEV mode is picked. Subsequently, the total electrical energy request is computed (Equation 3.29). The subscripts D and B stand for driving and braking, P_k^{EV} and P_l^{EV} are the battery power, Φ_k and Φ_l are the probability density function associated with the torque-speed combination, T_D and T_B refers to the time durations.

$$E_{EV} = \sum_{k=1}^{N} P_k^{EV}\, \Phi_k\, T_D + \sum_{l=1}^{M} P_l^{EV}\, \Phi_l\, T_B \tag{3.29}$$

If the strategy is applied to study HEV powertrain not belonging to the PHEV type, as it is the case of this research, as mentioned, a CS energy strategy is adopted to manage the battery. Avoiding excessive fluctuation in the battery state, this usage requires at the end of the optimization horizon the same initial SOC value. To satisfy this condition, the total electrical energy required E_{EV} should be less or equal than zero, which represents the total energy available E_{AV}.

STEP 3.3-3.4: HEV mode iterative selection

To satisfy the battery management requirement, the EV modes are iteratively substituted with HEV ones. The choice of the driving cycle points at which the substitution is performed depends on the efficiency difference reported at the 5th column of the Table 3.1. Consequently, at the torque-speed cell where the efficiency gap is the highest, the best HEV is chosen and the total electrical energy request is updated (Equation 3.30).

$$E_{EV_{new}} = E_{EV} + P_J^{HEV} \Phi_j T_D - P_J^{EV} \Phi_j T_D \tag{3.30}$$

Once more, Φ_j and T_D refer respectively to the probability density function and the time duration, while P_J^{HEV} and P_J^{EV} corresponds the battery power for the HEV and EV modes.

STEP 3.5: Fuel consumption and electrical energy calculation

After the mode shifting determination, the final electrical energy requirement is found as the last update value, whereas the fuel consumption is calculated summing up all the instantaneous injected contributions (Equations 3.31 and 3.32).

$$m_{fuel_j} = \frac{T_j\ \omega_j}{\eta_{ICE,i}\ Q_{LHV,i}} \tag{3.31}$$

$$m_{fuel_{tot}} = \sum_{j=1}^{n_{HEV}} m_{fuel_j} \tag{3.32}$$

The procedure of the step 3 are schematized in the flow chart of the Figure 3.2 [52].

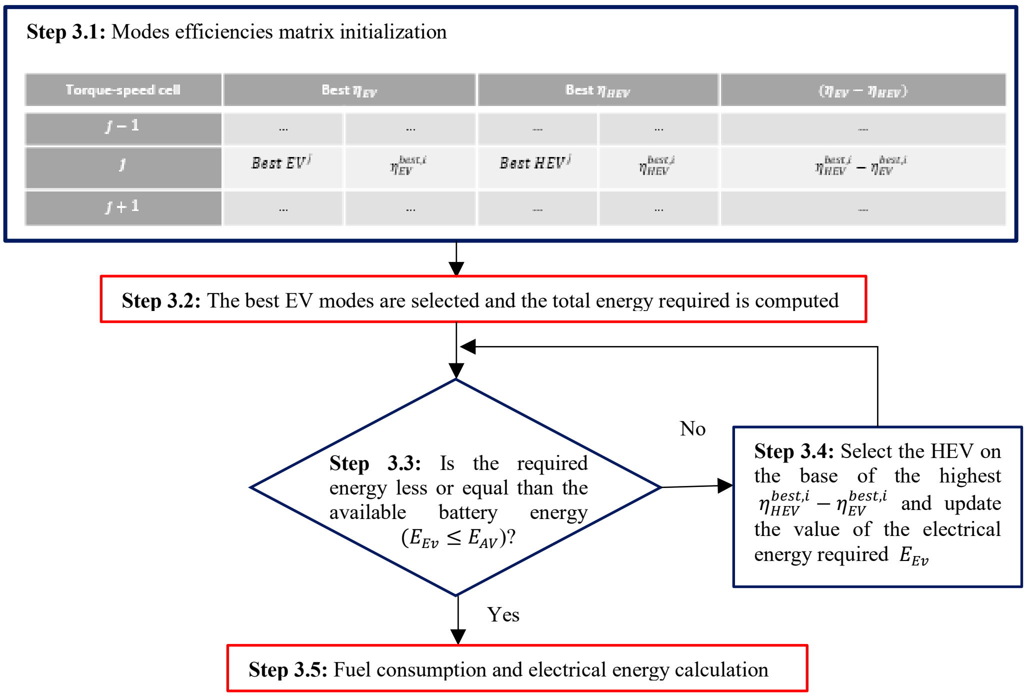

Figure 3.2 Flowchart step 3 of the PEARS algorithm

3.6 PEARS improvement

The PEARS algorithm has been proven to be about four orders of magnitude faster than DP while producing results which differs on the fuel consumption side by about 6% for some case of studies related to the single PG configuration [52]. However, one of the most important limitation of the strategy is related to the mode shift practicability. In fact, the generated shifting schedule might lead to a very frequent mode change without considering both the losses and the feasibility of the shifting operations. As a matter of fact, select another working mode may require either to open or to close clutches or manoeuvres of shafts speed synchronization which might not be achievable in practise. For this reason, another version of the algorithm, called PEARS$^+$ has been introduced by Zhang. This approach uses the PEARS for analysing the mode and DP for deciding the mode shifting strategy. Hence, in this case, the PEARS analysis allows to reduce the dimensions of the DP problem with a considerable advantage in terms of computational cost. The PEARS$^+$ logic is schematically reported in Figure 3.3, while the Equation 3.33 states the cost function used to find the optimal solution with DP [35].

$$J = \min \left[\sum_{t=1}^{N} \left(L_t + \gamma_1 \, \Delta\omega_e^2 + \gamma_2 \Delta\omega_{MG1}^2 + \gamma_3 \Delta\omega_{MG2}^2 \right) + \alpha \left(SOC_{desired} - SOC_N \right)^2 \right] \tag{3.33}$$

In this last $\gamma_1, \gamma_2, \gamma_3$ and α are some tuning coefficients used to take into consideration the shifting losses and to enforce the final constrain on the SOC value. It should be notice that an approach of this type does not allow to apply the optimal DP methodology using only the SOC as state variable. In fact, counting the shifting penalties requires to add the control of the selected mode at the current time step. Despite it has been shown how PEARS$^+$ can produce results close to the DP benchmark with a running time 10,000 faster, it has been used only for exploring the topologies belonging to the configuration of the 2nd generation of Toyota Hybrid System (THS-II) with the addition of clutches [35]. Furthermore, the PEARS$^+$ allow an important reduction of the computational burden, but still the time required to obtain the results does not permits to deal with the complete design space. The same authors have used PEARS$^+$ also for the exhaustive research of the best topologies in the whole design space. However, the strategy has been applied only after having substantially reduced the number of candidates with a fast analysis of the performances [54]. To address the issue of the mode shifting feasibility without compromising the computational cost, Anselma et al [41] proposed another version of the PEARS algorithm, which flow chart is the one reported in Figure 3.4. To demonstrate the benefit of this new proposal in terms of modes change uniformity a rough estimation of the shifting losses has been performed. It is considered that every time the operative mode is changed, 10% of the power produced or received by any of the powertrain components is wasted both at the current and at the successive time step (Equation 3.34). The aim is to show the positive impact of the strategy, despite the increase in the fuel consumption value.

In this dissertation this last version of the PEARS algorithm is the one to which we refer for the results comparison.

$$penalty = 10\% \left(\frac{P_{out^{ii}}}{\eta_{mode^{ii}}} + \frac{P_{out^{ii+1}}}{\eta_{mode^{ii+1}}} \right) \tag{3.34}$$

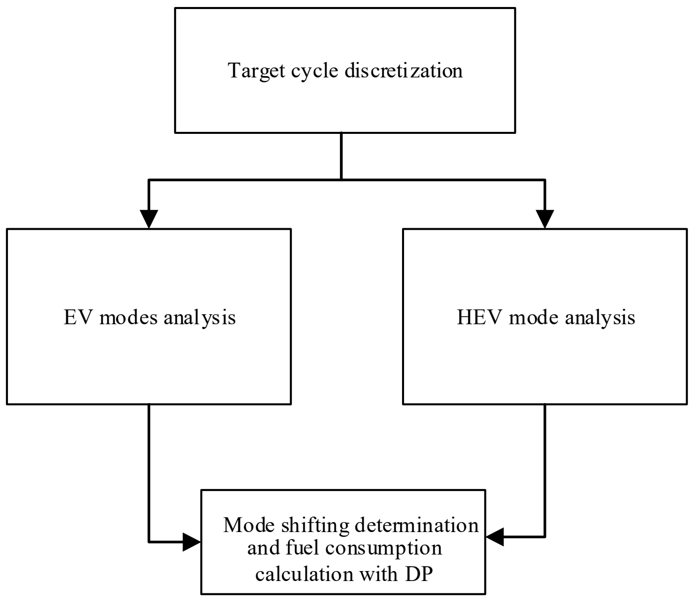

Figure 3.3 Flowchart PEARS+ algorithm

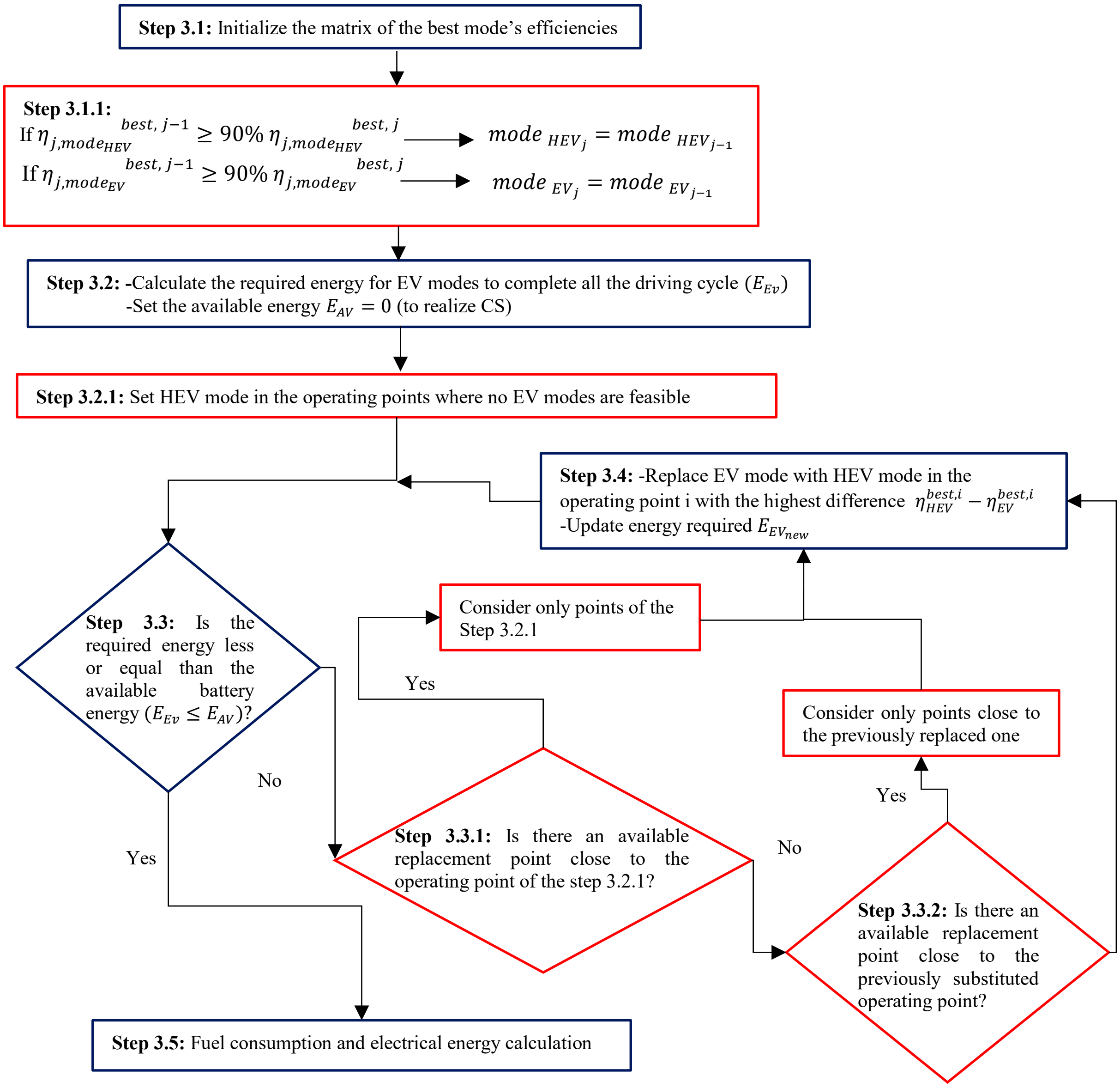

Figure 3.4 Flowchart of the improved version of the PEARS algorithm

3.7 Slope-weighted Energy-Based Rapid Control Analysis (SERCA)

The PEARS strategy introduced in the previous paragraph permits to address some of the issues of the design analysis, allowing to manage the battery in CS conditions without heuristic procedure of error and trial. Moreover, the algorithm fits the requirement related to the computational time. However, some researches have shown as the PEARS can exhibit in some occasion non-uniform propinquity with the global optimum solution, as can be notice in the cases of study reported in the Chapter 4. For this reason, in this thesis we have implemented a new approach for the HEV energy management problem called Slope-weighted Energy-based Rapid Control Analysis (SERCA). Firstly, the strategy is illustrated for the transmission realizing only two operative modes, as the one of the Chryslers Pacifica. Subsequently, the generalization to the multimode case is presented.

3.6.1 SERCA application for a dual mode transmission

The procedures of the SERCA algorithm [55], which are described in detail by following, can be summarized in 3 main phases:

- Subproblems exploration
- Generalized optimal point definition
- Energy Balance realization

STEP 1: Subproblems exploration

The first step of the algorithm involves the analysis of the driving cycle points, which represent the subproblems for the investigation. To increase the speed of the process, as for the PEARS, the driving cycle can be discretized along torque and speed [35].

STEP 1.1: Discretization of the control variable

The control variables of the problem which are torque and speed of the components are discretized according to the specific machine’s limits of maximum torque and speed. The adopted resolution depends on the component dimensions and it is a compromise between the results accuracy and the computational fastness.

STEP 1.2: Solution creation

In this step for each subproblem the solution candidates are originated according the PGs physical constraints. As discusses in the Chapter 2, both the speed and torque relations need to be satisfied (Figure 3.5).

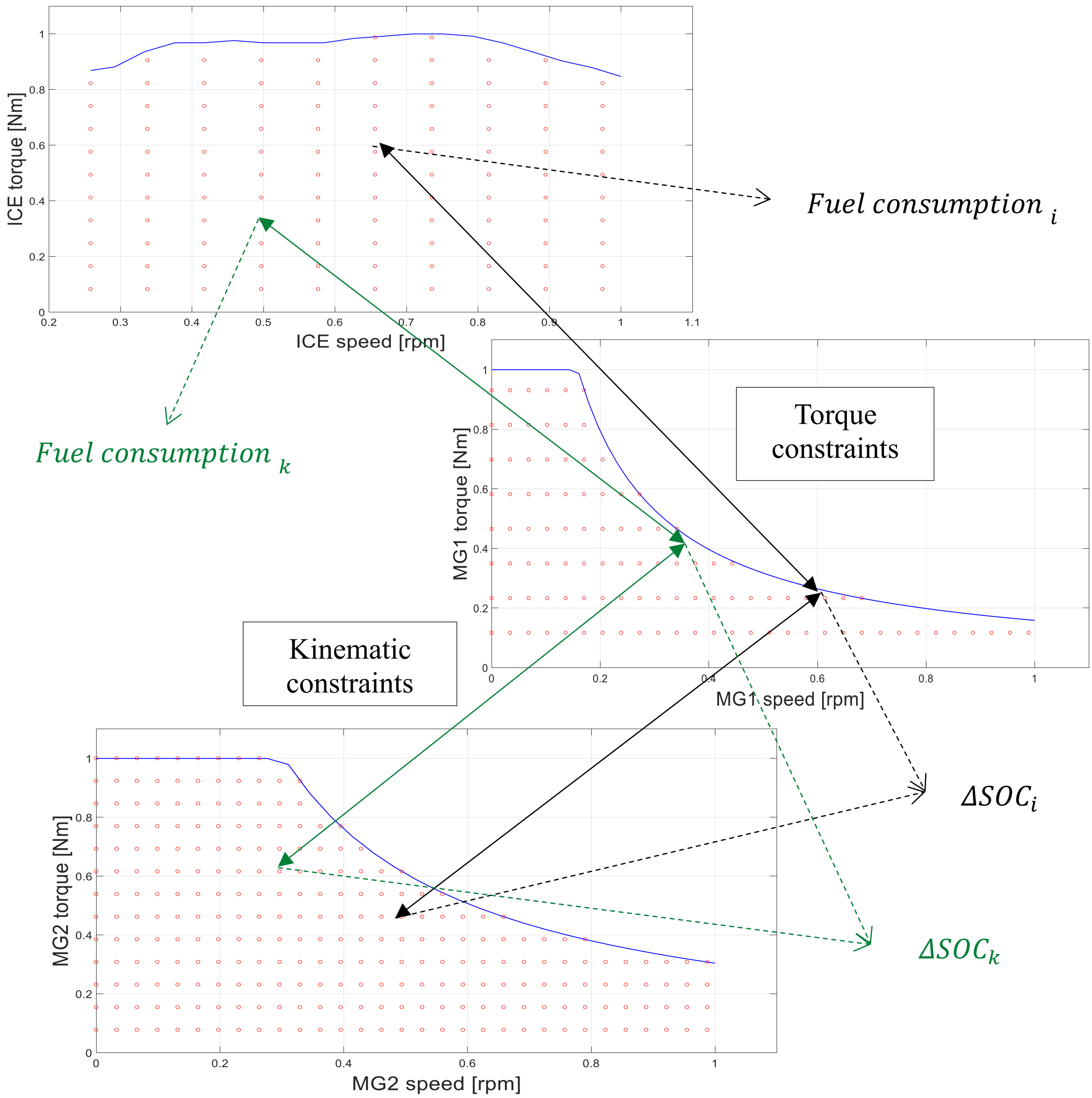

Figure 3.5 Example of solution creation

STEP 1.3: Solution evaluation

The points identified in the previous step are reported as fuel consumption and battery usage values according to the vehicle model presented in the Chapter 2. As concerns the EV modes, the optimal point is easily selected depending on the lowest battery request. Instead, as far as the HEV counterpart, a cloud of possible solutions as the one reported in Figure 3.6 is derived.

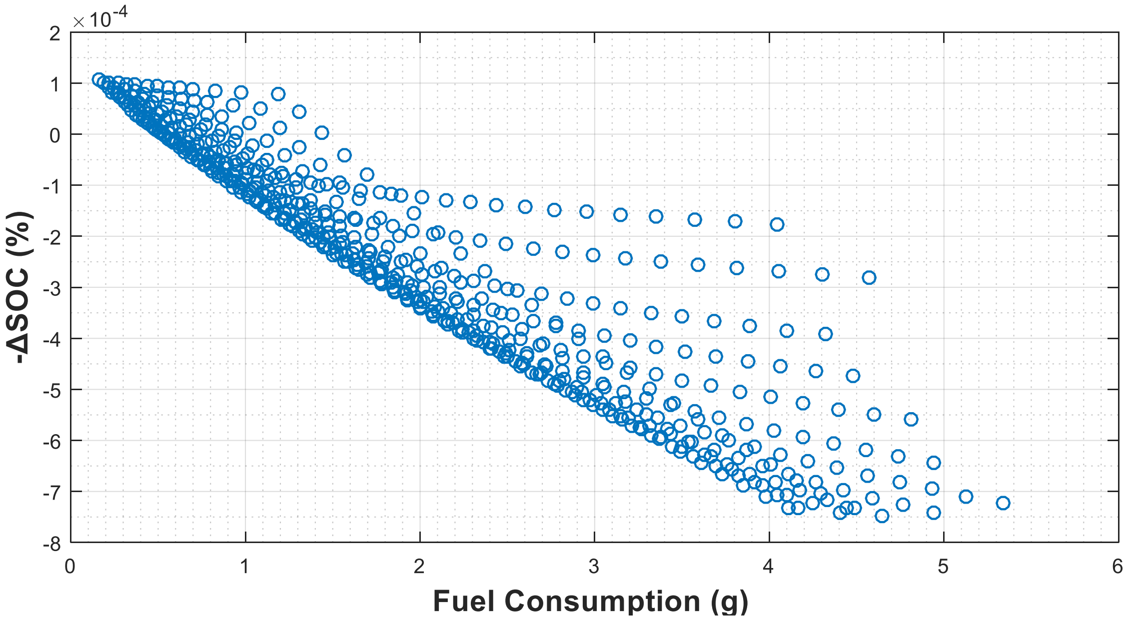

Figure 3.6 Example of possible solution for a local subproblem

The lower edge of this point cluster encloses the possible optimal solution points. In fact, fixing the amount of fuel burnt, these candidates are the one characterized by the lowest requirement in terms of battery usage. Consequently, this edge can be seen as a sort of Pareto optimal front [56]. The same derivation methodology has been followed to report the optimum engine operating line points as function of both battery power and fuel consumption for the application of the Pontryagin's minimum principle in [46]. However, a substantial difference in the SERCA approach, is the discretization of the control variables according the Step 1.1. As far as the meaning of the point cluster trend of the Figure 3.6, it is intuitive to notice that for a fixed output demand, increasing the amount of fuel burnt leads to a reduction of the battery use and vice versa.

STEP 2: Generalized optimal point definition

From the group of point built in the precedent passages, in this step only the identified optimal ones are picked as initial input data for the energy balance achievement.

STEP 2.1: Fuel consumption discretization interval

The fuel consumption is discretized from the lower to the highest value in intervals which wideness is, once more, a compromise between the results accuracy and the computational burden.

STEP 2.2: Identification of the optimal solution

For each fuel discretization interval, it is selected the point corresponding to the lowest battery use following the Equation 3.35.

$$min\left[P_{batt}\left(m_{fuel}\right)\right] \; subj.to: m_{fuel} \in \left[\left(m_{fuelk} - \frac{\Delta m_f}{2}\right)\left(m_{fuelk} + \frac{\Delta m_f}{2}\right)\right] \quad (3.35)$$

STEP 2.3: Slope-based filtration

After having identified the point candidates for the optimal solution, the results need to be filtered since there are concave part of the envelope which may be an obstacle in trying to converge to the optimality. Firstly, if moving to the left of the cluster towards points characterized by higher values of fuel consumption, the battery usage does not reduce or even increases, the point is discarded (Equation 3.36) for evident reasons.

$$SOC\left(m_{fuel,k}\right) < SOC\left(m_{fuel,k+1}\right) \quad (3.36)$$

At this stage the possible selected working points are connected to form an envelope of piecewise linear function starting from the EV mode. The slope connecting two consecutive points is defined according to the Equation 3.37.

$$\theta(k-1,k) = \frac{\Delta SOC}{\Delta m_{fuel}} = \frac{SOC(k) - SOC(k-1)}{m_{fuel}(k) - m_{fuel}(k-1)} \tag{3.37}$$

Despite the previous relaxation procedure, there may exist some area in which the envelope is concave leading to the problems previously discusses. To address this issue, another filtering technique is applied to the construction (Equation 3.38) ensuring the convexity. Figure 3.7 shows an example of the filtration procedure.

$$|\theta(k-1,k)| \geq |\theta(k,k+1)| \tag{3.38}$$

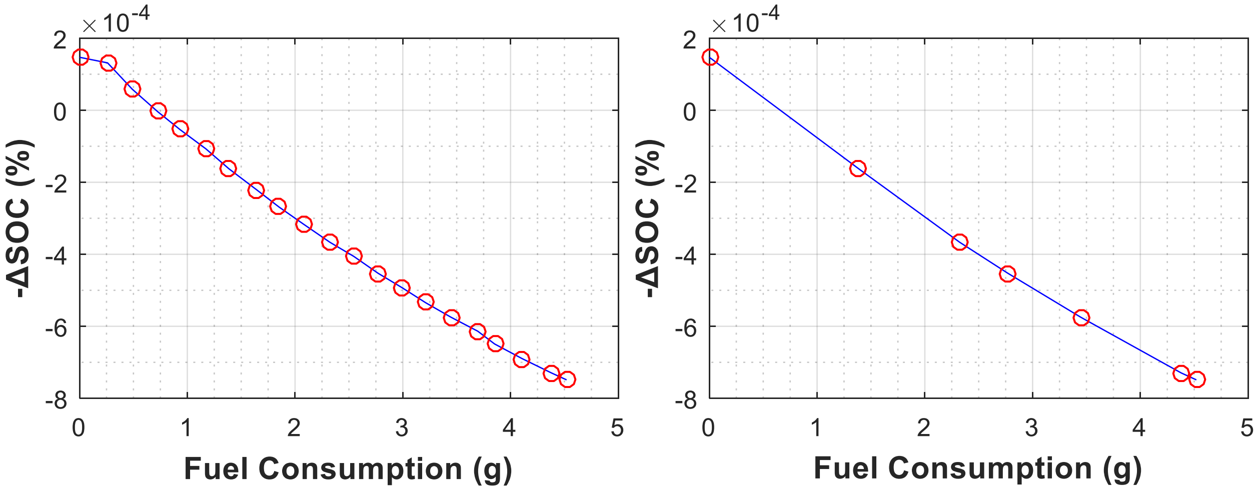

Figure 3.7 Example of SERCA envelope before and after the filtering procedures

Finally, for each driving cycle point, the envelope built up to this step is stored in matrix as fuel consumption, battery use and slope. Each row of the matrix corresponds to a point of the cluster from left to right (Equation 3.39). Subscript i and k respectively identify the driving cycle point and the row of the envelope matrix.

$$\begin{aligned} u_{1|i,k} &= \theta_i(k-1,k) \\ u_{2|i,k} &= SOC_i(k) - SOC_i(k-1) \\ u_{3|i,k} &= m_{fuel_i}(k) - m_{fuel_i}(k-1) \end{aligned} \tag{3.39}$$

STEP 3: Energy Balance Realization

After having repeated the previous steps for all the torque-cell combinations and having stored the results for the envelope, the energy balance is realized.

STEP 3.1: EV modes selection

First, similarly to the PEARS algorithm procedure, in each driving cycle point the best EV mode is selected. If the specific output requirement is not obtainable with any electric arrangement, the HEV mode is alternatively selected. Subsequently, the total electrical energy demand E_{EV} is computed.

STEP 3.2-3.3-3.4: HEV modes iterative selection

In these steps it starts the substitution process of the HEV modes. Each driving cycle point is labelled with the value of the slope connecting the best EV mode with the first point of the HEV envelope. In fact, after the filtering procedure (Equation 3.38), the first slope is the steepest for each construction. Indeed, the basic idea behind the SERCA strategy is to move towards points which can provide the maximum advantage in terms of battery usage relatively to the amount of fuel burnt. This relative magnitude is expressed through the slope concept. Accordingly, the driving cycle point at which the substitution takes place is selected on the base of the highest slope. After the substitution, the values of total electrical energy request, total fuel consumption and the value identifying the driving cycle point are updated (Equations 3.40 and 3.41). In other words, at the torque-speed demand at which the substitution has been performed the rows of the envelope matrix are shifted up, while the first row is discarded. The described procedure is iteratively repeated up to reaching CS conditions (Figure 3.8).

$$\begin{aligned} m_{fuel_{new}} &= m_{fuel} + (u_{1|i,k} - u_{1|i,k-1}) \\ E_{EV_{new}} &= E_{EV} + (u_{2|i,k} - u_{2|i,k-1}) \end{aligned} \tag{3.40}$$

$$u_{1|i,k} = u_{1|i,k+1}$$
$$u_{2|i,k} = u_{2|i,k+1} \qquad (3.41)$$
$$u_{3|i,k} = u_{3|i,k+1}$$

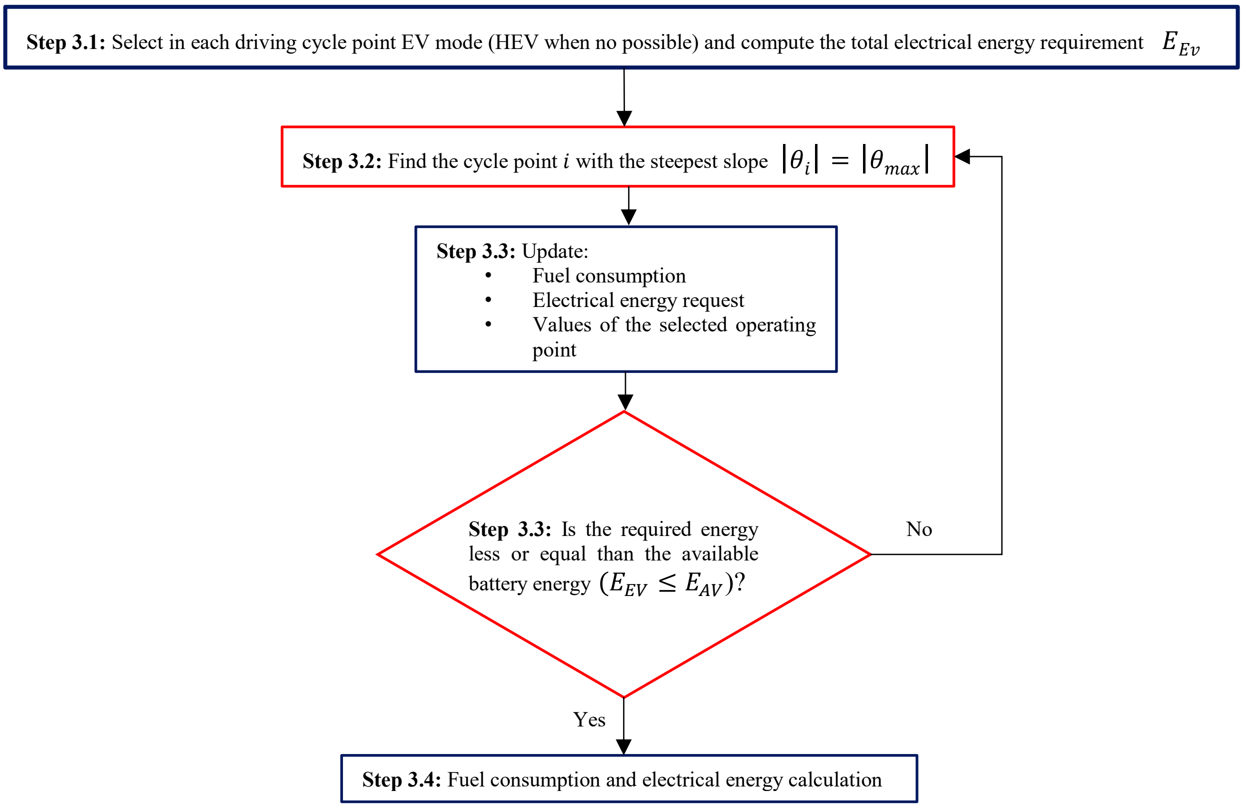

Figure 3.8 Flowchart SERCA algorithm for a dual mode transmission

3.6.1 SERCA extension to multimode transmissions

In this section we introduce the extension of the SERCA methodology for the multimode case and consequently for the application in the design activity.

STEP 1: Subproblems exploration

The first stage of the algorithm follows the procedure of the dual mode case, previously presented. The substantial differences are in the Step 1.3 which is related to the solution evaluation. Again, as far as the electric arrangement, in each driving cycle point, is chosen the EV mode achieving the highest efficiency. Instead, for the HEV modes, the possible solutions form a cluster of points for each achievable mode.

STEP 2: Generalized optimal point definition

In this step the clusters of points, representing the feasible power splits for the HEV modes, are transformed in envelopes of piece wise linear functions. For all the constructions the starting vertex is the best EV solution selected at the previous passage. Finally, after having applied the filtering criteria, detailed in the Step 2 of the dual mode application, the result at each output demand is a set of linear envelopes. An example is shown in Figure 3.9 for a case in which three HEV modes are present.

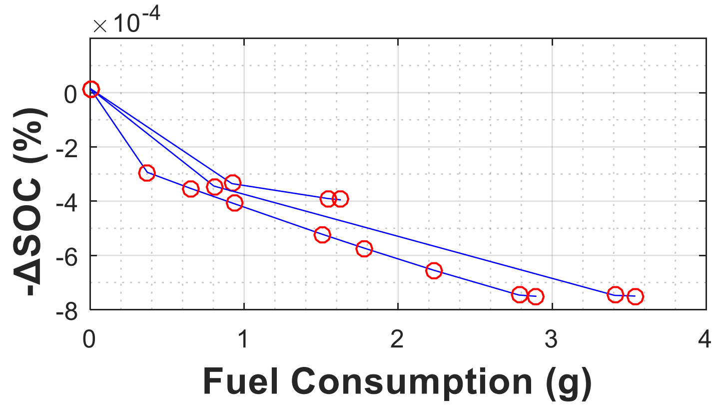

Figure 3.9 Example of SERCA envelope for a 3 modes transmission

STEP 3: Energy Balance Realization

In this final passage the mode shifting strategy and the power split are chosen. Once more as starting phase the best EV mode are picked first. Alternatively, when not feasible, it is chosen the HEV mode and the relative power split leading to the lowest fuel consumption. Subsequently, the total electrical energy requirement is computed. The iterative substitution of the HEV modes up to CS condition is performed, following the order identified by the slopes. Once the replacement has been effectuated, the value of the electrical energy demand and of the total fuel consumption are updated. A crucial passage is to correctly modify the stored data referred to the envelope in the driving cycle points for which the substitution has taken place. In fact, the common starting point of the envelope, is update to the selected HEV point. Before proceeding with the iteration passages, since the initial point has been modified, the filters (Equation 3.38) are re-applied guaranteeing the convexity of the construction. To avoid excessive mode shifting, after having identified the driving cycle point with the steepest slope, a comparison is made among the slope parameters related to mode adjacent to the driving cycle points for which the same HEV arrangement has already been selected. If a power split combination is labelled with a reasonably high value of slope, the correspondent HEV mode is preferred. The choice is weighted by a tuneable shifting penalty coefficient C_{shift} (Equation 3.42).

$$\theta_{max}^{i} \leq C_{shift}\theta_{max}^{i,HEV_j} \tag{3.42}$$

The algorithm steps are graphically reported in the flow chart of the Figure 3.10.

3.8 Comparison between PEARS and SERCA

Since the data set available for the simulation are representative of a typical minivan application, it is chosen to test the quality of the results generated comparing some topologies belonging to the same configuration of the Chrysler Pacifica (Table 3.2). Accordingly, the engine and the first electric machine are respectively connected with the carrier and the sun of the first planetarium, while the output and the second electric machine are coupled with the carrier and the sun of the second gear set. The parameters adopted for the simulation are reported in Table 3.3. The shifting coefficient used to generate a feasible mode shifting strategy is set at 0.9. As for all the results presented over the entire dissertation, the fuel consumption values are investigated on highway (HWFET) and urban driving cycles (UDDS). Nevertheless, for the purpose of this study, the most significant parameter in terms of comparison among different topologies is the averaged value of the fuel economy obtained weighting by 55 % the urban consumption and by 45 % the highway ones. The aim is to reduce the choice dependency by the type of analysed driving cycle [57].

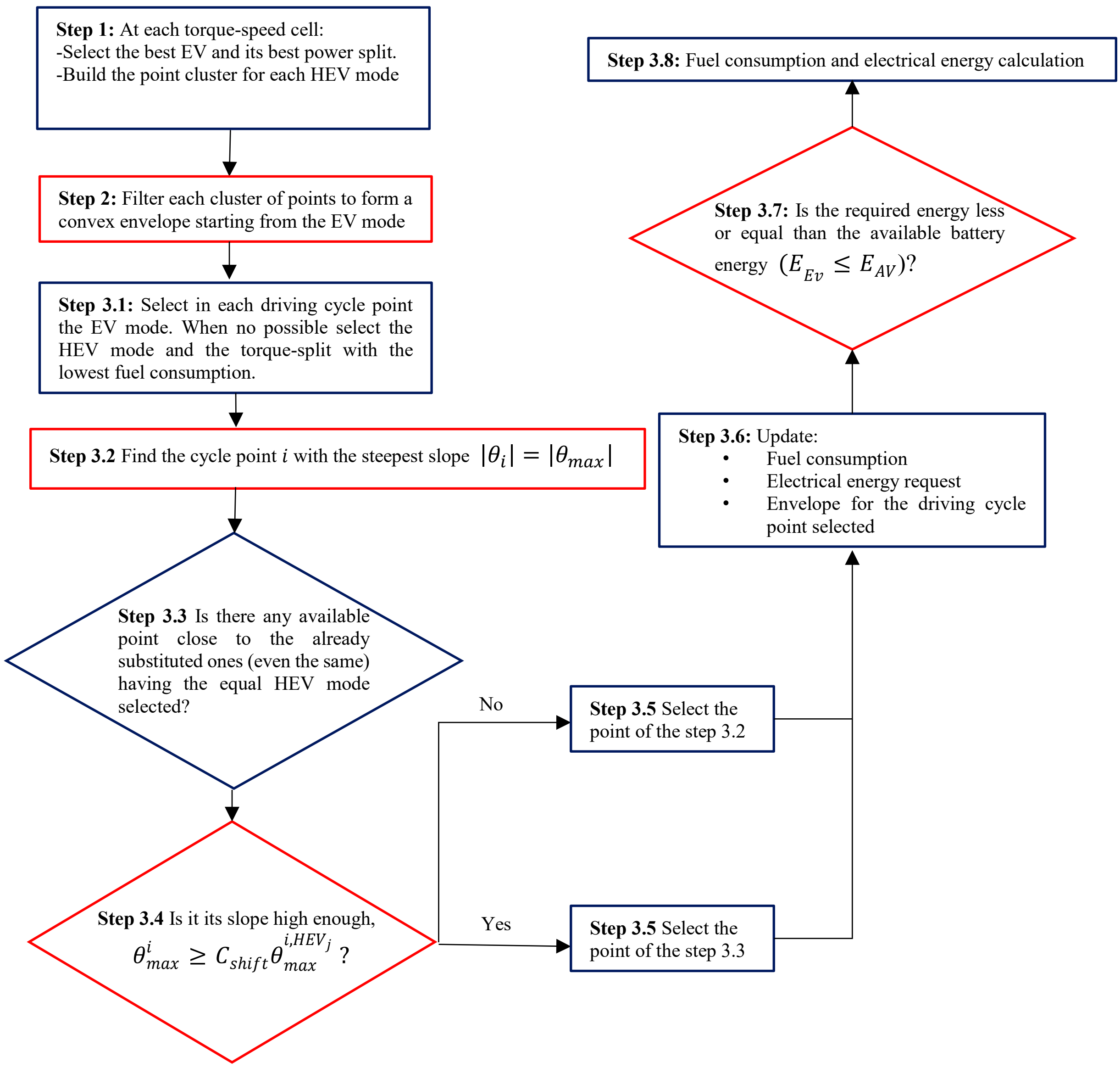

Figure 3.10 Flowchart SERCA algorithm multimode transmission

		PEARS (g)			SERCA (g)		
Nr.	**Modes**	**HWFET**	**UDDS**	**EFC**	**HWFET**	**UDDS**	**EFC**
1	3-4	664.05	341.7	486.7	648.1	327.4	471.7
2	22-71	828.6	411.3	599.0	736.5	321.3	508.1
3	92-98	646.4	331.9	473.5	621.8	312.1	451.5
4	112-116-122	**657.4**	367.0	**497.7**	**677.1**	358.8	**502.1**
5	3-6-75-78	638.3	391.0	502.3	612.8	354.3	470.6
6	3-40-98-108	649.1	**333.3**	**475.4**	624.1	**376.4**	**487.9**
7	3-75-78-113	**638.3**	397.6	505.9	**652.2**	355.6	489.1
8	3-4-112-113-114	**664.0**	341.7	**486.7**	**687.5**	336.1	**494.2**
9	77-92-98-108	640.6	332.2	471.0	618.7	308.3	448.0
10	112-113-114-116-122-123	657.4	**369.9**	**499.3**	647.0	**390.7**	**506.0**

Table 3.2 Comparison between PEARS and SERCA results

Driving cycle type	**Torque discretization (Driving cycle)**	**Speed discretization (Driving cycle)**	**Torque/Speed Sweep**	**Fuel mesh (SERCA)**
HWFET	100	85	50	50
UDDS	30	25	30	50

Table 3.3 Simulation parameters for PEARS and SERCA algorithm implementation

In bold are highlighted the topologies for which the PEARS strategy leads to better fuel consumption compared to SERCA. By observing these results referred to a small sample of possible topologies, it is possible to make some conclusions which can be extended to the entire results set. In some cases, the SERCA strategy might lead to better fuel economy and consequently to results closer to DP with a significantly lower computational cost compared with PEARS. However, the new strategy presents two main defects.

- In some cases, adding modes could worsen the fuel consumption instead of improving the transmission flexibility (e.g. results rows 1 and 8). The increase on HWFET (+6.1%) leads to results inaccuracies, finally changing the topologies rank which is the crucial output of the design activity. This issue might even occur for the PEARS evaluation (rows 3-10, 4-11, UDDS) but with an acceptable and contained growth (less than 1%).
- Some sensibility analysis performed have shown the presence of a strong dependency by two tuning factors: the number of intervals selected for torque and speed sweep and the amount of the steps adopted for meshing the fuel consumption. This dependency may lead to lack of consistency when increasing the mesh size is not beneficial for the results accuracy. Some example of the results variations with the tuning parameters on the UDDS driving cycle are reported in the following Figures.

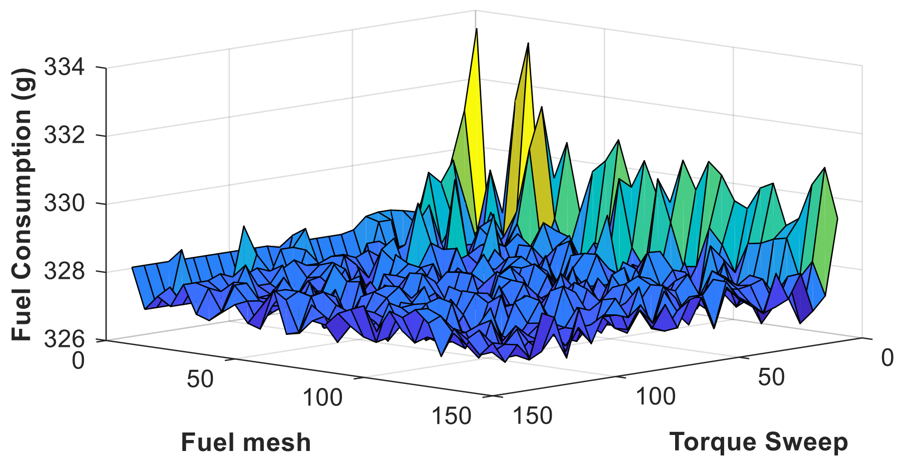

Figure 3.11 Tuning parameter dependency SERCA (UDDS), Topology Modes:3-4

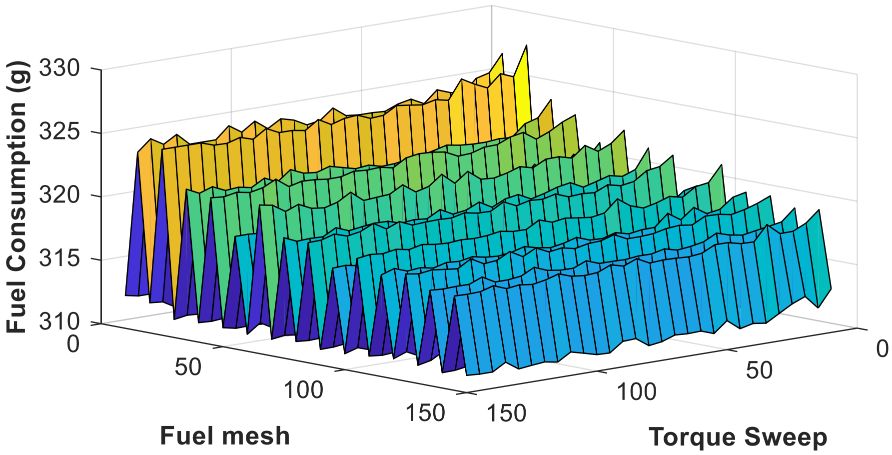

Figure 3.12 Tuning parameter dependency SERCA (UDDS), Topology Modes:92-98

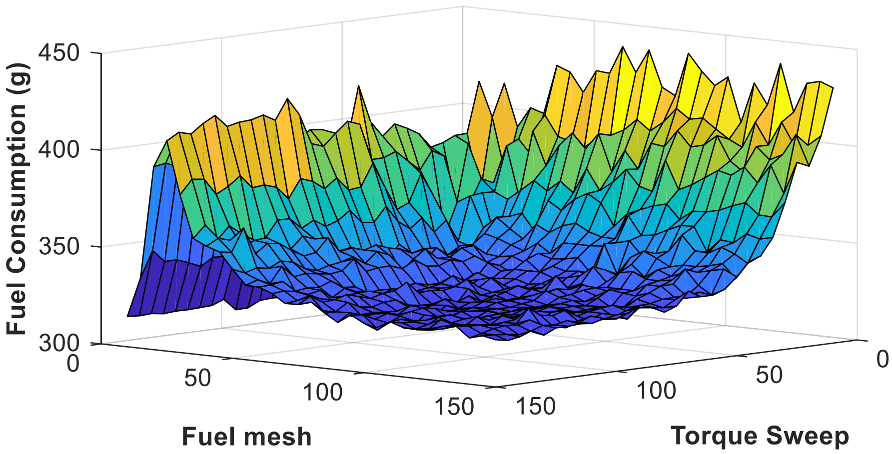

Figure 3.13 Tuning parameter dependency SERCA (UDDS), Topology Modes:3-6-75-78

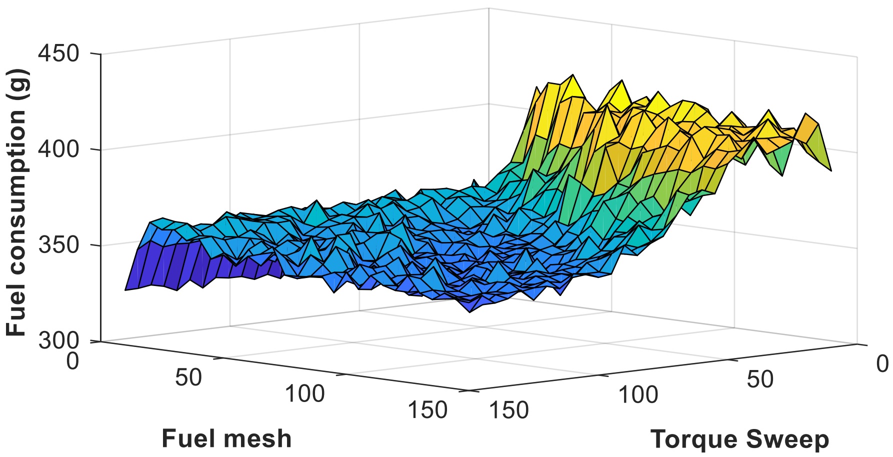

Figure 3.14 Tuning parameter dependency SERCA (UDDS), Topology Modes:3-40-98-108

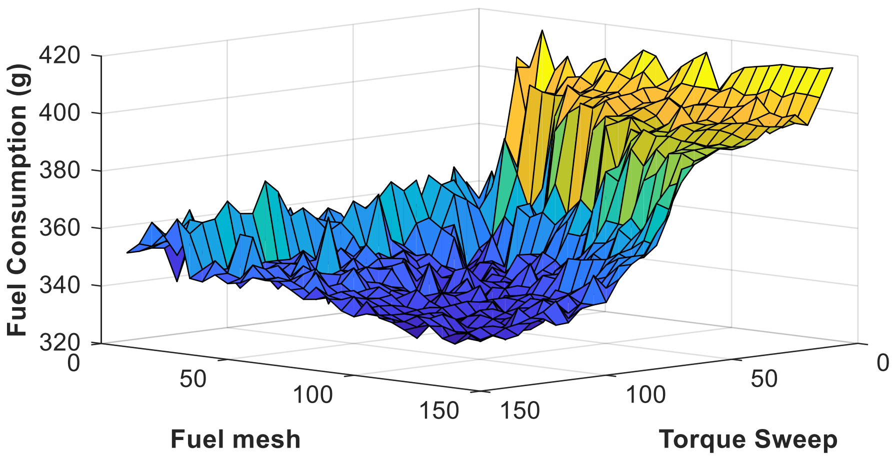

Figure 3.15 Tuning parameter dependency SERCA (UDDS), Topology Modes:3-75-78-113

The same results, previously shown in graphical form, are reported in Table 3.16 to underline the differences between the various topologies.

		Fuel consumption (g)				
Torque/Speed Sweep	**Fuel mesh**	**92-98**	**3-4**	**3-6-75-78**	**3-75-78-113**	**3-40-98-108**
10	55	312.5	328.7	342.8	323.6	318.5
10	60	312.8	328.3	340.2	**321.5**	319.3
10	100	312.6	328.2	344.2	326.2	312.0
10	105	312.6	328.2	352.6	328.5	**311.8**
25	10	328.1	331.7	406.9	391.1	415.6
40	30	312.8	327.7	355.4	370.8	340.3
50	50	311.5	327.9	342.6	353.7	342.0
60	20	312.9	**326.3**	399.3	416.5	396.7
90	90	311.4	327.0	336.8	342.5	322.8
110	140	311.4	327.7	338.4	346.9	326.0
115	140	318.0	327.2	**333.4**	342.3	325.5
140	80	311.5	327.6	356.4	363.1	329.1
150	130	**311.2**	328.2	341.4	349.2	325.5
Results Variability		16.9	7.4	84	105.2	129.6

Table 3.4 Mesh parameters dependency SERCA algorithm UDDS

The results bolded refer to the lowest fuel consumption achievable for each topology as function of the mesh parameters. It is important to notice how these minima occur for different values of the adjustable mesh factors. In other words, as anticipated, the parameters choice influences the results on the fuel economy side strongly compromising the choice of the best design candidates. This evidence is in contrast with the scope of the design activity for which, as mentioned in the previous paragraphs, the objective is to find an algorithm not dependent by any tuning factor. However, observing the proposed results, it is also central to notice the different tendencies for the dual mode transmission and for the multimode case. As a matter of fact, when only one HEV and one EV mode are present the results variability is acceptable (lower than 5%). For the multimode case, instead, the parameters of the mesh affect the fuel consumption to a larger extend (more than 30%). This consideration highlights the instability of the SERCA strategy in selecting the hybrid mode substitution.

3.9 SERCA$^+$ strategy

In the previous paragraphs two suitable energy management strategies for the design activity have been presented. Both are characterized by weakness and strength. In particular, PEARS is consistent but does not always show propinquity with the global optimum, while SERCA is fast but evidences a strong dependency by the mesh parameters. Consequently, the idea is to combine the two approaches to generate one unique strategy. The stability of PEARS can be used to determine the mode selection, while the stepwise procedure of SERCA can be applied to determine the power split (SERCA$^+$). By following are reported the step explaining the combined strategy.

STEP 1: Data preparation

In this step at each torque-speed cell the best EV mode and its relative power split are selected. Instead, as far as the HEV mode, the SERCA envelope is built and filtered. Subsequently, once the envelope is convex in each point of the construction the PEARS based efficiency (Equation 3.23) is computed. All the achievable HEV modes, for each driving cycle point are identified through their highest PEARS efficiencies. In fact, analysis conducted on the results sensibility have shown the robustness of this parameter in providing overall information about the operative modes.

STEP 2: PEARS mode selection

In this phase, for each driving cycle point, it is picked the HEV mode that might be selected in the substitution procedures. The choice is made on the base of the PEARS efficiency computed at the previous step. However, at the same time, to avoid an excessively frequent mode shifting, if the HEV mode selected at the previous driving cycle point is categorized by a high value of the average efficiency at the current output request, it is preferred to maintain the same operative mode (Equation 3.43).

$$If\ \eta_{j_{HEV_{best,\ j-1}}} \geq 90\%\, \eta_{j_{HEV_{best,\ j}}} \ \rightarrow\ mode_{\,HEV_j} = mode_{\,HEV_{j-1}} \tag{3.43}$$

Then as usual, at first, it is computed the total required electrical energy to complete the whole driving cycle in pure electric conditions, using the chosen HEV modes for the output demand at which no EV power split leads to a feasible solution.

STEP 3: Energy balance realization

The last step concerns the HEV modes substitution up to reaching CS conditions for the battery. Differently from the case of the SERCA extension to multi-mode powertrains, since the operative modes has already been selected in the Step 2 of the procedure, only a convex envelope is present at each driving cycle point output demand. The HEV modes are iteratively chosen for the replacement on the base of the steepest SERCA slope. In fact, the idea followed, as for the SERCA operations, is to select points capable to give the highest advantage relatively to the amount of fuel burnt. Furthermore, similarly to the case of the SERCA extension to the multi-mode case, during the mode substitution we try to discourage a frenetic mode shifting strategy looking at the slope values for points near or coincident to ones for which the same HEV mode has been already previously selected. Accordingly, if possible, after the comparison of the slope values, we prefer a more uniform mode selection. The SERCA$^+$ steps, which have been explained in this paragraph, are reported in graphical form in the flow chart of Figure 3.16.

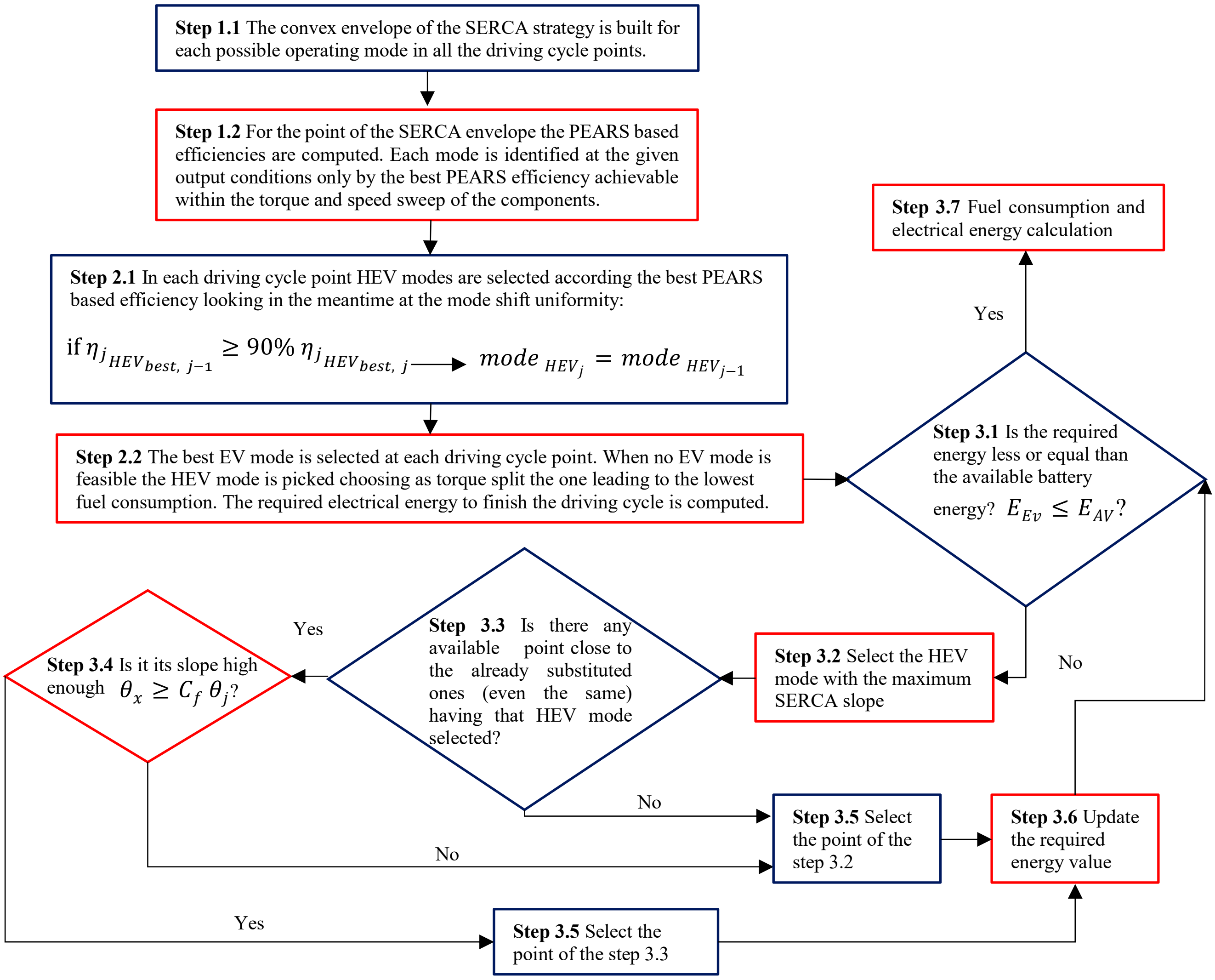

Figure 3.16 Flowchart SERCA⁺ algorithm

Subsequently, the SERCA$^+$ strategy has been implemented in the design activity. The results related to the same topologies previously reported are proposed in Table 3.5. As it is possible to notice, the fuel consumption values obtained are consistently always better if compared with the PEARS based ones. This conclusion holds for the whole design space.

		PEARS (g)			SERCA⁺ (g)		
Nr.	**Modes**	**HWFET**	**UDDS**	**EFC**	**HWFET**	**UDDS**	**EFC**
1	3-4	664.05	341.7	486.7	648.1	327.4	471.7
2	22-71	828.6	411.3	599.0	738.3	321.3	509.0
3	92-98	646.4	331.9	473.5	621.8	312.1	451.5
4	112-116-122	657.4	367.0	497.7	628.8	336.6	468.1
5	3-6-75-78	638.3	391.0	502.3	608.5	306.9	442.6
6	3-40-98-108	649.1	333.3	475.4	619.7	306.7	447.6
7	3-75-78-113	638.3	397.6	505.9	614.1	310.4	447.0
8	3-4-112-113-114	664.0	341.7	486.7	648.1	327.4	471.7
9	77-92-98-108	640.6	332.2	471.0	621.8	312.1	451.5
10	112-113-114-116-122-123	657.4	369.9	499.3	628.8	339.3	469.6

Table 3.5 Comparison between PEARS and SERCA⁺ results

Driving cycle type	Torque discretization (Driving cycle)	Speed discretization (Driving cycle)	Torque/Speed Sweep	Fuel mesh (SERCA)
HWFET	100	85	50	50
UDDS	30	25	30	50

Table 3.6 Simulation parameters for PEARS and SERCA⁺ algorithm implementation

To investigate the benefit of the new implementation regarding consistency and robustness behaviour, a study of the sensibility to the tuning parameters is performed. The results for the same topologies investigated with SERCA can be observed in the following Figures.

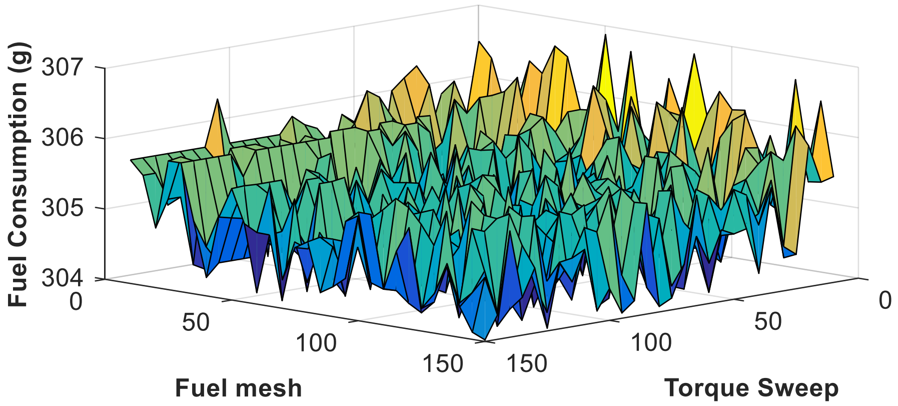

Figure 3.17 Tuning parameter dependency SERCA⁺ (UDDS), Topology Mode:3-6-75-78

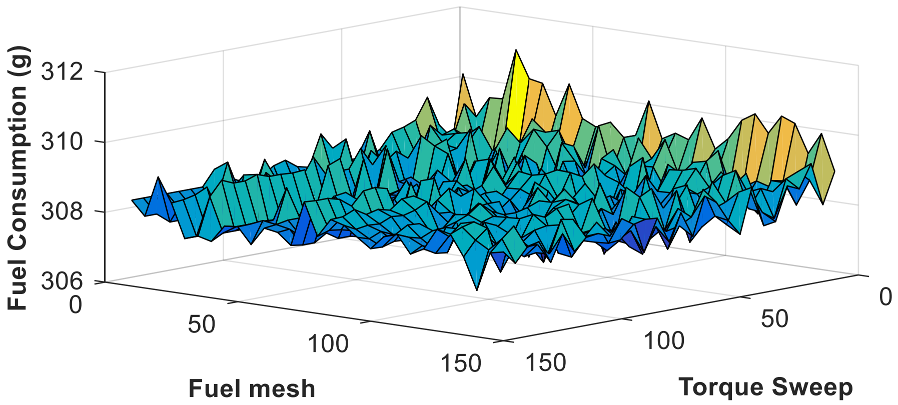

Figure 3.18 Tuning parameter dependency SERCA⁺ (UDDS), Topology Mode:3-40-98-108

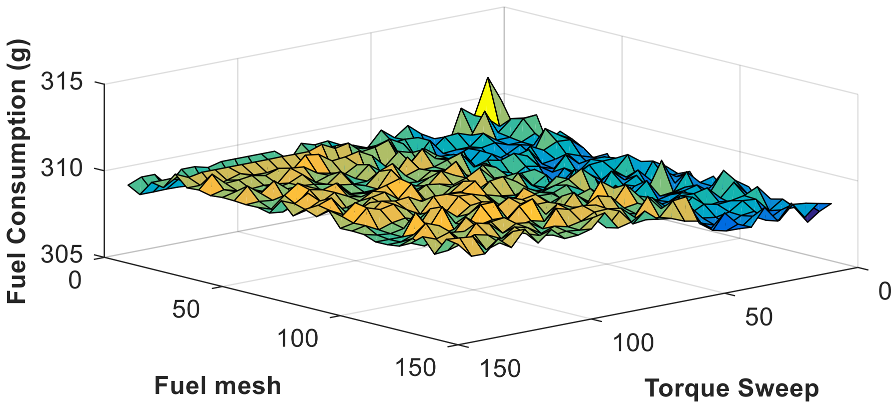

Figure 3.19 Tuning parameter dependency SERCA⁺ (UDDS), Topology Mode:3-75-78-113

Noticing the scale of the graphs, it is evident the contained results fluctuation compared to the SERCA strategy. To have a better perception, the same results are proposed in tabular form (Table 3.7), highlighting with the bold line the lowest fuel consumption obtainable as function of the tuning parameters.

		Fuel consumption (g)		
Torque/Speed Sweep	**Fuel mesh**	**3-6-75-78**	**3-75-78-113**	**3-40-98-108**
10	35	306.4	309.1	308.8
10	100	305.7	308.4	309.8
10	110	305.7	308.6	309.8
25	10	305.8	309.8	309.9
40	30	305.6	308.7	308.5
50	50	305.8	308.8	308.3
90	90	304.9	307.6	309.8
110	140	305.6	308.4	309.8
115	140	305.4	308.1	309.7
140	80	305.1	307.5	310.5
130	50	304.3	309.0	309.7
140	150	304.4	**307.3**	309.9
140	10	305.6	309.5	**307.6**
150	150	**304.0**	308.5	310.8
Results Variability		2.9	3.9	4.1

Table 3.7 Mesh parameters dependency SERCA$^+$ algorithm-UDDS

The results variability row clearly underlines the negligible dependency by the adjustable factors and consequently the overall consistency achieved by the new solution proposed. Furthermore, SERCA$^+$ offers great advantages in terms of lower computational effort. To obtain the fuel consumption results for the whole design space, the ATDT design tool needs roughly 72 hours using the PEARS strategy, while only almost 18 hours are needed with the SERCA$^+$ using the same driving cycle discretization parameters. This computational cost values have been obtained with a processor Intel® Core™ i7-6700 CPU 3.40GHz with 32 GB RAM. More generic results referred to different configurations obtained with ATDT are presented in the Chapter 4.

Chapter 4: Results and Future Work

In this chapter some significant results obtained with the SERCA$^+$ strategy introduced in the Chapter 3 are presented. Fist, the algorithm performances are shown for some powertrains coming from the state of art. Subsequently, a comparison among different control strategies is proposed for the Chrysler Pacifica and the Chevrolet II generation topologies. Moreover, the fuel consumption values for best and worst candidates generated for a given configuration with the SERCA$^+$ approach are compared with the ones obtained with another strategy called Greedy. Finally, research conclusions and achievements are discussed together with the project future work and objectives.

4.1 Analysis of Powertrains from state-of- art

In this section SERCA$^+$ is used as energy management strategy to determine the fuel consumption of three arrangement coming from the state-of-art [58]. The first is the Prius 2010^{++} which is a conceptual evolution of the Toyota Prius 2010 powertrain with the addition of three clutches [53]. The second and the third are respectively the Chevrolet Volt II generation [26] and the Chrysler Pacifica [28], which transmissions have been introduced in the Chapter 1. The three topologies are represented in the Figures below, while their PGs geometrical parameters are reported in the Table 4.1.

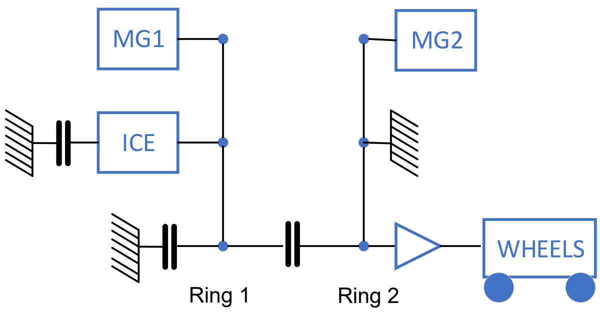

Figure 4.1 Prius 2010++ topology

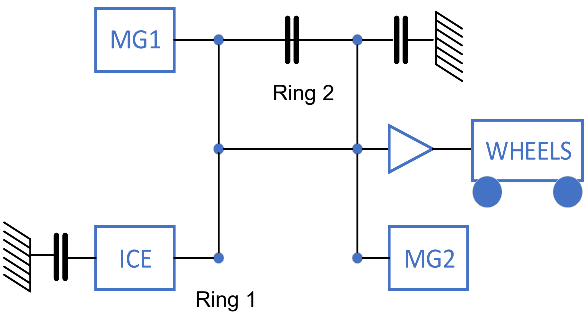

Figure 4.2 Chevrolet II generation topology

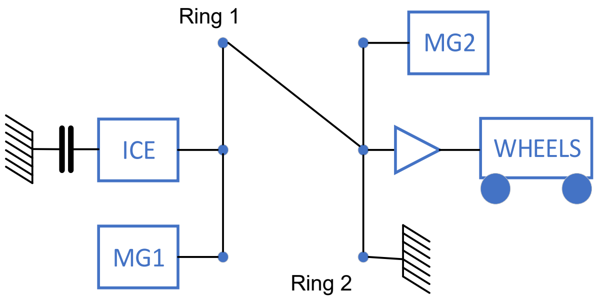

Figure 4.3 Chrysler Pacifica topology

	Ratio 1	Ratio 2	Final Drive
Prius 2010++	2.6	2.63	3.2
Chevrolet Volt II	1.87	2.077	2.64
Pacifica	3.15	1.59	3.59

Table 4.1 State-of-art PGs geometrical parameters

The predicted fuel consumption values obtained with SERCA^{+} in highway and urban driving conditions are presented in Table 4.2. It should be underlined that the results have been generated with the same powertrain components dimensions and maps presented in the Chapter 2. In fact, since the design tool is capable to generate any feasible arrangement, the aim is to evaluate the performances of the most popular powertrains for a hypothetic mini-van application. However, since powertrain position and gears parameters are choices intimately connected, the gears ratios are modified according the real vehicle values, as reported in the Table 4.2.

	HWFET		UDDS		EFC	
	g	L/100 Km	g	L/100 Km	g	L/100 Km
Prius 2010++	607.4	5.04	311.5	3.52	444.6	4.20
Chevrolet Volt II	641.0	5.32	314.5	3.56	461.4	4.35
Pacifica	621.8	5.16	312.1	3.42	451.5	4.20

Table 4.2 Estimated fuel consumption state-of-art powertrain (SERCA^{+})

The Chrysler Pacifica is the only minivan among the analysed vehicles. Therefore, its transmission results can be roughly compared with the real fuel consumption evaluated by the United States Environmental Protection Agency (EPA). Accordingly, the fuel economy in real condition stands at 32 mpg which corresponds to 7.35 L/100 km [59]. This value is almost 1.75 times lower compared to the amount predicted with the SERCA^{+}

strategy. In addition to the different maps and data, there are several possible reasons behind this diverge. First, despite a shifting coefficient has been introduced to penalize an excessively frequent mode shifting, the mode change losses are not properly taken into account in the algorithm implementation. Furthermore, other losses relate to the powertrain components have been neglected. Indeed, as exposed in the Chapter 2, the analysis performed for the design activity is a quasi-static one. Consequently, the transient phenomena have not been considered. Finally, since 2008 EPA has changed its fuel consumption estimation methodology adding three different tests in the analysis. They account respectively for the faster speed and acceleration rates, for the air conditioning use and for the cold temperature starting phases [60]. All these factors are expected to increase the fuel consumption to different extend. Furthermore, the significant gap among the values underlines the fundamental role assumed by the control strategy in the fuel consumption determination. For each powertrain arrangement investigated in this section the ATDT has been used to generate the complete set of topologies belonging to the same configuration preserving the geometrical gears' parameters. The results obtained are shown in Figure 4.4, where the circles identify the fuel consumption for the actual design, while the x-marks denote the averaged fuel consumption of the candidates for which changing clutches and connections has been beneficial. As already mentioned before, the simulation results do not refer to the real vehicles specifics but only to the powertrain arrangements. In fact, the purpose of this comparison is to show that for any possible application, there is a potentially large space to improve the design. Consequently, we expect a significative amount of design candidates capable to improve the fuel economy performances. As summarized in the Table 4.3, these topologies represent a consistent fraction of the generated candidates. Despite the vehicle data are referred to a typical minivan application it is interesting to notice the large amount of solutions which might improve the Chrysler Pacifica powertrain. The reason behind this evidence can be found in the limited number of modes realized by the actual vehicle. On the other hand, for the Prius 2010^{++} topology, although the different powertrain components and vehicles sizes, a reduced part of solutions features better fuel economy. This evidence can be justified considering that the discussed design already represents an improved version of the original arrangement.

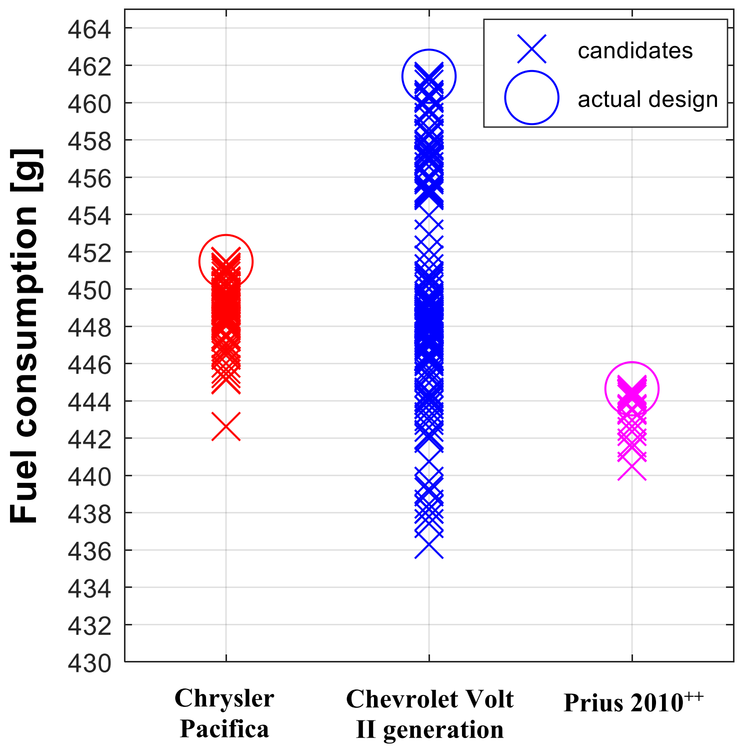

Figure 4.4 Possible candidates improving the state-of-art powertrains topologies

	Prius 2010^{++}	Chevrolet Volt II	Chrysler Pacifica
Topologies total	406	452	508
Topologies better fuel	51 (12.6 %)	186 (41.1 %)	104 (20.5 %)

Table 4.3 Outlook of the state-of-art topologies possible improvement

4.2 Case of Study: Chrysler Pacifica Powertrain

To achieve a first validation of the quality of the results produced by the tool we refer to the DP optimal benchmark. As first, we present a case of study concerning the analysis the Chrysler Pacifica design since, as already mentioned, the data used for the simulation are referred to a representative minivan powertrain. The modes achievable with the Pacifica arrangement are reported by following together with the static equation implemented to express the components torque and speed.

EV MODE (2MGU-1DOF)

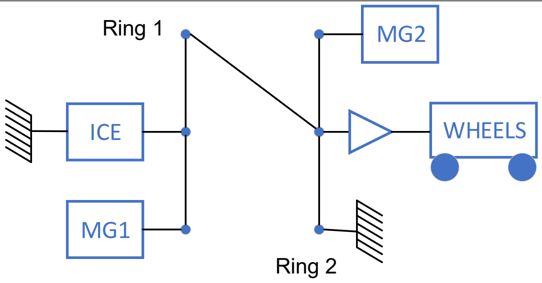

$$\omega_{MG1} = -\omega_{OUT}\, r_1$$

$$\omega_{MG2} = \omega_{OUT}(1 + r_2)$$

$$T_{MG2} \;\; swept$$

$$T_{MG1} = \frac{-T_{OUT} + T_{MG2}(1 + r_2)}{r_1}$$

HEV MODE (INPUT-SPLIT)

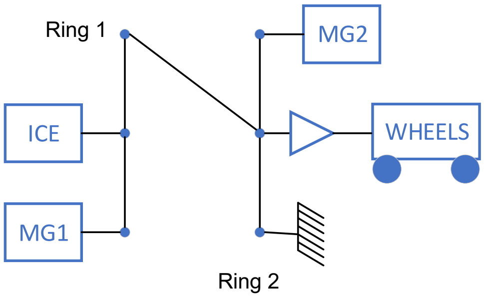

$$\omega_{ICE} \;\; swept$$

$$\omega_{MG1} = \omega_{ICE}(1 + r_1) - \omega_{OUT}\, r_1$$

$$\omega_{MG2} = \omega_{OUT}(1 + r_2)$$

$$T_{ICE} \;\; swept$$

$$T_{MG1} = \frac{-T_{ICE}}{1 + r_1}$$

$$T_{MG2} = \frac{T_{OUT} - T_{ICE}\dfrac{r_1}{1 + r_1}}{1 + r_2}$$

To generate the DP results it has been used a general-purpose tool developed at ETH of Zurich [44]. Among the different options, the method used to deal with the state final constraint is the boundary line [61]. The results obtained with the DP are compared with the ones based on PEARS, SERCA^{+} and Greedy strategies. The Greedy algorithm is a simple approach minimizing at each time step the cumulative cost function obtained considering several working points defined by power split and selected mode. The local cost function on which the algorithm is based is reported below in the Equation 4.1.

$$J_{x_k \in X(t)}(t) = m_f(t) + \alpha(\Delta SOC) + J_{x_j \in X(t-1)}(t-1) \tag{4.1}$$

$J_{x_k \in X(t)}(t)$ represents the cost for reaching the point x_k belonging to the set of feasible point at the current time t, starting from the point x_j, which denotes the local optimum solution at the previous time step. The comparison of the results as fuel consumption and battery SOC for the four strategies are plotted in Figure 4.5.

In Table 4.4, instead, we synthetically report the final values of fuel consumption and the required computational effort.

	HWFET		**UDDS**	
	Fuel cons. (g)	**Comp. Cost**	**Fuel cons. (g)**	**Comp. Cost**
DP	614.6	4.2 h	306.1	2 h
Greedy	618.8	216 s	310.8	298 s
***SERCA$^+$**	621.8	2.4 s	312.1	2.5 s
***PEARS**	646.4	10.1 s	331.9	11.4 s

*Table 4.4 Strategies comparison for Chrysler Pacifica Topology (*Results obtained with ATDT)*

Before commenting the simulation outcome, it is worth to notice that for a dual mode application the SERCA and SERCA$^+$ algorithms generate the same results with a difference only in the computational cost. In fact, there is no need to evaluate the PEARS based efficiencies when only one HEV mode is present. However, the scope of the comparative analysis is to demonstrate what has been asserted in the Chapter 3. In fact, the PEARS strategy is clearly an outlier with an uncontrolled management of the battery SOC. Contrarily, the slope method shows a good level of suboptimality. For the studied driving cycles the difference with DP is around 2% and 1.2 % respectively for UDDS and HWFET. On the other hand, the PEARS low performances can be explained by the lower amount of information used. Finally, another noticeable characteristic of the strategy is the advantageous computational cost.

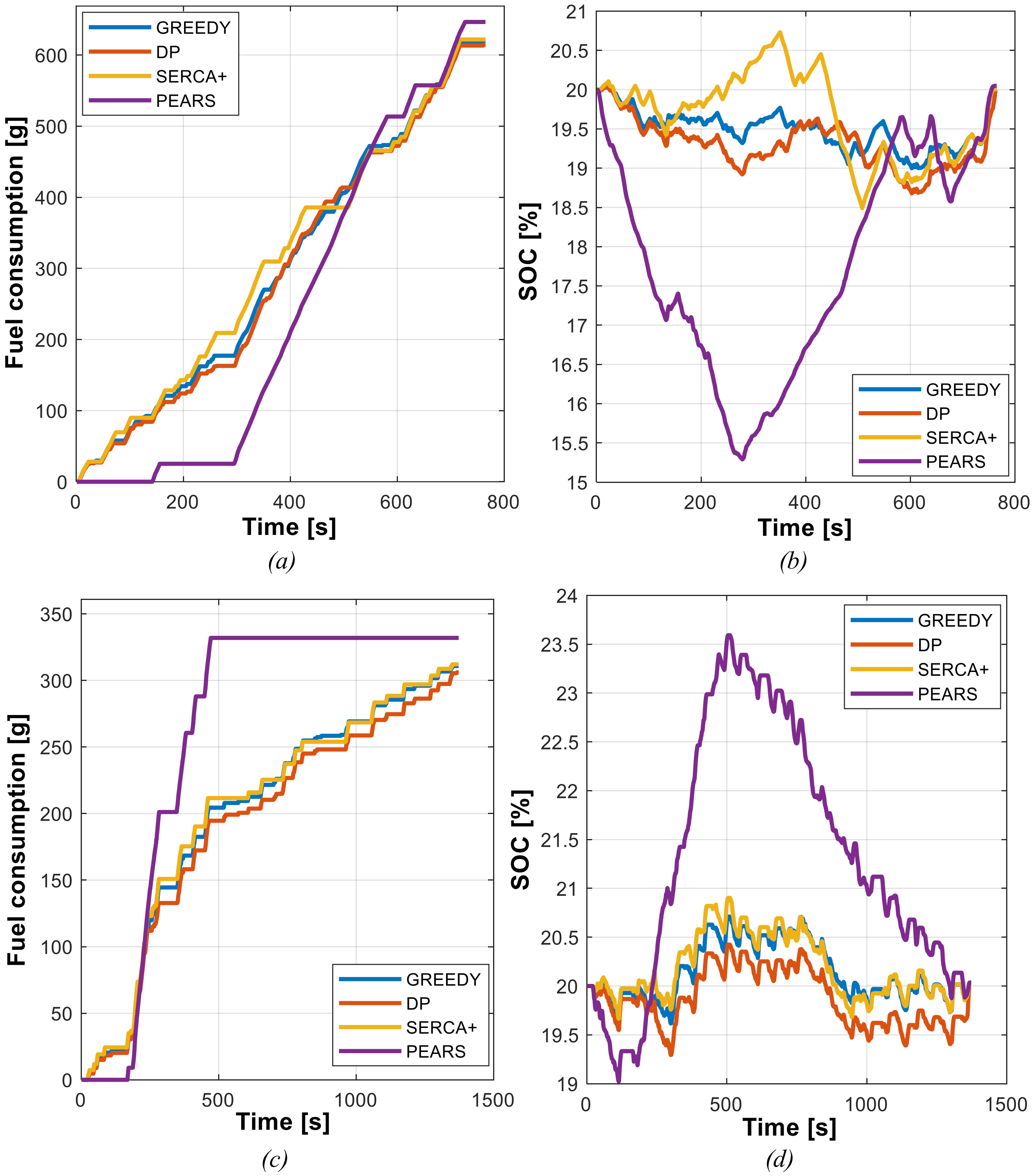

(a) *(b)* *(c)* *(d)*

Figure 4.5 Strategies comparison for Chrysler Pacifica Topology, (a)-(b) HWFET, (c)-(d), UDDS

4.3 Case of Study: Chevrolet Volt II generation topology

Since the SERCA and SERCA$^+$ algorithms approach is conceptually the same for the case of a dual mode transmission, it is chosen to investigate the design of the General Motors Chevrolet Volt II generation. Once more, the data used for the simulation are not related to the real vehicle model. Furthermore, for the analysis we consider all the modes achievable by this type of design regardless the actual implementation in the commercial application, illustrated in the Chapter 1. By following are reported the operative modes representation together with the static equations of the modes torque and speed.

EV MODE (2MGU-2DOFs)

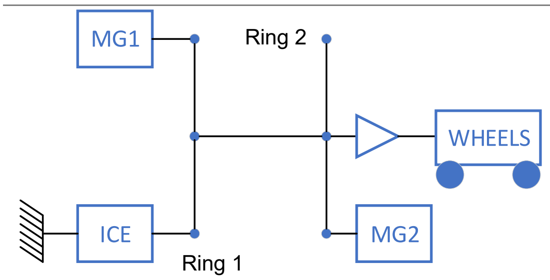

$$\omega_{MG2}\ swept$$

$$\omega_{MG1} = \omega_{OUT}\ (1 + r_1)$$

$$T_{MG2}\ swept$$

$$T_{MG1} = \left(T_{OUT} - T_{MG2}(1 + r_2)\right)\left(\frac{1}{1 + r_1}\right)$$

EV MODE (2MGU-1DOF)

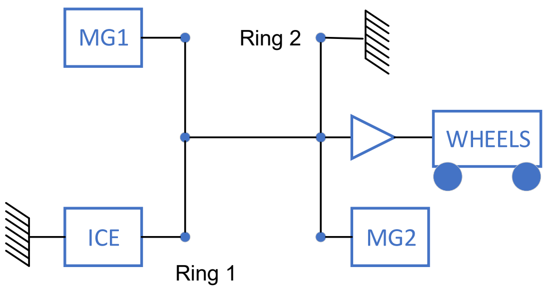

$$\omega_{MG2} = \omega_{OUT}\ (1 + r_2)$$

$$\omega_{MG1} = \omega_{OUT}\ (1 + r_1)$$

$$T_{MG2}\ swept$$

$$T_{MG1} = \left(T_{OUT} - T_{MG2}(1 + r_2)\right)\left(\frac{1}{1 + r_1}\right)$$

EV MODE (2MGU-1DOF)

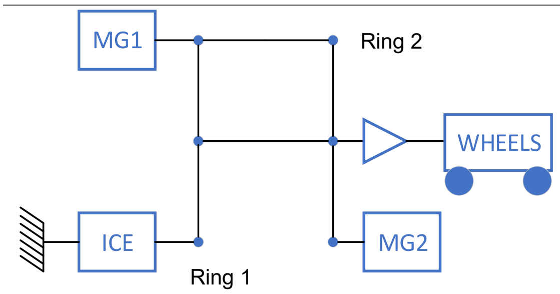

$$\omega_{MG1} = \omega_{OUT}\ (1 + r_1)$$

$$\omega_{MG2} = \omega_{OUT}\ (1 + r_2) - \omega_{MG1}\ r_2$$

$$T_{MG2}\ swept$$

$$T_{MG1} = \left(T_{OUT} - T_{MG2}(1 + r_2)\right)\left(\frac{1}{1 + r_1}\right) + T_{MG2}\ (1 + r_2)\ /\left(1 + \frac{1}{r_2}\right)$$

HEV MODE (INPUT-SPLIT)

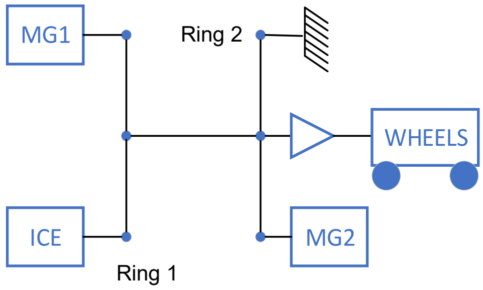

$$\omega_{MG2} = \omega_{OUT}\,(1 + r_2)$$

$$\omega_{ICE}\ swept$$

$$\omega_{MG1} = \omega_{OUT}\,(1 + r_1) - \omega_{ICE}\, r_1$$

$$T_{ICE}\ swept$$

$$T_{MG1} = \frac{T_{ICE}}{r_1}$$

$$T_{MG2} = \left(T_{OUT} - T_{MG1}(1 + r_1)\right)\left(\frac{1}{1 + r_2}\right)$$

HEV MODE (PARALLEL FIXED GEAR-1MGU)

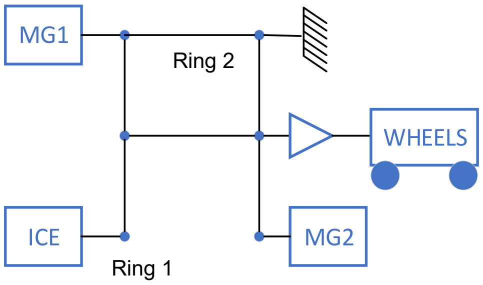

$$\omega_{MG2} = \omega_{OUT}\,(1 + r_2)$$

$$\omega_{ICE} = \omega_{OUT}\,\left(1 + \frac{1}{r_1}\right)$$

$$T_{ICE}\ swept$$

$$T_{MG2} = \left(T_{OUT} - T_{ICE}\left(1 + \frac{1}{r_1}\right)\right)\left(\frac{1}{1 + r_2}\right)$$

HEV MODE (COMPOUND SPLIT-2DOFs)

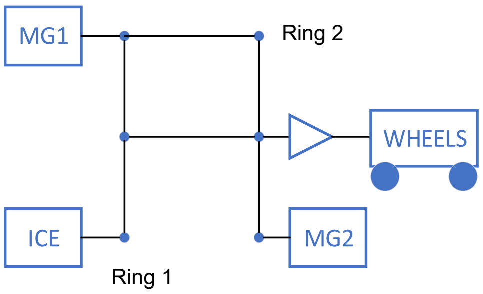

$$\omega_{ICE}\ swept$$

$$\omega_{MG1} = \omega_{OUT}\,(1 + r_1) - \omega_{ICE}\, r_1$$

$$\omega_{MG2} = \omega_{OUT}\,(1 + r_2) - \omega_{MG1}\, r_2$$

$$T_{ICE}\ swept$$

$$T_{MG1} = \frac{T_{ICE}}{r_1}\left(1 - \frac{1 + r_1}{1 + r_2}\right) + \frac{T_{OUT}}{1 + r_2}$$

$$T_{MG2} = \left(T_{OUT} - T_{ICE}\,\left(1 + \frac{1}{r_1}\right)\right)\left(\frac{1}{1 + r_2}\right)$$

The results obtained comparing DP, Greedy, PEARS and SERCA^{+} strategies are presented in the Table 4.5 and in the Figure 4.6. As for the analysis of the Chrysler Pacifica, it is evident the advantage of the proposed methodology in terms of computational cost over the other EMS proposed in the study. On the fuel consumption side, in this case the difference for the UDDS case is only 1.5%, while it reaches 8.1 %

in HWFET. These results obtained in a six modes application confirm the value of the proposed approach for the design activity.

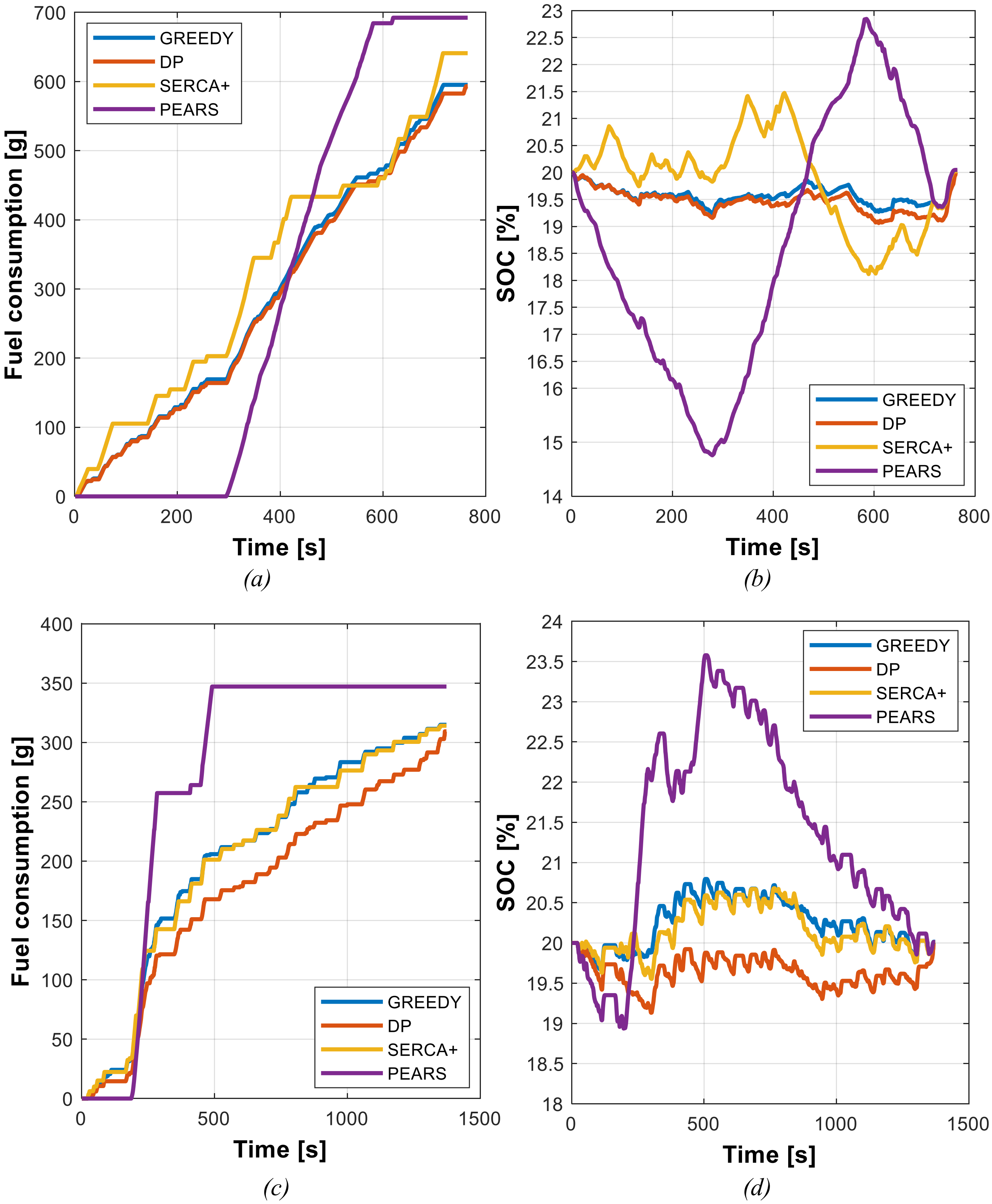

Figure 4.6 Strategies comparison for Chevrolet Volt II generation Topology, (a)-(b) HWFET, (c)-(d), UDDS

	HWFET		UDDS	
	Fuel cons. (g)	Comp. Cost	Fuel cons. (g)	Comp. Cost
DP	593.2	8.2 h	309.4	4.6 h
*Greedy	595.2	112.3 s	314.9	74.6 s
*SERCA$^+$	641.0	1.4 s	314.1	1.2 s
*PEARS	692.3	5.1 s	347.1	3.5 s

*Table 4.5 Strategies comparison for Chevrolet Volt II generation Topology (*Results obtained with ATDT)*

4.4 Discussion of the design tool results

In this paragraph we propose a comparison between the SERCA$^+$ and the Greedy algorithms. The results refer to the best and worst topologies generated with ATDT for the topologies belonging to the same configuration of the Chrysler Pacifica (Table 4.6 and 4.7). The aim of the comparison is to have an overview related to to the quality of the results generated. For both strategies, as usual, the reference driving cycles are HWFET and UDDS.

		SERCA$^+$ (g)			GREEDY (g)		
Nr.	Modes	HWFET	UDDS	EFC	HWFET	UDDS	EFC
1	3-6-75-78	608.5	306.9	442.6	613.3	301.2	441.7
2	96-98-102-104-108	620.2	301.8	445.1	631.2	313.1	456.2
3	74-75-76-83-84	613.6	307.3	445.2	614.6	312.7	448.5
4	10-11-12-117-118	608.6	312.0	445.4	644.3	325.3	468.8
5	10-11-12-69-70	609.0	312.1	445.7	626.6	332.5	464.8
6	74-76-77-79	614.2	308.4	446.0	619.5	313.5	451.2
7	10-11-12-69-117	609.0	313.5	446.4	644.1	331.9	472.4
8	96-98-99-101-108	619.7	304.7	446.4	625.4	315.6	455.0

9	3-35-65-108-110	614.0	309.0	446.6	609.3	310.1	444.8
10	3-76-88-98-108	620.2	304.7	446.7	623.3	307.3	449.5

Table 4.6 Comparison of the 10 best SERCA⁺ topologies with Greedy strategy

		SERCA⁺ (g)			**GREEDY (g)**		
Nr.	Modes	HWFET	UDDS	EFC	HWFET	UDDS	EFC
1	74-75-76	1236.7	404.9	779.2	810.7	373.6	570.3
2	74-76-81	1195.2	373.3	743.2	810.6	373.6	570.3
3	16-74-76	1005.9	362.4	652.0	810.7	373.6	570.3
4	3-64	977.2	340.4	626.9	989.4	347.1	636.1
5	74-76	900.9	351.1	598.5	813.7	377.2	573.6
6	11-69	928.6	325.4	596.8	938.8	338.1	608.4
7	3-11-69	928.6	325.4	596.8	931.7	325.7	598.4
8	10-11-69	928.6	325.4	596.8	938.8	338.0	608.4
9	11-66-69	928.6	325.4	596.8	936.5	335.0	605.7
10	10-11-13-69	928.6	325.4	596.8	938.8	338.0	608.4

Table 4.7 Comparison of the 10 worst SERCA⁺ topologies with Greedy strategy

An initial important observation is that none of the two methods can be generally identified as better in terms of suboptimality level. As matter of fact, alternatively either one or the other strategy predict a lower amount of fuel consumption. Nevertheless, both generate values reasonably close, which consequently allow to obtaining a near ranking of the candidates. This conclusion is crucial because this type of design tool requirement is to identify the most promising topologies independently by the fuel economy predicted, as it has been stated at the beginning of the dissertation. Thus, the purpose of the comparison is to demonstrate that the best and the worst topologies according the

SERCA$^+$ evaluation are similarly judged by another control strategy. However, once more, it is also central to notice the difference in the computational cost. Indeed, SERCA$^+$ is more than 300 times faster as running time than GREEDY. Another fundamental observation is referred to the best topologies, which are characterized by additional achievable modes when compared to the worst candidates. This consideration confirms the improvement on the flexibility side potentially obtainable increasing the number of clutches and justifies the interest towards this research activity. In fact, it is intuitive to recognise that the higher cost of the transmission needs to be balanced with the lower fuel expenses.

Figure 4.7 reports the averaged fuel consumption values foreseen related to the whole set of results generated with the ATDT for the topologies of the Chrysler Pacifica configuration. The reduced span of the histogram (17 grams) evidences the large amount of the design solutions characterized by nearby values of fuel consumption.

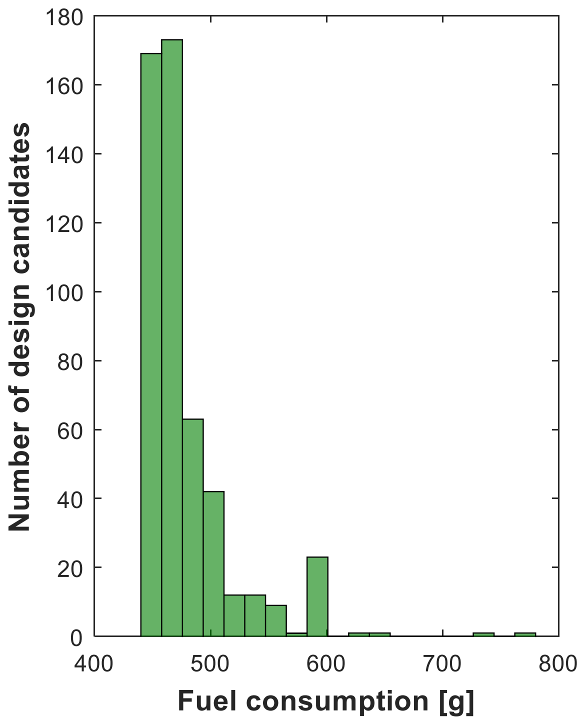

Figure 4.7 Combined fuel consumption results for topologies belonging to the Pacifica configuration

This evidence and the previous comparative analysis suggest the following conclusions:

- The fuel consumption cannot evidently be the only design criterion. To decide the proper architecture, the evaluation of other parameters as the pollutant emissions and the vehicle performances is fundamental.
- Being a large part of the design space compressed in a narrow band in terms of fuel economy the proper selection would necessitate a more precise evaluation of the mode shifting losses. It is crucial to point out the impact that they have on the powertrains is very different depending on the operative modes. For example, in some previous research [39] to have a rough estimation of the different cost, the shifting losses have been first divided in direct and indirect, according whether an intermediate mode is required for the mode change. Additionally, the direct mode shifting has been separated in conditional and unconditional dependently on the way on which the clutch speed requirement is met. If only clutch disengaging operation are required, the mode shifting is said to be direct unconditional. Similar criteria can be implemented in ATDT to make the selection more accurate. Furthermore, a precise model would be needed for the powertrain components and, in general, for the whole vehicle.
- The current version of the design tool can be used for a reverse purpose. Instead of selecting the most suitable topologies among the design space it can be used with the aim of reducing the outlier candidates. This reduction would allow more precise evaluation of the remaining arrangements.

As matter of example, we have added to the results of the previous histogram the engine starting phases (Figure 4.8). First, we have avoided frequent on-off switches, leaving the engine running if the gap between two consecutive start events was less than four seconds. Subsequently, we have introduced the start event at the time steps preceding the ones at which the engine power was needed. As shown in the new histogram distribution, also simple and practical considerations create an appreciable gap among the alternatives, reducing the candidates in the first bin.

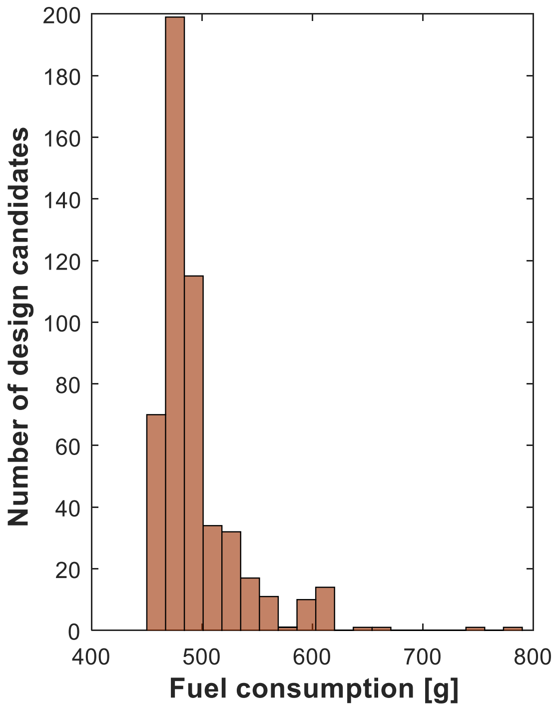

Figure 4.8 Combined fuel consumption results for topologies belonging to the Pacifica configuration with ICE start events

4.5 Conclusion and future work

In this thesis a design methodology for multimode power split HEV has been presented. The motivation behind this study relies in the advantages and flexibility of this hybrid category. A huge pool of design alternatives exists when choosing the component positions and the node connections. Many of these candidates are unexplored and, therefore, there might be topologies capable to improve the vehicle fuel consumption, performances and emissions. This was the drive behind the study and the improvement of a code called "Analytical Transmission Design Tool" (ATDT).

The main personal contributions of this research are listed by follow.

- Implementation of practical considerations to speed up the ATDT.
- Extension of the SERCA algorithm procedures to the multimode case and related implementation in ATDT.
- Introduction of the SERCA$^+$ strategy and application in ATDT.

In particular, the SERCA$^+$ methodology is the main intellectual achievement of this dissertation. This new EMS uses the PEARS algorithm to select the operative mode and the SERCA slope to decide the power-split. The SERCA$^+$ approach has been proven in the case of studies to reach results nearby the benchmark identified by DP. However, a full validation of the strategy is not obtainable since it would require the comparison with DP for all the design candidates.

Furthermore, since numerous arrangements are present, many of them are labelled by adjacent values of fuel economy. This evidence does not allow to use the ATDT for the selection of the best design alternative.

Consequently, the tool can be used in the first phase of a cascade design process to drastically squeeze the design space dimension. In fact, the most important benefit of the proposed procedure is the extremely low computational cost required for the simulation.

In fact, the reduction of the number of design alternatives allow the use of more sophisticated algorithms and model for the further selection. In the successive steps of the design activity, it will be crucial to introduce a precise evaluation of the mode shifting losses. At that stages, it will not be possible anymore to apply fast strategies as PEARS or SERCA. Additionally, it will be required to evaluate the components dynamic behaviour, especially for the ICE. In fact, the transient phenomena might affect the fuel economy to a large extend.

Finally, it will be essential to focus on parameters beyond the fuel economy considering for example vehicle performances and pollutant emissions. In this scenario, the new concept of Real Driving Emissions (RDE) will require analysis of the solution dependency from the driving cycles implemented in the simulation activity.

Bibliography

[1] A. Emadi, «Transportation 2.0,» *IEEE Power & Energy Magazine,* vol. 9, pp. 18-29, 2011.

[2] «Standards, A Brief History of U.S. Fuel Efficiency,» [Online]. Available: https://www.ucsusa.org/clean-vehicles/fuel-efficiency/fuel-economy-basics.html#.W-2JgpNKjIU.

[3] N. Hooftman, M. Messagie, J. Van Mierlo e T. Coosemans, «A review of the European passenger car regulations – Real driving emissions vs local air quality,» *Renewable and Sustainable Energy Reviews,* vol. 89, pp. 1-21, 2018.

[4] «cars, Reducing C02 emission from passengers,» [Online]. Available: Available:https://ec.europa.eu/clima/policies/transport/vehicles/cars_en#tab-0-0.

[5] C. Chan, «The State of the Art of Electric, Hybrid, and Fuel Cell Vehicles,» *Proceedings of the IEEE,* vol. 95, pp. 704-718, 2007.

[6] «Lohner-Porsche Mixte Voiturette,» [Online]. Available: https://www.ultimatecarpage.com/car/3456/Lohner-Porsche-Mixte-Voiturette.html.

[7] A. Emadi, K. Rajashekara, S. S. Williamson e S. Lukic, «Topological Overview of Hybrid Electric and Fuel Cell Vehicular Power System Architectures and Configurations,» *Vehicular Technology, IEEE Transactions,* vol. 54, pp. 763-770, 2005.

[8] B. Bilgin, P. Magne, P. Malysz, Y. Yang, V. Pantelic, M. Preindl, A. Korobkine, W. Jiang, M. Lawford e A. Emadi, «Making the Case for Electrified Transportation,» *IEEE Transactions on Transportation Electrification,* vol. 1, pp. 4-17, 2015.

[9] S. Lukic e A. Emadi, «Effects of Drivetrain Hybridization on Fuel Economy and Dynamic Performance of Parallel Hybrid Electric Vehicles,» *Vehicular Technology, IEEE Transactions ,* vol. 53, pp. 385 - 389, 2004.

[10] Y. Guezennec e G. Rizzoni, «Optimal Energy Management in Series Hybrid Electric Vehicles,» in *American Control Conference (ACC)*, Chicago, IL, 2000.

[11] S. Barsali, C. Miulli e A. Possenti, «A Control Strategy to Minimize Fuel Consumption of Series Hybrid Electric Vehicles,» *IEEE Transactions on Energy Conversion,* vol. 19, n. 1, pp. 187-195, 2004.

[12] G. Song e G. Yan, «Study on Power Train Parameters Matching of Series Hybrid City Bus,» in *IEEE International Conference on Vehicular Electronics and Safety*, Shanghai, 2006.

[13] Y. Yang, K. Arshad-Ali, J. Roeleveld e A. Emadi, «State-of-the-art electrified powertrains – hybrid, plug-in, and electric vehicles,» *Int. J. Powertrains,* vol. 5, n. 1, pp. 1-29, 2016.

[14] S. Delprat, J. Lauber, T. Guerra e J. Rimaux, «Control of a parallel hybrid power train: Optimal control,» *IEEE Transactions on Vehicular Technology,* vol. 53, n. 3, p. 872–881, 2004.

[15] A. Sciarretta, M. Back e L. Guzzella, «Optimal control of parallel hybrid electric vehicles,» *IEEE transactions on Control System Technology,* pp. 352-363, 2004.

[16] X. Zeng e J. Wang, in *Analysis and Design of the Power-Split Device for Hybrid Systems*, 2017.

[17] J. M. Miller, «Hybrid electric vehicle propulsion system architectures of the e-CVT type,» *IEEE Transactions on Power Electronics,* vol. 21, n. 3, pp. 756-767, 2006.

[18] T. A. Burress, S. L. Campbell, C. Coomer, C. W. [. Ayers, A. A. [. Wereszczak, J. P. Cunningham, L. D. Marlino, L. E. Seiber e H.-T. Lin, «Evaluation of the 2010 Toyota Prius Hybrid Synergy Drive System,» Oak Ridge National Lab. (ORNL), Oak Ridge, TN (United States). Power Electronics and Electric Machinery Research Facility, 2011.

[19] A. Kawahashi, «A new-generation hybrid electric vehicle and its supporting power semiconductor devices,» in *Proceedings of the 16th International Symposium on Power Semiconductor Devices and ICs*, Kitakyushu, Japan, Japan, 2004.

[20] B. Conlon, «Comparative analysis of single and combined hybrid electrically variable transmission operating modes,» in *SAE World Congress*, Detroit, MI, 2005.

[21] «Global Car Sales Analysis 2017,» [Online]. Available: http://carsalesbase.com/global-car-sales-2017/.

[22] M. R. Schmidt, D. Klemen, L. T. Nitz e A. G. Holmes, «Two-Mode, Compound-Split Hybrid Electro-Mechanical Transmission having Four Fixed Ratios». U.S. Brevetto 6953409, October 2005.

[23] Y. Yang e A. Emadi, «Integrated electro-mechanical transmission systems in hybrid electric vehicles,» in *IEEE Vehicle Power and Propulsion Conference*, Chicago, IL, 2011.

[24] M. Miller, A. G. Holmes, B. M. Conlon e P. J. Savagian, «The GM "Voltec" 4ET50 Multi-Mode Electric Transaxle,» in *SAE 2011 World Congress and Exhibit*, Detroit, MI, 2011.

[25] N. Kim, J. Kwon e A. Rousseau, «Comparison of Powertrain Configuration for Plug-in HEVs from a Fuel Economy Perspective,» in *SAE 2012 World Congress & Exhibition*, Detroit, MI, 2012.

[26] «Gen 2 Volt Transmission Operating Modes Explained,» [Online]. Available: https://gm-volt.com/2015/02/20/gen-2-volt-transmission-operating-modes-explained/.

[27] «Deep Inside the Chrysler Pacifica hybrid system,» [Online]. Available: https://www.allpar.com/mopar/transmissions/hybrid-automatic.html .

[28] M. Pittel e D. Martin, «eFlite Dedicated Hybrid Transmission for Chrysler Pacifica,» in *WCX World Congress Experience*, Detroit, MI, 2018.

[29] Karlsson, Hammarström, Sörensen e Eriksson, «Road surface influence on rolling resistance: coastdown measurements for a car and an HGV,» Swedish Road Administration, VTI, 2011.

[30] P. G. Anselma, Y. Huo, J. Roeleveld, G. Belingardi e A. Emadi, «Slope-weighted Energy-based Rapid Control Analysis for Hybrid Electric Vehicles,» *Submitted to: IEEE Transactions on Vehicular Technology,* 2018.

[31] J. Liu e H. Peng, «Control optimization for a power-split hybrid vehicle,» in *American Control Conference*, Minneapolis, MN, 2006.

[32] H. Benford e M. Leising, «The Lever Analogy: A New Tool in Transmission Analysis,» in *SAE International Congress and Exposition*, 1981.

[33] Z. Weichao, Y. D. Xiaowu Zhang, W. Liangmo e H. Xiaosong, «Comparison of multi-mode hybrid powertrains with multiple planetary gears,» *Applied Energy,* vol. 178, pp. 624-632, 2016.

[34] X. Zhang, H. Peng, J. Sun e S. Li, «Automated Modeling and Mode Screening for Exhaustive Search of Double-Planetary-Gear Power Split Hybrid Powertrains,» in *ASME Dynamic Systems and Control Conference*, San Antonio, Texas, 2014.

[35] X. Zhang, S. Eben Li, H. Peng e J. Sun, «Efficient Exhaustive Search of Power-Split Hybrid Powertrains With Multiple Planetary Gears and Clutches,» *Journal of Dynamic Systems Measurement and Control,* vol. 137, n. 12, 2015.

[36] J. Liu e H. Peng, «A systematic design approach for two planetary gear split hybrid vehicles,» *Vehicle System Dynamics,* vol. 48, n. 11, pp. 395-1412, 2010.

[37] A. Bayrak, N. Kang e P. Papalambros, «Decomposition-Based Design Optimization of Hybrid Electric Powertrain Architectures: Simultaneous Configuration and Sizing Design,» *Journal of Mechanical Design,* vol. 138, n. 7, 2016.

[38] Q. Zhaobo, L. Yugong, Z. Weichao, P. Ziheng, K. Li e P. Huei, «Simultaneous optimization of topology, control and size for multi-mode hybrid tracked vehicles,» *Applied Energy,* vol. 212, n. 1627–1641, 2018.

[39] X. Zhang, *Design of Power Split Hybrid Powertrains with Multiple,* A dissertation submitted in partial fulfillment in The University of Michigan, 2015.

[40] W. Zhuang, X. Zhang, H. Peng e L. Wang, «Rapid Configuration Design of Multiple-Planetary-Gear Power-Split Hybrid Powertrain via Mode Combination,» *IEEE/ASME Transactions on Mechatronics,* vol. 6, n. 2924-2934, p. 21, 2016.

[41] P. G. Anselma, Y. Huo, A. Edris, J. Roeleveld, A. Emadi e G. Belingardi, «Mode-shifting Minimization in a Power Management Strategy for Rapid Component Sizing of Multimode Power Split Hybrid Vehicles,» *SAE Technical Papers,* 2018.

[42] L. Serrao, S. Onori e G. Rizzoni, «A Comparative Analysis of Energy Management Strategies for Hybrid Electric Vehicles,» *Journal of Dynamic Systems, Measurement, and Control,* vol. 133, n. 3, 2011.

[43] R. E. Bellman, Dynamic programming, Princeton - N.J.: Princeton University Press, 1957.

[44] O. Sundstrom e L. Guzzella, «A generic dynamic programming Matlab function,» in *IEEE Control Applications, (CCA) & Intelligent Control, (ISIC)*, St. Petersburg, 2009.

[45] A. Sciarretta e L. Guzzella, «Control of hybrid electric vehicles,» *IEEE Control Systems Magazine,* vol. 27, n. 2, pp. 60-70, 2007.

[46] N. Kim, S. Cha e H. Peng, «Optimal Control of Hybrid Electric Vehicles Based on Pontryagin's Minimum Principle,» *IEEE Transactions on Control Systems Technology,* vol. 19, n. 5, pp. 1279-1287, 2011.

[47] Q. Jiang, F. Ossart e C. Marchand, «Comparative Study of Real-Time HEV Energy Management Strategies,» *IEEE Transactions on Vehicular Technology,* vol. 66, n. 12, pp. 10875-10888, 2017.

[48] L. Chan-Chiao, P. Huei e G. J. W., «A stochastic control strategy for hybrid electric vehicles,» in *Proceedings of the 2004 American Control Conference*, Boston, MA, 2004.

[49] K. Namwook e R. Aymeric, «Sufficient conditions of optimal control based on Pontryagin's minimum principle for use in hybrid electric vehicles,» *Proceedings of the Institution of Mechanical Engineers, Part D: Journal of Automobile Engineering,* vol. 226, n. 9, pp. 1160-1170, 2012.

[50] G. Paganelli, G. Ercole, A. Brahma, Y. Guezennec e G. Rizzoni, «General supervisory control policy for the energy optimization of charge-sustaining hybrid electric vehicles,» *JSAE Review,* vol. 22, n. 4, pp. 511-518, 2001.

[51] G. Paganelli, T.-M. Guerra, S. Delprat, J.-J. Santin, M. Delhom e E. Combes, «Simulation and assessment of power control strategies for a parallel hybrid car,» *International Journal of Automotive Engineering ,* vol. 214, pp. 705-717, 2000.

[52] X. Zhang, H. Peng e J. Sun, «A near-optimal power management strategy for rapid component sizing of power split hybrid vehicles with multiple operating modes,» in *American Control Conference*, Washington, DC, USA, 2013.

[53] X. Zhang, C. Li, D. Kum e H. Peng, «"Prius+ and Volt-": Configuration Analysis of Power-Split Hybrid Vehicles With a Single Planetary Gear,» *IEEE Transactions on Vehicular Technology,* vol. 61, n. 8, pp. 3544-3552, 2012.

[54] X. Zhang, S. E. Li, H. Peng e J. Sun, «Design of Multimode Power-Split Hybrid Vehicles—A Case Study on the Voltec Powertrain System,» *IEEE Transactions on Vehicular Technology,* vol. 65, n. 6, pp. 4790-4801, 2016.

[55] P. G. Anselma, Y. Huo, J. Roeleveld, A. Emadi e G. Belingardi, «Slope-weighted Energy-based Rapid Control Analysis for Hybrid Electric Vehicles,» *Submitted to: IEEE Trasactions on Vehicular Technology,* 2018.

[56] K. Ahn, S. Cho e W. Cha, «Optimal operation of the power-split hybrid electric vehicle powertrain,» *Proceedings of the Institution of Mechanical Engineers, Part D: Journal of Automobile Engineering,* vol. 222, n. 5, pp. 789-800, 2008.

[57] «Gasoline Vehicles: Learn More About the New Label,» [Online]. Available: http://www.fueleconomy.gov/feg/label/learn-moregasoline-label.shtml.

[58] P. G. Anselma, Y. Huo, J. Roeleveld, A. Emadi e G. Belingardi, «Rapid optimal design of a multimode power split hybrid electric vehicle transmission,» *Proceedings of the Institution of Mechanical Engineers. Part D, Journal of automobile engineering,* 2018.

[59] «2016 - 2019 Chrysler Pacifica,» [Online]. Available: https://www.fueleconomy.gov/feg/PowerSearch.do?action=noform&path=1&year1=2016&year2=2019&make=Chrysler&baseModel=Pacifica&srchtyp=ymm

[60] «2017 Ratings Changes,» [Online]. Available: https://www.fueleconomy.gov/feg/ratings.shtml.

[61] O. Sundström, D. Ambühl e L. Guzzella, «On Implementation of Dynamic Programming for Optimal Control Problems with Final State Constraints,» *Oil & Gas Science and Technology,* vol. 65, n. 1, pp. 91-102, 2010.

[62] P. G. Anselma, J. A. Yi Huo e B. Giovanni, «Rapid optimal design of a multimode power split hybrid electric vehicle transmission».